Design of an Animal Model for Testing Alginate Tissue Repair Scaffolds in Spinal Cord Injury

A Thesis Submitted to the College of

Graduate Studies and Research

In Partial Fulfillment of the Requirements

For the Degree of Master of Science

in the Division of Biomedical Engineering

University of Saskatchewan

Saskatoon

By

Huishu Hou

PERMISSION TO USE

In presenting this thesis in partial fulfilment of the requirements for a Postgraduate degree from the University of Saskatchewan, I agree that the Libraries of this University may make it freely available for inspection. I further agree that permission for copying of this thesis in any manner, in whole or in part, for scholarly purposes may be granted by the professor or professors who supervised my thesis work or, in their absence, by the Head of the Department or the Dean of the College in which my thesis work was done. It is understood that any copying or publication or use of this thesis or parts thereof for financial gain shall not be allowed without my written permission. It is also understood that due recognition shall be given to me and to the University of Saskatchewan in any scholarly use which may be made of any material in my thesis.

Requests for permission to copy or to make other use of material in this thesis in whole or part should be addressed to:

Head of the Division of Biomedical Engineering

University of Saskatchewan

Saskatoon, Saskatchewan, S7N 5A9

Canada

ABSTRACT

Current treatments for spinal cord injury (SCI) are extremely limited due to the fact that the central nervous system lacks the intrinsic ability to regenerate, and constitutes a poor environment for regenerative axon growth. Nerve tissue engineering is an emerging field with the aim of repairing or creating new nerve tissues to promote functional recovery by using artificial tissue repair scaffolds. The design of a stable and consistent animal model of SCI is essential to study the effectiveness of scaffolds in promoting nervous system repair. In this study, a partial transection animal model was created with a three dimensional lesion at T8-T9 that disrupts axonal pathways unilaterally in the dorsal columns of the rat spinal cord. Alginate hydrogel scaffolds incorporating living Schwann cells were fabricated to evaluate the abilities of those scaffolds to foster axonal regeneration. The surgical technique was improved to provide better outcomes related to bleeding during surgery, weight control, neurological function and surgery duration. The survival rate of animals during the surgical procedure and post-surgery period was ultimately increased to 100%. Histology and immunohistochemistry results indicated that implanted alginate scaffolds may induce larger cavities and extenuate harmful inflammation responses, but that effect was ameliorated by inclusion of Schwann cells in the scaffold. However, neither plain alginate scaffolds nor scaffolds containing living Schwann cells were able to improve regeneration of identified axon tracts in the spinal dorsal columns. This research also employed a synchrotron based x-ray phase contrast imaging technique coupled with computed-tomography to visualize the low optical density structural features of scaffolds and spinal cord tissues in formaldehyde fixed specimens. The imaging results suggest that this is a promising method for analyzing the structure of tissue repair scaffolds within the spinal cord. This degree of structural characterization, potentially applicable to living tissue, is not afforded by other conventional image analysis techniques.

DEDICATION

I dedicate this work to my beloved parents Dr. Liancheng Hou and Mrs. Wei Song for their love, support, patience and care. They are my treasures forever.

ACKNOWLEDGMENTS

I would like express my extreme gratitude to my supervisors, Dr. Daniel Chen and Dr. David Schreyer, for their excellent guidance, tremendous support, patience, encouragement and enthusiasm during my graduate studies, research and thesis work. Without them, I couldn't finish this work. I also want to extend my gratitude to Dr. William Dust (Department of Surgery) and Dr. Michael Kelly (Department of Surgery), serving as members of my advisory committee and providing me with valuable comments.

I thank all my colleagues and friends at the Tissue Engineering Research Group, including Dr. Ning Zhu, Dr. Ajay Rajaram, Mindan Wang, Peng Zhai, Ning Cao, Chenglin Liu, Zohreh Izadifar, and at the Cameco MS Neuroscience Research Center, including Tangyne Berry and Ruiling Zhai for their valuable advice and technical support during my experiments. Also, I thank Dr. Dean Chapman, Dr. George Belev and Dr. Adam Webb who provided me with technical advice at the Canadian Light Source. They are excellent people with kind hearts. Special thanks to Dr. Sally Caine, who provided enormous help during the thesis preparation process.

In addition, I would like to acknowledge the financial support I received from the Saskatchewan Health Research Foundation (SHRF), and the CIHR Training Grant in Health Research Using Synchrotron Techniques Fellowship (CIHR-THRUST).

TABLE OF CONTENTS

page

LIST OF TABLES

LIST OF FIGURES

LIST OF ABBREVIATIONS

3D	Three dimensional
AREB	Animal Research Ethics Board
ATCC	American Type Culture Collection
BBB	Basso, Beattie and Bresnahan
BMIT	BioMedical Imaging and Therapy
BMS	Basso Mouse Scale
BMSC	Bone marrow stem cell
BSA	Bovine serum albumin
BWS	Body-weight supported
Calcein-AM	Acetoxymethyl ester of calcein
CLS	Canadian Light Source
CNS	Central nervous system
CSPGs	Chondroitin sulfate proteoglycans
CST	Corticospinal tracts
CT	Computed tomography
DMEM	Dulbecco's Modified Eagle Medium
ECM	Extracellular matrix
EDTA	Ethylenediaminetetraacetic acid
FBS	Fetal bovine serum
FGF	Fibroblast growth factors
HEPES	Hydroxyethyl piperazineethanesulfonic acid
IL	Interleukin

HA	Hyaluronic acid
MAG	Myelin-associated glycoprotein
MEP	Motor evoked potential
MPSS	Methylprednisolone sodium succinate
NGF	Nerve growth factor
NPC	Neural progenitor cell
NSC	Neural stem cell
O.C.T	Optimal cutting temperature (tissue embedding medium)
OEC	Olfactory ensheathing cell
OMGP	Oligodendrocyte-myelin glycoprotein
OsO_4	Osmium tetroxide
PBS	Phosphate buffered saline
PCI	Phase contrast imaging
PF	Paraformaldehyde
PGA	Poly (glycolic acid)
PLA	Poly (lactic acid)
PLGA	Poly (lactic glycolic acid)
PNS	Peripheral nervous system
SCI	Spinal cord injury
SEM	Standard error of the mean
SSEP	Somatosensory evoked potential
TNF-α	Tumor necrosis factor-α
UCACS	University Committee on Animal Care and Supply

Chapter 1. Introduction and Objectives

Spinal cord injury (SCI) can cause permanent neurologic deficits, severely affecting the quality of life for patients (Lawrence S Chin 2013, Nor 2006). Up to now, there is no treatment that can effectively improve the rehabilitation of spinal cord injuries, even though functional training would cost years to recover a little motor and sensory function. In the nervous system of mammalian animals, peripheral nervous system (PNS) injuries can be repaired and regenerate efficiently at any time during the embryonic phase and adulthood. However, recovery from injuries in the adult central nervous system (CNS) such as brain or spinal cord is not as simple as in PNS. The possibility of regeneration is extremely limited, although the CNS neurons have the ability to recover in the embryonic phase (Brittis and Flanagan 2001).

Early *in vitro* study illustrated that the CNS lacks regeneration ability not only because of intrinsic deficits, but also because it provides an unfavorable environment for axon regeneration. The unfavorable environment is due to substances produced by slow Wallerian degradation (Mietto et al. 2011, Rotshenker 2011), myelin and myelin-associated axonal growth inhibitors (Hu and Strittmatter 2004) and astrocytic scars (Wanner et al. 2013). Researchers have been focusing on overcoming these negative cues in the growth-inhibitory environment at the molecular level. One of the promising methods is the use of bioengineered tissue repair scaffolds as a bridge to reconstruct the lesion area and provide positive guidance factors to induce or promote axonal regeneration through scaffolds (GrandPre, Li, and Strittmatter 2002, Cui et al. 2006).

Tissue engineering is a multi-disciplinary scientific field with roots in life science, material science and clinical medicine which is still at the early stage (Nor 2006). Alginate is a natural material that has been widely used in tissue engineering, especially in skin repair (Mano et al.

2007). It has already been reported that alginate sponge can help CNS axon regeneration by providing a favorable environment in young rats (Kataoka et al. 2004). Properly designed animal models are of great value in helping scientists understand the mechanisms of SCI and evaluating potential therapies. Meanwhile, the development of understanding of SCI mechanisms could also help scientists to design and develop better animal models for studying SCI (Kwon, Oxland, and Tetzlaff 2002). A large variety of animal species can be used in injury experiments (Fernandez et al. 1991) but different injury paradigms are designed to address different questions. Therefore, choosing the right animal models requires consideration of the advantages and disadvantages of each injury paradigm as well as the natural properties of each animal model species.

1.1 CNS Injury

1.1.1 SCI in humans

SCI causes thousands of people to suffer paraplegia or tetraplegia each year. Epidemiologic research has demonstrated that the annual incidence of SCI is approximately 40 persons per million in the United States. There are over 12,000 new spinal cord injury cases occurring each year in the United States, with a total of 273,000 patients, living with a spinal cord injury. The range of prevalence is 238,000 to 332,000 (Starkweather 2013). In Canada, it is estimated that over 86,000 people live with SCI and 4,300 new SCI cases occur each year (Canada 2014). SCI can be caused by many reasons: the largest percentage is due to road traffic accidents, which account for 36.5%. Sports-related accidents are the second reasons, especially accidental falls (28.5%) and diving injuries (9.2%). Additionally, violence such as gunshot wound and knife injuries also constitute 14.3% of SCIs (Whitwell 2005). SCIs are commonly seen in young

individuals involved in traffic accidents and violence or older individuals who sustain falls. Governments invest billions of dollars each year to help recovery of SCI patients.

Trauma causes dysfunction of the spinal cord, result in devastating and permanent loss of neurological function. Sensory and motor function is lost in those body regions served by spinal cord caudal to the point of injury. Multiple secondary health problems include pressure sores, cardiac dysfunction, respiratory dysfunction, autonomic dysfunction, stroke, depression and urinary tract infection (McKinley et al. 1999). Recently, strides have been made in physiology, pharmacology and rehabilitation, which provide hope for promoting the quality of life of spinal injured patients. However, the practical impact on patients and their treatment has remained almost at a standstill.

1.1.2 Anatomy of the human and rat spinal cords

To understand the mechanism of spinal cord injury, it is first necessary to appreciate the basic structure of the spinal cord and the pathophysiology of SCI. The nervous system can be divided into two parts, the CNS (brain, retina, optic nerve and spinal cord) and the PNS (generally, all nerves and ganglia outside the CNS). The spinal cord (Figure 1.1) is a longitudinal structure of nerve fibers and cells arranged in a rostral – caudal direction running down the middle of the back. There are four major levels of the spinal cord: cervical, thoracic, lumbar and sacral/coccygeal whereby afferent (sensory) information enters, and motor (efferent) information exits. Cervical segment 1 is connected with the brain through the medulla. The spinal cord of humans consists of 31 segments each supporting a pair of spinal nerves. The nerves of the PNS are connected with the spinal cord through nerve roots and travel to specific parts of the body to control motor, sensory and autonomic functions.

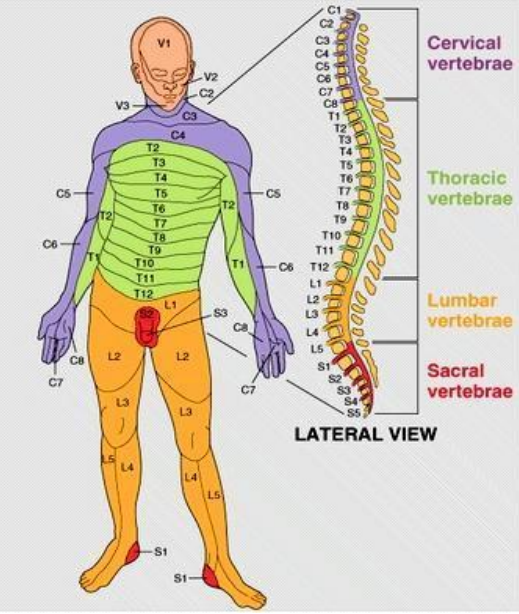

Figure 1.1. Schematic diagram of human spinal cord. The spinal cord is located inside the vertebral canal, which consists of 7 cervical, 12 thoracic, 5 lumbar and 5 sacral vertebrae. Each spinal segment includes motor, sensory and autonomic neurons that are topographically related to different parts of body (Spinal cord injury, http://www.sci-recovery.org/sci.htm).

CNS tissues in both brain and spinal cord contain gray matter and white matter. The gray matter in the spinal cord is in its center, and is composed of neurons and neuropil (complex meshwork of glial cells, dendrites, axon terminals and synapses). The location of white matter columns is outside and surrounding the gray matter, and includes bundles of ascending and descending, myelinated or unmyelinated axons. In the white matter, axons travel across different spinal levels and with the brain to establish contacts with other neurons (Figure 1.2), often over long distances. Dorsal roots of peripheral nerves transmit sensory information to the posterior horn of the gray matter, and motor information leaves the anterior horn through the ventral roots to innervate muscles.

The organization of white matter is complex; different ascending and descending axon tracts convey information relevant to different somatic sensations and movements (Figure 1.2). There are several major ascending tracts and descending tracts. One of the ascending tracts, for example, the dorsal columns include the fasciculus cuneatus and fasciculus gracilis, transmitting ascending touch information. The dorsal spinocerebellar tract (Flechsig's tract) transmits ascending unconcious proprioceptive information from the body to the cerebellum. The spinothalamic tract conveys nociceptive information up to the brain regions related to pain sensation (Naseri et al. 2013, Zhang et al. 2000). The corticospinal tract (CST) is a major descending tract that control the voluntary skilled movements and the fine musical movements on face and neck as well as all four limbs. Along with the CST, the rubrospinal tract has a similar function but the rubrospinal tract is largely limited to controlling the upper limbs. The tectospinal

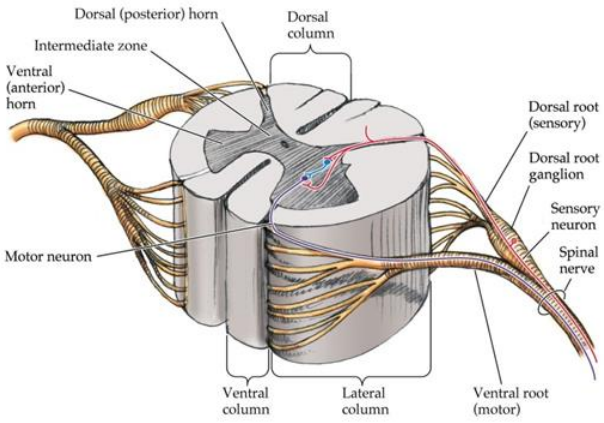

Figure 1.2. Structure of human spinal cord and distribution of dorsal and ventral roots.

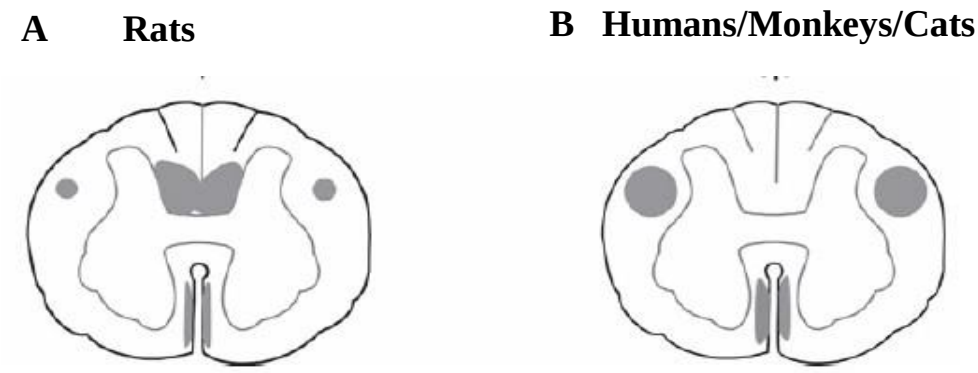

Figure 1.3. Schematic drawings of CST anatomy in the spinal cord in rodents, and in humans/monkeys/cats. (A) Location of CST in rodents. (B) Location of CST in humans/monkeys/cats.

tract conducts descending multi-synaptic connections to motor neurons of neck muscles along with the vestibulospinal tracts.Vestibulospinal tracts (lateral and medial) coordinate the head movements and the upright posture of primates (Voron 2011, Miselis 2011). The current repair strategies are not only focusing on how to regrow these tracts after injury, but also on how to make the axons within these tracts reconnect to the right place.

Injuries occuring in one spinal segment will disconnect all the spinal segments below the lesion from communicating with the brain through the affected tracts, leading to a complete or partial loss of function. Therefore, the closer to the head the spinal cord injury is, the greater the area of the body that may be affected (Tortora and Derrickson 2011). For example, a patient with an injury at the level of the tenth thoracic segment may lose use of his legs but his/her arms will not be affected. Another patient with an injury at the level of the fourth cervical segment may lose use of his/her legs and arms. Accordingly, animal models of SCI can be designed by understanding the relationships between the various levels of the spinal cord and their topographical relationship to the rest of the body.

Rat spinal cord is similar to human spinal cord but has some differences. The human spinal cord has 31 segments, while the rat spinal cord has 34 segments. Each segment possesses a dorsal root and a ventral root connecting the CNS with the PNS. Dorsal roots convey sensory information to the dorsal horn of the gray matter, and the motor information leaves the ventral horn through the ventral roots. There are some differences in the organization of white matter tracts comparing rat with human spinal cord. A major difference is that the position of the CST in the rat is different from human. This is off practical, experimental importance because in the last two decades, many animal studies have focused on the improvement of the CST as a hallmark of repair. The CST contributes significantly to the control of skilled movements in

mammals (Oudega and Perez 2012). In the rat spinal cord, CST axons are mainly (95%) located in the ventral aspect of the dorsal columns and the rest (3-5%) are located in the medial aspect of the ventral columns (Brosamle et al. 2000). The lateral columns also contain two minor CST components (Fig 1.3.A;(Joosten et al. 1992)). In contrast, humans, non-human primates and cats all have similar CST anatomy which is mainly located in the dorsal aspect of the lateral columns, with a minor component in the medial aspect of the ventral columns (Fig 1.3.B; (Nyberg-Hansen and Brodal 1963, Lemon and Griffiths 2005)).

Injuries in the spinal cord axon tracts can cause functional loss in the affected body part. For example, transection of the half part of one segment which includes the dorsal columns can block the flow of afferent nerve information up to the brain, thus causing injured animals to lose unilateral sensory function which was dominated by the injured segment. Many studies reported that hemisection of one side of the spinal cord that involves segments T8 to T12 will result in contralateral loss of pain and temperature sensation and paralysis of the ipsilateral leg, and slight reduction in ipsilateral muscle tone in the lower abdomen (Fig 1.2) because pain and temperature ascending sensory tracts have crossed the midline below the lesion, and descending motor tracts have crossed the midline above the lesion. No loss of sensation or paralysis to the upper limbs will ensue. These phenomena has been called Brown-Séquard syndrome in humans.

1.1.3 Spinal cord injury response

Injury of spinal cord is usually not followed by regenerative repair. An understanding of the pathophysiological mechanisms of SCI is necessary for the development of new repair strategies and technologies. Generally, SCI has four types: *1*) cord maceration/compression, *2*) cord lacerations (gun shot or knife wounds), 3) contusion injury, and 4) solid core injury (Norbert Pallua 2011). Compared to the latter two injuries, the first two could cause the surface of the

cord to be lacerated and have more connective tissue response. In each type of injury, three phases of SCI can be identified: the acute, secondary (sub-acute), and chronic injury processes. In the acute phase, tissue destruction occurs within seconds to minutes from the initial trauma. Mechanical damage associated with the neural lesion may also include blood vessel, bones, intervertebral discs, and ligaments. At the cellular level, instantaneous mechanical and ischemic insults could lead to cell death or necrosis. This is usually more severe in grey matter than in the white matter in a contusion injury.

Secondary injury usually develops minutes to weeks after the acute phase, leading to damage of a variety of neural and other tissues surrounding lesions which were unaffected by the primary traumatic event. During this phase, the trauma site continues to enlarge. Mechanisms of secondary injury include, but are not limit to, immune system response or inflammation, delayed apoptosis, ischemia, and excitotoxicity.

The inflammatory response begins immediately and persists through the acute phase to chronic phase after initial SCI. It is a critical component in the secondary injury cascade. (Fehlings and Nguyen 2010). The role of the inflammatory response is to clear cellular debris. This debris from the injury could prevent the regeneration of surviving neurons. Neutrophils (the first immune cells response to the injury), macrophages and resident microglia are activated and invade the spinal parenchyma from the circulatory system within 24 h and can reach a peak within 48 h. However, it is controversial whether an uncontrolled immune response may be harmful for the survival of spared axons and for axon regeneration in SCI. The active microglia and macrophages release increased cytokines, which include chemokines, interleukin (IL)-1β and tumor necrosis factor-α (TNF-α), etc. These cytokines were observed to be elevated in the

enlarged lesion and ultimately cause neuron injury or death by inducing axon demyelination and neuronal apoptosis (Catharyn T. Liverman 2005, Popovich and Jones 2003).

Apoptosis is a secondary cell death process that is different from necrosis. Necrosis mostly happened in the acute phase of SCI derive from the rupture and swelling of cells, caused by external factors. In contrast to necrosis, apoptosis is a programmed cell death process that requires a specific program of enzyme activation, and ultimately results in less harmful substances released as cells die. It involves several cellular events which include cell shrinkage, DNA fragmentation and compartmentalization of cytoplasmic parts into membrane-bound 'apoptotic bodies'. In SCI, apoptosis normally starts within a few hours after injury and can be activated in both neurons and glial cells. Apoptosis is not only observed in the injury site, but also extends to spinal cord tissues away from the center of the injury. Typically, the cells at the center of the lesion die by necrosis because of the direct trauma. Necrosis triggers dead cells to release potassium, calcium, proteases and numerous other factors that change the microenvironment as well as activate the inflammation response. Apoptotic cell death is not directly caused by external force, but because the changes of the local chemical and signaling environment (Zhang et al. 2012). Therefore, how to improve the microenvironment of cells to prevent apoptosis has become an extremely important focus.

When neuron death occurs it leads to release of excitatory neurotransmitters into the microenvironment, and nearby healthy neurons get overexcited to release even more neurotransmitters. This cycle is another important contributor to damage during the secondary phase. This is called excitotoxicity which not only involved with SCI, but also been found in stroke, Alzheimer's, Huntington's, Parkinson's diseases and other neurodegenerative diseases. Glutamate is the most important neurotransmitter that is released when cell death occurs

resulting in excitotoxicity (Xu et al. 2005). The excessive accumulation of glutamate binds with receptors on neurons causing a rush of Ca^{2+} into unimpaired cells, contributing to damage.

Ischemia, the interruption of blood flow, plays an important role in both primary and secondary injury mechanisms. Mechanical force compresses or tears the spinal cord microvasculature causing hemorrhage in the following hours, especially in grey matter. Loss of blood flow deprives neurons of oxygen and glucose, and contributes to neuronal depolarization resulting in transmitter release and excitotoxicity. Another possible cause of ischemia is vasogenic edema caused by a breakdown of the blood-brain barrier, leading to increased pressure and metabolic perturbation (Chodobski, Zink, and Szmydynger-Chodobska 2011).

A chronic phase of SCI occurs weeks to months after the injury. During the chronic phase, fibroblastic and astrocytic scar formation is the predominate reason that prevents the regenerative recovery of axons. The scars usually form from reactive astrocytes and microglial cells that hypertrophy and proliferate at the interface between the intact tissue and the injury site. In the acute and secondary phases of injury, the formation of glial scars may help stop hemorrhage, minimize inflammatory damage and stabilize the microcirculation in surrounding intact tissue. However, in the chronic phase, the glial scars become physical and biochemical barriers that prevent axon regeneration. Astrocyte scars at the injury site can secrete inhibitory molecules that partially cause the failure of regeneration, such as ephrin B3, semaphorin 4D, and chondroitin sulfate proteoglycans (CSPGs). Several additional growth-inhibitory proteins are associated with myelin debris that can induce growth cone collapse and inhibit axon extension. These myelin-derived axon inhibitors include myelin-associated glycoprotein (MAG), oligodendrocyte-myelin glycoprotein (OMGP) and nogo A. Removal or neutralization of these inhibitory signals might lead to improved axonal regeneration.

Microglia, astrocytes and invasive macrophages are responsible for removing myelin debris in the epicenter and surrounding of injury site in CNS whereas Schwann cells and macrophages are responsible for cleaning myelin debris in injured PNS. Clearance of myelin debris is much slower in the CNS than in the PNS. Ultimately, surviving or regenerating axons must undergo remyeleination. Several studies (de Guzman et al. 2008, Oudega and Xu 2006, Agudo et al. 2008) suggest that introduction of Schwann cells into injured CNS may help improve axon regeneration and accelerate the re-myelination process.

1.2 Therapeutic Strategies for Spinal Cord Repair

1.2.1 Conventional therapies for SCI

Primary mechanical forces initiate nervous tissue damage in SCI. Persistent compression of the spinal cord is often treated with surgical decompression after the SCI occurs. However, because of the absence of randomized, controlled clinical trials, how surgery will improve neurological recovery is still controversial. Studies revealed that decompressed surgery performed within the first 24 h of injury could be conducted safely. However, the patient must exhibit stabile hemodynamics in order for urgent decompression to be performed within the first 24 h after an isolated cervical SCI (Consortium for Spinal Cord 2008).

Since the use of surgical and post-surgical interventions are limited to the first 24 h of injury, pharmacological treatments are applied more widely in the recovery procedure following SCI. The strategy of neuroprotection in acute SCI aims at prevention of secondary injury as well as rescuing spared axons and cell bodies at and around the primary lesion. Pharmaceutical agents such as methylprednisolone sodium succinate (MPSS), is currently used in the clinic. High-dose MPSS targets several different early molecular events to reduce excitotoxicity, inhibit calcium influx, ischemia and inflammatory responses (Fehlings 2001). It can be used in the first 8 h after

trauma and continued during the secondary injury phase (Gorio et al. 2005). However, high-dose MPSS has severe adverse side effects that make its use very controversial. MPSS is not recommended for blunt SCI.

Injuries in spinal cord could lead to demyelination of preserved spinal tracts, thus influencing the transmission of electrical impulses. Axon demyelination leaves previously covered potassium channels exposed. This phenomenon will put axons in danger of conduction block when the action potential enters the demyelinated region. Based on this mechanism, researchers hypothesized that HP184, a blocker which can antagonize both exposed potassium and sodium channels on demyelinated axons has been developed to restore the ability of demyelinated axons to transmit electrical impulses. This therapeutic strategy is still undergoing clinical trials.

Physical rehabilitation is a significant part of long-term recovery strategies after surgical and pharmacological treatments in SCI. Gait rehabilitation is suitable for persons in the secondary injury phase and chronic phase of SCI. One method of gait rehabilitation is body-weight supported (BWS) training, which can be combined with treadmill-based gait training. In recent studies (Field-Fote 2001), the combination of BWS and treadmill showed positive results. This method can stimulate the lower limbs to produce effective rhythmic swing in paraplegic subjects. This provides evidence supporting the idea that there is a central pattern generator in human spinal cord, which can act in the absence of supraspinal influence. Similar to lower mammals, the central pattern generator in the spinal cord may control involuntary locomotor movement according to the central pattern generator theory. However, compared with other intensive rehabilitation therapies, BWS treadmill training has not been proven to have more benefit than other rehabilitation strategies (Lam et al. 2007).

1.2.2 Tissue engineering strategies for SCI

Besides the conventional therapies listed above, the emerging techniques of bioengineered tissue repair scaffolds can be used to combine several restorative strategies together. Broadly speaking, tissue repair scaffold therapy combines medicine with biomaterial science and engineering. The medical part is related to the surgery, neuro-regenerative and cell-mediated repair. The main idea of tissue repair scaffold therapy is fabricating a scaffold from a composite biomaterial and then implanting the scaffold, with growth-promoting factors and inhibition-neutralizing factors enclosed, into the injured part of spinal cord. The regeneration of axons might then proceed through the internal physical structure of the scaffold.

Development of tissue repair scaffolds requires the integration of several different design strategies, and can target different phases of repair. Current research focuses on three phases of scaffold design; (1) synthesize and characterize suitable composite biomaterials that do not provoke an inflammatory response in the host tissue; (2) design and fabricate scaffolds with appropriate physical properties and microstructure; and (3) integrate strategies for promoting axon regeneration and antagonizing inhibitory effects *in vitro* and *in vivo*, that can eventually be applied in clinical trials.

To date, significant achievements have been made in the first two phases. A variety of biomaterials, both synthetic and natural, have been modified to fabricate tissue repair scaffolds. Natural biomaterials including alginate, hyaluronic acid (HA), collagen, agarose, chitosan, Matrigel^{TM}, and methylcellulose hydrogels have been reported to be suitable to fabricate scaffolds, although none of them is perfect. Combination of different materials may perform better than only one material.

Synthetic materials such as poly (lactic acid) (PLA), poly (glycolic acid) (PGA), and their copolymers poly (lactic glycolic acid) (PLGA) may also play an important role in tissue engineering (Vacanti and Vacanti 2000). Because of their good biodegradability and bioresorbability *in vivo*, PLA, PGA, and PLGA have been considered to be the gold standards in tissue engineering. However, the mechanical properties of synthetic materials may be unsuitable for application in SCI repair, creating a mismatch between scaffold flexibility and spinal cord flexibility. Since both natural and synthetic materials have shortcomings, combinations of natural and synthetic materials could preserve advantageous properties, meanwhile minimizing any harmful effects.

Alginate hydrogel is a natural material that has been widely used in tissue engineering due to its high level of biocompatibility and biodegradability as well as its nontoxicity. It has been well established that alginate hydrogels can enhance skin repair (Huang and Fu 2010), and serve as a substrate for both *in vitro* cell culture and *in vivo* drug release (Rupenthal, Green, and Alany 2011). It has also been reported that alginate can act as an effective cell carrier for neuronal stem cell transplantation (Rupenthal, Green, and Alany 2011). Further studies demonstrated that alginate sponge could present a favorable environment for axon regeneration in the spinal cord and sciatic nerve (Kataoka et al. 2004). These studies suggest that the use of alginate-based scaffolds in spinal cord regeneration is promising.

Alginate is a bioresorbable polysaccharide extracted from brown seaweed. In chemical structure, alginate is a linear copolymer composed of 2 monomeric units, β-D-mannuronic acid (M units) and α-L-guluronic acid (G units) (Sriamornsak and Sungthongjeen 2007). Within the alginate molecule, these monomers are sequentially assembled as regions made up of either M blocks or G blocks, or as an alternating sequence of MG blocks (Usov 1999) (Figure 1.4).

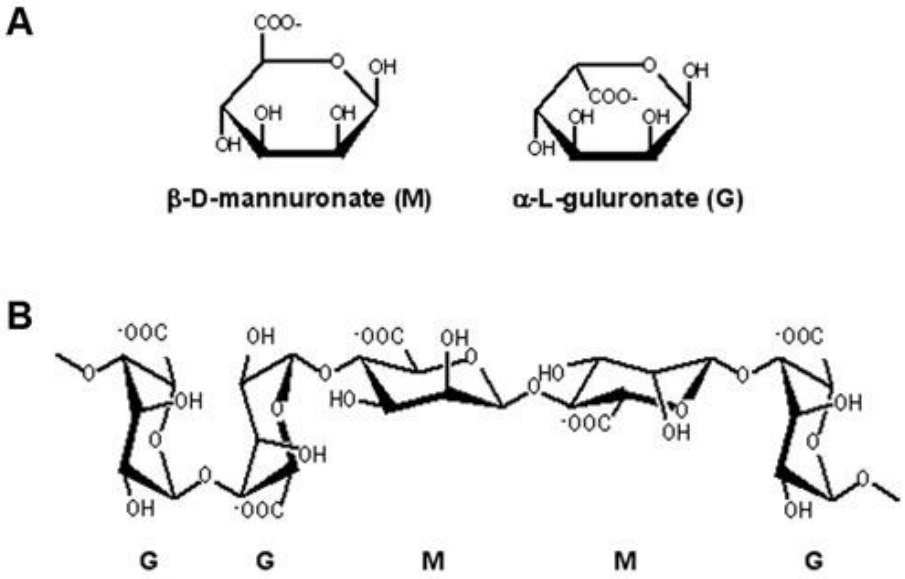

Figure 1.4. Chemical structure of alginate. (A) The monomers in alginate. (B) The alginate chain.

Gelation of alginate is generally carried out by ionic crosslinking using a divalent cation, typically calcium (Lee and Mooney 2012). Different crosslinks occurring between monomers would cause different mechanical properties for alginate hydrogels. For example, the crosslinking that happens between the α-L-guluronic residues (G residues) produces brittle gels with good heat stability, whereas the crosslinking that happens between the β-D-mannuronic residues (M residues) produces weak, elastic gels with good freeze-thaw behavior. Besides that, calcium ions also play an important role in regulating the elastic modulus of alginate hydrogel.

The biocompatability of alginate, and the mild conditions under which it is handled, make it a suitable material for inclusion of living cells that might assist the repair process after implantation of a tissue scaffold. The mechanical properties of alginate could influence proliferation, differentiation, location, and morphology of living cells included during fabrication (Banerjee et al. 2009). However, the concentrations of alginate and, particularly, high levels of calcium ions, may inhibit the growth of cells in culture.

A variety of cell types include neural stem cells (NSCs), neural progenitor cells (NPCs), bone marrow stem cells (BMSCs), Schwann cells, and olfactory ensheathing cells (OECs) have already been studied for their usefulness in cell-mediated tissue repair following SCI (Friedman et al. 2002, Schmidt and Leach 2003, Nomura, Tator, and Shoichet 2006). Immature stem cells such as NSCs, NPCs and BMSCs have the ability to proliferate, migrate and differentiate to vary kinds of cells that help improve locomotor recovery, with diminished astrocytic scarring (Chen et al. 2010, Wilcox et al. 2014). Pluripotent cells descended from BMSCs have the ability to migrate towards a lesion and secret growth factors that facilitate regeneration and lesion repair (Vawda, Wilcox, and Fehlings 2012). Previous studies (Assun et al. , Wong, Chan, and Lo 2014) also show the promise of using mature cells in tissue repair scaffolds in improving regenerative

repair of PNS and CNS, especially in SCI. In this method, scaffolds made from biomaterials are seeded with viable cells, such as Schwann cells or OECs that act to support and promote regeneration of severed axons.

One important component in the process of PNS nerve regeneration is the presence of growth-promoting Schwann cells (Moon and Bunge 2005). In the normal intact peripheral nerve Schwann cells produce the myelin sheaths around large-diameter axons. Non-myelinating Schwann cells also enclose the small-diameter, unmyelinated axons. However, after peripheral nerve injury, proliferation of Schwann cells is triggered by damaged axons membrane and myelin debris. Schwann cells remove the myelin debris and pass them to macrophages, and then macrophages engulf the debris. When Schwann cells migrate to a distal nerve stump, they align themselves into Bands of Büngner. The formation of the Bands of Büngner after PNS injury can promote axonal growth (Cote et al. 2011). Moreover, Schwann cells can secret extracellular matrix (ECM) proteins such as laminin and collagen that can help axon regeneration. Schwann cells also produce nerve growth factor (NGF)，BDNF and fibroblast growth factors (FGFs) as well as antagonize CNS myelin-associated inhibitors to improve the microenvironment surrounding the lesion (Goto et al. 2010, Deng et al. 2011, Wilhelm et al. 2012). Several studies (Hill et al. 2006, Oudega and Xu 2006) reported that Schwann cells can myelinate surrounding axons near the scaffolds after implantation within channels containing extracellular matrix in SCI models. However, the safety of transplantation of Schwann cells in humans hasn't been proven yet. For example, there are no relevant studies to test whether transplantation of Schwann cells into humans could form tumors or not.

OECs are a type of myelinating glial cells located in the olfactory nerve and they can continuously produce neurotropic factors to enhance axon regeneration and mediate

remyelination (Ramon-Cueto and Avila 1998). OECs and Schwann cells have some similar properties. They secrete several of the same growth factors and can express similar cell membrane adhesion molecules. In addition, OECs have better migratory potential to penetrate glial scars (Verdu et al. 1999). However, Deumens et al. (2006) reported OECs did not migrate well in the host spinal cord, but are limited to a small area of lesion. Furthermore, there were few OECs still alive after three or four weeks' implantation on rats *in vivo* which indicate they may not suitable for long term implantation (Andrews and Stelzner 2007).

1.3 Animal Models for SCI

1.3.1 Animal species used in SCI

Animal models offer a great opportunity to help scientists understand the deeper mechanisms of SCI and evaluate potential therapies. Conversely, the development of understanding in SCI could also help to develop and refine experimental animal models of SCI. A variety of animal species can be used in injury experiments, depending on the injury paradigms and the questions to be answered. Thus, one needs to choose the right animal models considering the advantages and disadvantages of each injury paradigm as well as the natural properties of each animal model species.

Currently, scientists are commonly using rat and mouse as animal models in their experiments. Rodents are easy to access and raise, relatively inexpensive, have transgenic potential, and are relatively easy to care for post-operatively, with few surgical infections (Pritchard et al. 2010, Khan et al. 1999). However, issues such as size, gait, and neuroanatomical, and neurophysiological and behavioral differences complicate comparisons between rodents and humans. Thus, there are limitations when assessing the efficacy and safety of treatments in

humans compared to rodents. Also, rodents have high rates of spontaneous recovery from induced spinal cord injury. This could cause difficulty in identifying whether the recovery derives from treatments or are more intrinsic to the animals themselves.

Non-human primates and other larger mammals can serve as an intermediate step between rodents and humans to aid in translation of effective therapies to the clinic (Courtine et al. 2007). One advantage of large animal models is that experimental surgery can be more precise because their size. For cats and non-human primates, the organization of spinal cord is much like humans, especially the main part of the CST. Ultimately, their use is imperative to prove safety and efficacy prior to human experimentation. The major drawbacks of using large animals as models are the extreme expense and the high level of breeding environment that is demanded. These disadvantages make it more difficult to show reproducibility in non-human primate models. There are also ethical concerns about using non-human primates because they are too close to human.

1.3.2 Injury paradigms

Three major injury paradigms have been used to study SCI in animal models: transection, contusion and compression models. Complete or partial transection of spinal cord is an easier model in which to evaluate the effectiveness of interventions with regard to both axonal regeneration and functional recovery. In studies of bioengineered tissue repair scaffold therapy, complete transection can provide a gap into which the scaffold is implanted, and can make the observation of axons regeneration more unambiguous (Kwon, Oxland, and Tetzlaff 2002). However, complete anatomic transection of the spinal cord is rare in humans. Therefore, partial transection models more closely mimic real cases of human SCI. It is easier to nurse post-operative animals following partial spinal cord transection because we can selectively damage

only certain tracts of the spinal cord, resulting in only partial loss function. However, compared with complete transection, it is more difficult to determine whether the functional improvement following partial transection originates from true regeneration of the injured tract or to functional compensation from other neural systems that are spared. Nevertheless, transection models still have unquestionable value in the study of axonal regeneration because specific axon groups can be targeted and evaluated.

Although transection or laceration SCI is seen in the clinic, blunt contusive or compressive force to the spinal cord occurs more frequently in human SCI. Surgical clips and balloon compressive models are commonly used to induce compressive injury in experimental animals. Balloon compressive injury can be created without making a laminectomy, offering the possibility of easier and less traumatic surgery. The typical contusive injury model is weight-drop injury. The principle is to use mechanical force to damage the tissue in the spinal cord without disrupting the dura covering the spinal cord. Compressive and contusive injury models can be reproducible with low morbidity rates (Jun Chen 2009). However, most of compressive and contusive models require an injury device. Importantly, it is very difficult in compressive or contusive injury models to identify which tracts been damaged and to assess the severity of damage (Lee and Lee 2013).

1.4 Imaging Techniques for Tissue Engineering

1.4.1 Conventional biological visualization techniques for tissue engineering

To investigate the performance of bioengineered scaffolds *in vivo*, a non-invasive imaging technique to observe changing microarchitectures of the scaffold during the recovery process is essential. Conventional visualization techniques, such as scanning electron microscopy

(SEM), transmission electron microscopy (TEM) and confocal laser scanning microscopy (CLSM), can be used to study morphological aspects of scaffolds and tissues obtained from *in vivo* and postmortem *in vitro* animal experiments (Zhu et al. 2011). These methods typically use optical or electron microscopy to detect changes in scaffold architecture after *in vivo* placement and interactions between the host tissue and scaffold. These conventional histological methods occur postmortem and require many individual steps including fixation, embedding, sectioning, staining, and mounting. However, these steps are destructive and invasive and could therefor damage the samples for further analysis such as immunohistochemistry.

Radiological approaches are more suitable for examining scaffolds and surrounding tissues *in situ* in living animal models and in human patients. For conventional X-ray imaging, X-rays are absorbed and attenuated when they penetrate through optically dense samples. Tissue and scaffold materials each have their own X-ray attenuation coefficient. Soft tissues and scaffolds are hard to be distinguished because they each have similar, low X-ray attenuation coefficients (Kim et al. 2008). In order to solve this problem, phase contrast imaging (PCI) based on X-ray refraction and analyzed using computed tomography (CT) is more suitable for the study of scaffold-based nerve tissue engineering (Guan 2010).

1.4.2 Synchrotron radiation imaging techniques for tissue engineering

The synchrotron radiation PCI technique is a new imaging method that allows structural visualization of low density scaffolds and nerve tissues without fixation, sectioning and staining. Synchrotron radiation provides a spatial resolution almost two orders of magnitude higher than conventional X-rays from a tube. As such, it can provide detailed information of tissue regeneration and insight that would not be possible from conventional imaging methods. In-line PCI is a technique that is sensitive to the boundary between tissues and/or biomaterials with

different refractive indices. Synchrotron PCI coupled with CT can provide not only easy sample preparation but also visualization ability of the low density scaffolds in soft tissue without damaging the samples. However, in these studies, a single axon still cannot be resolved in the images. Currently available synchrotron PCI technology has a resolution limit of 1 μm, but only at high radiation doses.

1.5 Research Objectives

The aim of this research is to design a stable, effective animal model for evaluation of axon regeneration and functional recovery using tissue repair scaffolds following SCI. The focus is on the development of alginate hydrogel tissue repair scaffolds that include living Schwann cells, development of a surgical procedure for the SCI animal model, and evaluation of axon regeneration. Synchrotron-based PCI-CT will be employed to characterize the features of alginate hydrogel scaffolds and surrounding soft tissues. The first hypothesis is that **a partial transection animal model could be suitable for the placement of 3D tissue repair scaffolds, have simple surgery process and easy post-operative care**. The second hypothesis is that **alginate hydrogel scaffolds, with or without inclusion of living Schwann cells, could provide a favorable microenvironment to regenerate injured spinal axons**. The ultimate goal is that this animal model could be used in the future to test the efficiency and biocompatibility of 3D scaffolds for SCI repair *in vivo*. Particularly, the following objectives are to be achieved.

(1) Develop solid alginate hydrogel scaffolds with encapsulated Schwann cells and explore the interaction of Schwann cells with alginate hydrogels for Schwann cell survival and proliferation inside of scaffolds *in vitro*. Design an animal model for spinal cord tissue engineering and optimize the surgery procedure

(2) Evaluate and analyze the functional recovery and axon regeneration by means of behavioral tests, histology and immunohistochemistry methods.

(3) Illustrate the merits of synchrotron based PCI-CT in low density biological samples, such as spinal cord tissue and alginate hydrogel scaffold, and characterize the features of 3D grid-pattern alginate hydrogel scaffolds.

1.6 Thesis Organization

This thesis consists of six chapters: four experimental chapters are put into context with a beginning introductory chapter, and a concluding discussion chapter. Each experimental chapter is comprised of three main sections: introduction, materials and methods, results and discussion.

The first chapter of this thesis is focused on reviewing the problem of SCI and experimental approaches to the study of SCI, as well as outlining the structure of the thesis. This chapter presents the anatomy of human and animal spinal cord, the physiological and pathological changes after spinal cord injury and the current therapies for SCI. Also, a literature review about the application of tissue engineering in SCI and the importance of animal models are elucidated in this chapter.

Chapter 2 presents the surgical procedure and post-operative care for a novel scaffold implantation animal model. The two series of surgery process were compared and the improvements that have been made were described. This chapter also introduces a method to fabricate alginate hydrogel scaffold and encapsulate Schwann cells as well as the scaffold implantation procedure.

Chapter 3 presents the behavior test results of all animals during the six weeks recovery time after surgery. The classic test, Basso, Beattie and Bresnahan (BBB) open field locomotion

scale is used to examine functional recovery following SCI. The result comparisons were between two series of surgeries and also between left and right hindlimbs.

Chapter 4 provides postmortem histology and immunohistochemistry analysis on the response of different neuronal and non-neuronal cells after spinal cord injury. The activities of macrophages, microglia, astrocytes and two populations of spinal cord axons were examined within the normal healthy spinal cord, injured spinal cord and scaffold treated groups for direct evaluation and analysis of axon regeneration in this research.

In Chapter 5, a preliminary, new method for the visualization of low-density hydrogel scaffolds in soft tissue by means of synchrotron based PCI-CT is presented and discussed. The samples are prepared so as to mimic the environment *in vivo*. A newly developed 3D grid-pattern hydrogel scaffold is tested with the same technique.

Chapter 6 discusses the results and conclusions drawn from Chapter 2 to 5, followed by explanations for the limitations of present work and an exploration of potential future directions.

Chapter 2. Animal Model and Surgery Methods for SCI Repair

2.1. Introduction

There are three common SCI experimental models in rodents: transection, contusion and compression. Hemisection and complete transection are commonly used in animal models, although transection injuries represent only a minority of cases occurring in humans (Mahdi Sharif-Alhoseini 2014). However, transection models are much easier to evaluate the effectiveness of interventions with regard to both axonal regeneration and functional recovery. Post-operative care is hard to manage in any animal, but is easier in rodents.

Compare to the hemisection and complete transection, partial transection may be more suitable for evaluating the success of implanted tissue repair scaffolds (Straley, Foo, and Heilshorn 2010). This type of model uses cutting instruments or needle aspiration to damage a focal area in the spinal cord. Different from hemisection, this method entails less bleeding and secondary reactions. In the case of needle aspiration, the removal area can provide a cavity that is suitable for placing implants or experimental scaffolds. The investigator can control what tracts are removed or transected. In addition, targeting the removal area only on one side can leave healthy, corresponding tracts on the other side to serve as a control to assess effectiveness of the surgery and intervention.

In this project, the dorsal columns are targeted to be removed from one side of the spinal cord. The dorsal columns include the CST and the fasciculus graculis The CST are major descending tracts which, in rodents, are located principally at the ventral part of the dorsal columns of the spinal cord (Figure 2.1). They conduct motor impulse from the brain to the spinal cord. These tracts control discrete voluntary skilled movements, such as precise movement of the

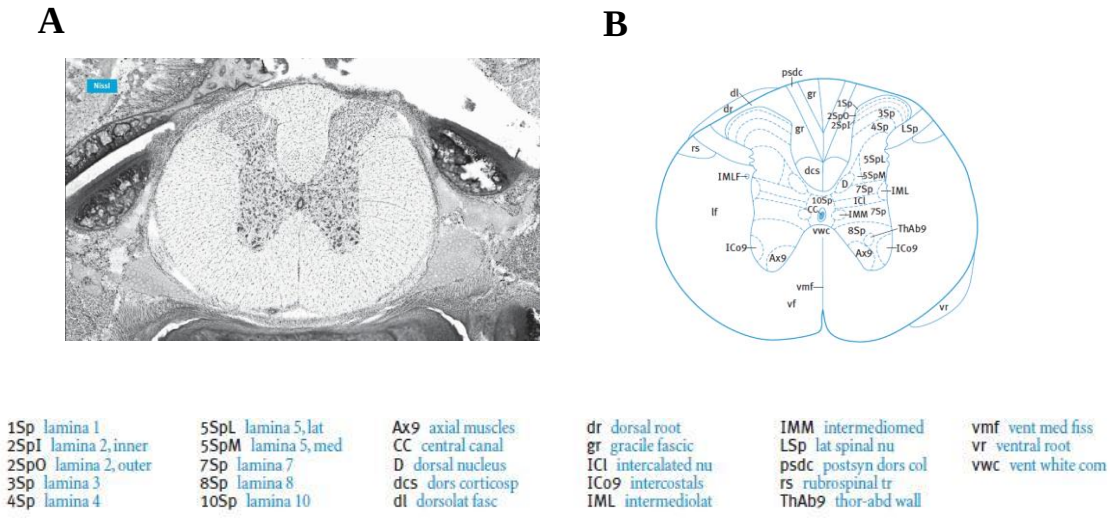

Figure 2.1. Rat T8 structure. (A) Nissl stained transverse sections from T8. (B) Detailed diagram of T8, delineating the laminae of Rexed and all other significant neuronal groupings.

paws and toes. The corticospinal tracts at T8 to T10 are specifically devoted to muscular contractions of the trunk and precise movement of the toes of the hindlimb. The fasciculus graculis is an ascending sensory tract that conveys proprioception, fine touch, and vibratory senses from the skeletal muscles to the brain. The fasciculus graculis is derived from spinal level T6 and below. The damage created at the lesion is expected to impair control of muscular coordination of the lower trunk and precise movement of toes, as well as proprioception, fine touch, and vibratory senses of the hindlimb on one side. However, these damages would not cause them to be totally paralyzed, and they would still hold the ability to walk.

In the peripheral nerve regeneration process, tissue engineering studies show evidence of successful nerve regeneration at six weeks by encapsulating isogenic bone marrow stromal cells with autograft in a 20mm nerve gap (Siemionow et al. 2011). In this project, six weeks as a reasonable time point can be adopted to monitor the central nervous axons regeneration.

2.2. Materials and Methods

2.2.1 Animals

All animals used in this study were obtained and cared for in accordance with the guidelines of the Canadian Council on Animal Care. All experimental and surgical procedures were approved by the University Committee on Animal Care and Supply (UCACS) of our local Animal Research Ethics Board (AREB).

Adult male Sprague Dawley rats were purchased from Charles River, Inc. (Wilmington, MA, USA). They weighed 250-300 grams upon arrival and were maintained in the animal facilities with a 12 hour light/dark cycle at 25 ºC, and fed rat chow with the limitation of 12-15 g per day.

2.2.2 Alginate scaffolds

Triangular prism alginate tissue scaffolds with a length of 5 mm and triangular edges of 1.2 mm x 1.2 mm x 0.6 mm were designed to be implanted in a spinal cord lesion cavity. A nylon mould was fabricated to cast these scaffolds (Figure 2.2 A-D) by the Engineering Workshop at the University of Saskatchewan.

For scaffold fabrication, animal-culture-tested alginate (Sigma-Aldrich, A2158) was purchased and sterilized by freeze dryer (Labconco Co.). To determine the suitable concentration of alginate solution to fabricate scaffolds, the alginate solution was prepared at concentrations of 2% or 4%. To achieve gelation through ionic crosslinking, the mould containing alginate scaffolds were placed in Dulbecco's Modified Eagle Medium (DMEM) with different concentrations of added calcium chloride (Sigma Aldrich, ON, CA) (Table 2.1). In preliminary studies, the cross-linked scaffolds were maintained in DMEM in 24-well plates at 37℃ to simulate an *in vivo* environment. The scaffolds were observed by microscope in order to monitor any morphological changes from day 1 to day 14. The appropriate alginate and calcium chloride concentrations were chosen that provided enough mechanical strength to maintain the shape of scaffold during the surgical implantation procedure.

2.2.3 Culture for Schwann cells

A Schwann cell line (RSC 96, CRL- 2765) was purchased from American Type Culture Collection (ATCC; Manassas, VA). Schwann cells were harvested between passage number 9 and 13 and maintained in standard DMEM supplemented with 10% fetal bovine serum (FBS, Invitrogen Co., Carlsbad, CA) supplemented with 1% antibiotics. Cells were placed into 10 cm

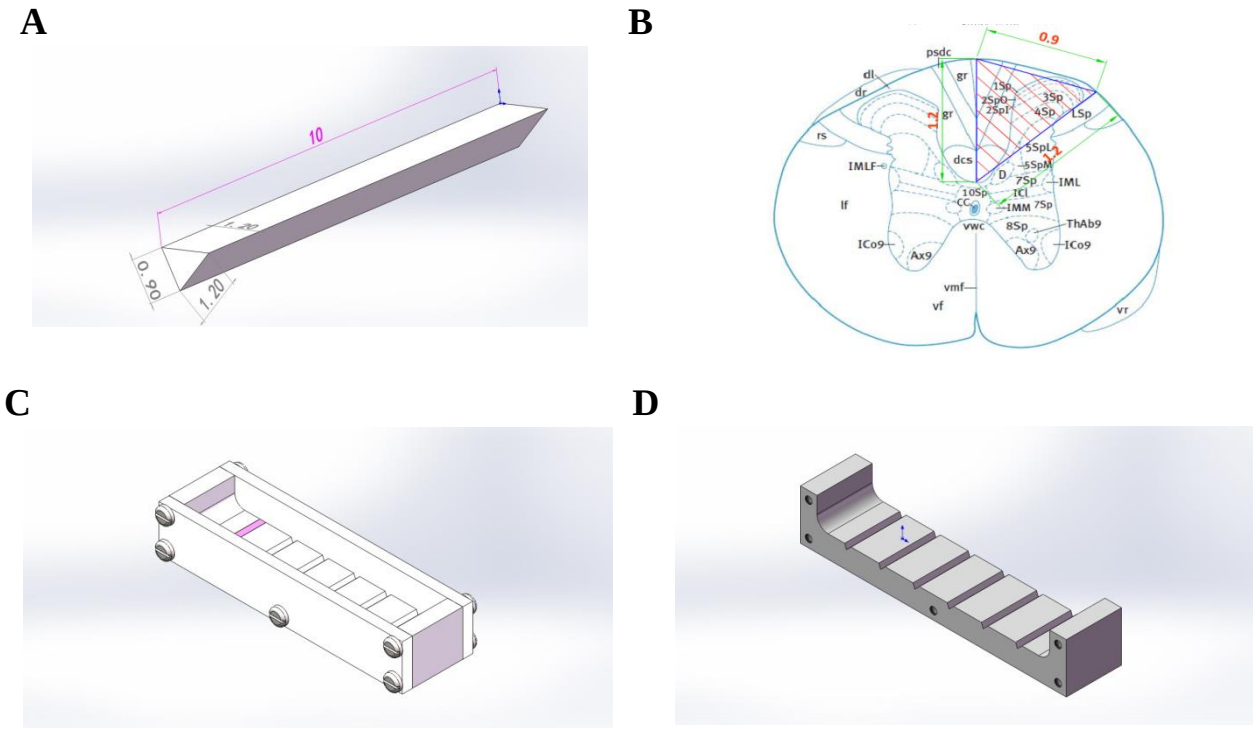

Figure 2.2. Design of scaffold shape. (A) Triangular prism alginate tissue scaffolds. (B) Excision of T8-T9 triangle area during surgery to include the gracile fasciculus and the major, dorsal CST. (C) The mould to cast the scaffolds. (D) The main part of the mould to cast the scaffolds.

tissue culture dishes (BD Falcon™, USA) at 37°C in a 5% CO_2 humidified incubator. Growth medium was changed every other day. When cell density achieved 100% confluence, cells were washed with 1 mL 0.25% trypsin containing ethylenediaminetetraacetic acid (EDTA) (Invitrogen Co., Carlsbad, CA) for 1 minute to detach the cells from the dish. Then cell suspensions were delivered into a sterile 15 mL falcon tube and centrifuged at 800 rpm for 5 minutes. The cells were counted and re-suspended with fresh medium to a density of 1.2×10^7/ml to 1.8×10^7/ml.

2.2.4 Encapsulation of Schwann cells and cell viability studies in alginate scaffolds

Our preliminary results showed that a hydrogel made from 2% alginate solution had enough mechanical strength to maintain the integrity of a scaffold for 14 days. In contrast, 4% alginate or higher concentration increases the difficulty of evenly mixing suspended cells into the alginate solution. Therefore, sterilized alginate was dissolved in DMEM to obtain 2.5% concentration alginate solution; then Schwann cells were added as a suspension (prepared as in section 2.2.3) to create a final mixture with Schwann cells at a density of 1.5 x 10^7 cells/mL in 2% alginate. The mixture was turned upside down gently to insure that Schwann cells were distributed evenly in the alginate solution. A pipette was used to dispense alginate solution containing Schwann cells into the scaffold mould immediately after mixing. Calcium chloride was dissolved into deionized water at 100 mM and was poured into the upper chamber of the mould to promote the formation of a hydrogel. Thirty minutes later, the hydrogels were rinsed three times, submerged in DMEM medium which contains 10% FBS and 1% antibiotics, and incubated at 37 ℃ in a 5% CO_2 humidified environment. The cell growth medium was refreshed every other day.

The integrity and morphology (i.e. the presence of processes) were monitored in Schwann cell cultures at days 1, 3, 5 and 7. Meanwhile, the cell viability and distribution of cells within the scaffold were assessed by staining with acetoxymethyl ester of calcein (calcein-AM; Anaspec,

Table 2.1 Numbers of scaffolds fabricated and distributed in 24-well plates.

Ca^{2+} Concentration in Medium / Concentration of Alginate Solution	Control group(DMEM)	4 mM $CaCl_2$ (DMEM+2 mM $CaCl_2$)	8 mM $CaCl_2$ (DMEM+6 mM $CaCl_2$)	16 mM $CaCl_2$ (DMEM+14 mM $CaCl_2$)
2% Alginate	3	3	3	3
4% Alginate	3	3	3	3

Table 2.2 Groups and number of animal surgeries.

Group	Number of rats		Scaffolds implanted
	First series	Second series	
S	2	2	(sham surgery)
L(-)	5	3	No scaffold
L(A)	6	3	Alginate
L(A+S)	6	4	Alginate + Schwann cells
Total	19	12	

CA, USA) which labeled the living RSC96 cells within the scaffolds. Scaffolds were washed in 10 mM hydroxyethyl piperazineethanesulfonic acid (HEPES) buffer and then submerged in HEPES containing 1 μg/ml calcein-AM for 30 minutes. Repeat washes with only HEPES buffer were done prior to the analysis of the cells. Calcein-AM penetrates into the cytosol of living cells and stains them green. The hydrogel patterns were imaged using a fluorescent microscope (Carl Zeiss Axiovert 100, Germany) equipped with the Northern Eclipse imaging module (Empix Imaging, Inc., CA). Image acquisition by stacking optical sections was done using the Northern Eclipse imaging module. Cell viability was presented as the percentage of cells that remained alive after 24 hours compared to the percentage of live cells immediately after mixing with alginate. The images of the alginate scaffold also detailed the cellular distribution.

2.2.5 Surgery procedure and postoperative care

In this study, two series of experiments of implanting scaffolds in rats were performed. In the first series, nineteen male Sprague-Dawley adult rats were used; in the second series, twelve were used with improved procedures. In each series, there were four groups: Group S (sham-operated) rats only received the laminectomy part of the surgery without damage to spinal cord tissue. Group L(-) rats received the spinal cord lesion, but did not receive a tissue repair scaffold. Group L(A) rats underwent the spinal cord lesion procedure, then a scaffolds composed of alginate alone was implanted into the lesion cavity. Group L(A+S) rats underwent the spinal cord lesion procedure, then received scaffolds composed of alginate and living Schwann cells (Table 2.2).

All experimental surgery was performed at least one week after the rats had arrived, ensuring that they were in the stable condition. To perform laminectomy surgery at the thoracic level, rats were given pre-operative analgesic with an initial injection of buprenorphine (25

ug/ml), then were anesthetized using 2% isoflurane (Baxter Corporation, Toronto ON, CA) delivered by inhalation using an anesthetic vaporizer (Medishield Products Ltd. Rexdale, ON, CA). The animals were positioned in a stereotaxic frame designed for vertebral column stabilization (Figure 2.3 A,B). Isoflurane at a concentration of 1.5-2% was delivered in 100% O_2 through a nose cone using a closed circuit at a flow rate of 1 L/min. Deep anesthesia was confirmed by pinching the hind paw with forceps and noting the absence of a withdrawal reflex.

Anesthesia administration and the entire surgical procedure were done under aseptic conditions. Body temperature was maintained using an electrically heated pad set at the 'low' setting. Care was taken to continuously monitor the breathing signs of the rat, as well as the color of the paws and eyes during the entire surgery. The skin over the spinal cord region was shaved, disinfected by wiping with chlorhexidine gluconate and 70% alcohol. Surgical instruments and drapes packs were autoclaved one day before the surgery. A glass bead sterilizer was available for re-sterilizing instruments during the surgery.

A midline incision was made using a size 21 stainless steel Paragon sterile surgical blade in the lower back. After paravertebral muscles and other subcutaneous tissues were separated and retracted, two clamps attached to the T7 and T10 spinous processes were used to immobilize the vertebral column (Fig. 2.3 C), and then a laminectomy of vertebrae T8 to T9 was performed using small rongeurs. The dura enclosing the spinal cord was slit with a microknife at the dorsal midline, avoiding any midline blood vessels. The microknife was then manipulated with the stereotaxic device to place a longitudinal cut at the dorsal midline. A sharpened stainless steel

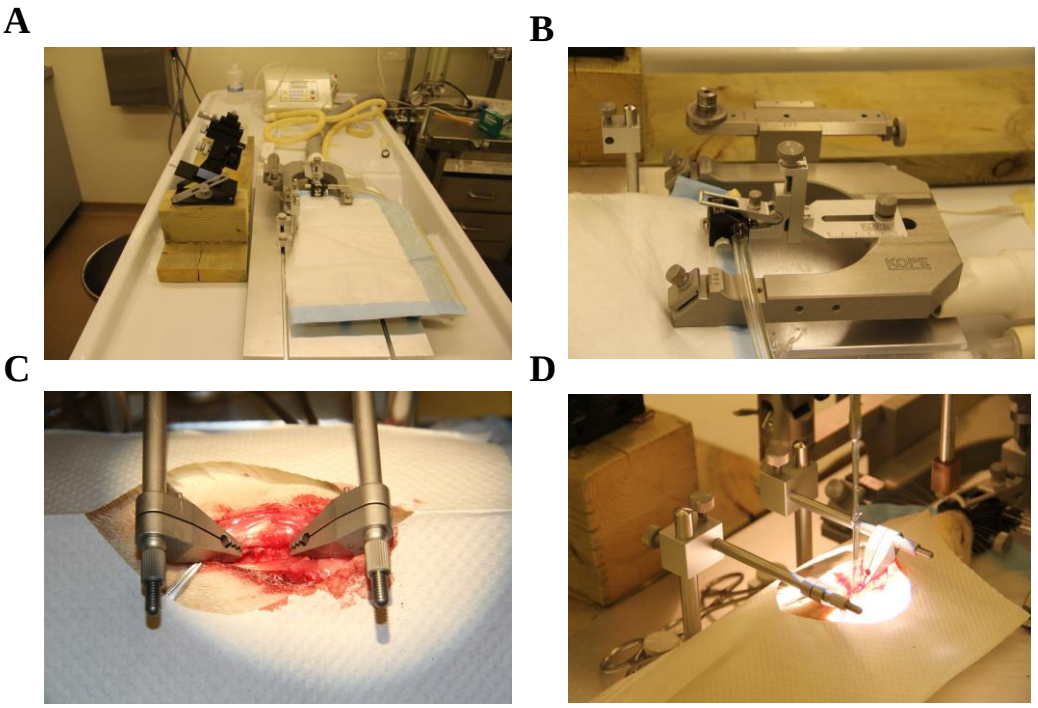

Figure 2.3. Instruments used in the surgery. (A) The stereotaxic frame with other instruments used for surgery. (B) The anesthesia delivery nose cone and scale parts of the stereotaxic frame. (C) The clamps used to immobilize the vertebral column. (D) The stereotaxically-controlled knife holder.

spatula was inserted into the midline cut to the depth of the dorsal columns to create a physical barrier between the left and right sides. (Spatula placement was eliminated in later surgeries.) The stereotaxically drive microknife was then manipulated to make a second longitudinal cut at the medial aspect of the entering dorsal rootlets (Fig.2.3 D). A steel cannula connected to a vacuum line was used to aspirate the dorsal columns on the targeted side of the spinal cord to a depth sufficient to transect the dorsal columns and the corticospinal tract (approximately 1.2 mm), along a rostrocaudal extent of 10 mm or (later) 5 mm, leaving over 75% of the transverse extent of the spinal cord intact. Bleeding was controlled with GelFoam. Group L(A) and L(A+S) rats received placement of a triangular prism alginate tissue scaffold within the lesion cavity. Group L(-) received no tissue scaffold placement. After scaffold placement, a GelFoam pad was inserted to replace bone tissue removed during the laminectomy. In later surgeries, the GelFoam pad was replaced by fibrin glue. The damaged muscle was sutured using 6.0 Viacril dissolving sutures (Ethicon Inc., Johnson and Johnson, NJ, USA). The external incision in the skin was then sutured using 4.0 silk sutures (Ethicon Inc., Johnson and Johnson, NJ, USA).

At the end of surgery, the anesthesia was discontinued and the recovery of rat was monitored. The rat was then transferred back to a clean cage. Buprenorphine analgesia was administered every 6 hours for the first 24 hours or longer if necessary. Ringer's lactate solution (3 ml) was injected subcutaneously after surgery (Teng et al. 2002, Pritchard et al. 2010). The rats were housed in a separate recovery room for 6 weeks.

2.3. Results and Discussion

2.3.1 Schwann cell incorporation into alginate scaffolds

The longevity of 2% and 4% alginate scaffolds *in vitro* was monitored for 14 days. The appropriate concentration of alginate scaffolds should have the strength to maintain the integrity of scaffold when placed into the surgical cavity, continuing for at least two weeks after implantation into the spinal cord. During the two weeks *in vitro* observation period, both 2% and 4% alginate scaffolds keep good shape. Compared to 2% alginate, 4% alginate is too dense to mix with Schwann cells evenly. Since 2% alginate gels are better for integration of added Schwann cells, 2% alginate was chosen for use in the following experiments.

Cell survival in the alginate scaffolds was measured in 2% alginate hydrogels held *in vitro*, using the calcein-AM assay. Alginate cell mixtures were crosslinked with 100 mM calcium solution for 30 mins to form hydrogels and then calcein-AM was used for imaging cells alive within the hydrogels. The results are shown in Figure 2.4. It can be observed that the survival rates were stable and slowly increased among different time points during the period of measurements. Meanwhile, there was no sign showing that cells proliferated out of the scaffold, suggesting that cell survival and proliferation occurred within the environment the scaffold provided.

2.3.2 Surgical outcomes

Two series of surgeries were performed in this study. In the first series, we attempted to create a lesion cavity in the dorsal columns of the low thoracic spinal cord with a length of 10 mm for scaffold implantation. A variety of surgical difficulties were encountered, leading to poor survival rates and surgical outcomes. These difficulties included extensive damage to paravertebral musculature and up to five vertebrae, heavy bleeding during lesion placement, and prolonged anesthesia. Three of nineteen rats in this first surgical series died during the surgical procedures, and an additional five died or were euthanized during the six-week recovery period.

Two of the eight rats that died prematurely showed significant lateral curvature of the spine and had abdominal swelling on the left side. Euthanasia was used for these unusual outcomes. (Figure 2.5).

Based on these experiences, a second series of surgeries was carried out with a number of important modifications to the surgical protocol. As a result, all twelve rats in the second surgical series survived the surgeries and lived for six weeks before planned euthanasia. Changes and improvements made in the second surgical series can be summarized as follows:

(1) Lesion design: The length of lesion cavity created in the spinal dorsal columns was shortened from 10 mm to 5 mm. This strategy required only partial laminectomy of the two vertebrae, and reduction in associated tissue damage. Furthermore, modifications and simplifications were introduced to the stereotaxic placement procedures, for example elimination of the placement of a midline barrier, which allowed the surgery to proceed more quickly.

(2) Anesthesia: A surgical assistant was tasked with continually monitoring animal physiology and depth of anesthesia. Good results were obtained with all animals by inducing anesthesia with 2% isoflurane in oxygen at 1 L/min, which was reduced after stabilization to 1.5% isoflurane at 700 ml/min, with adjustment upward to 1.75% isoflurane at 700 ml/min as necessary. Also, because of other improvements in the procedure (see above and below), the typical time under anesthesia was greatly reduced, from approximately 3 hours in the first series, to 1.5 to 2 hours in the second series.

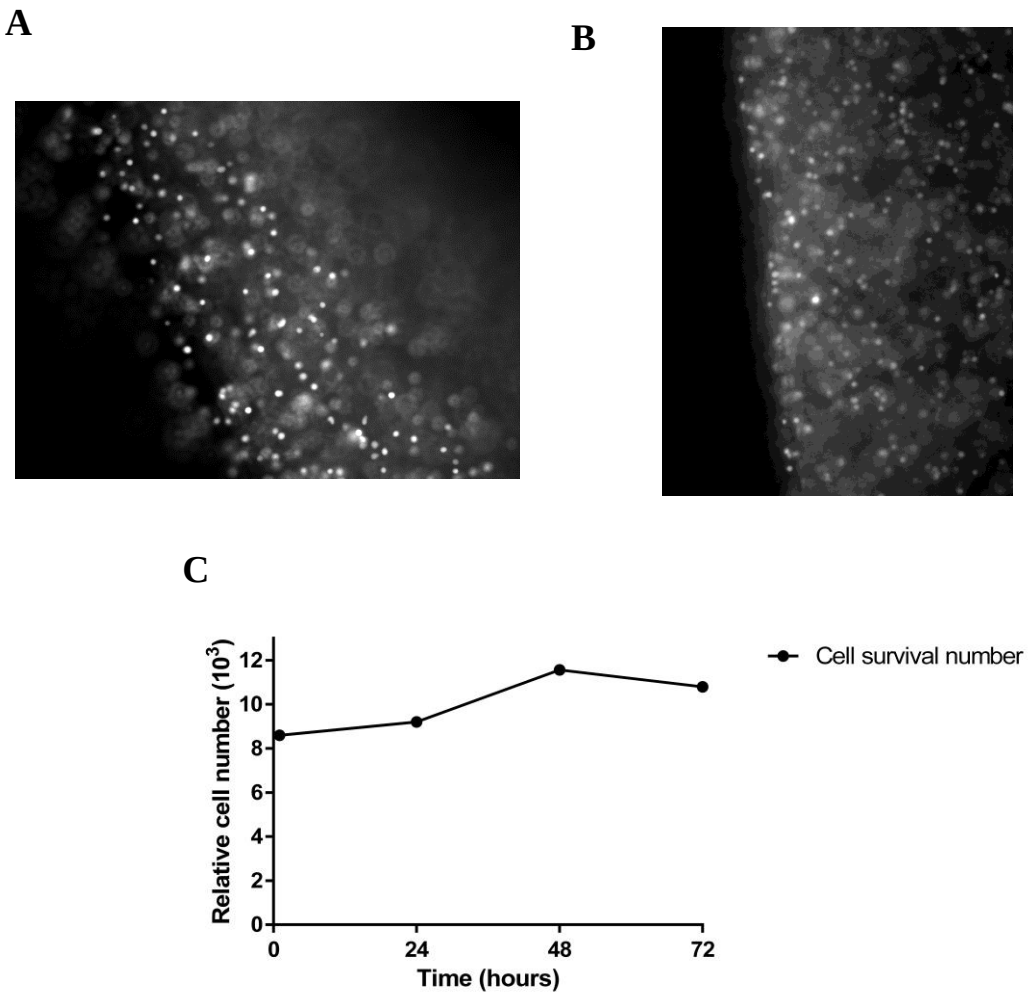

Figure 2.4. Calcein-AM staining for living Schwann cells survival in an alginate scaffold. (A) Optical imaged immediately after mixing (B) Optical imaged 24 hours after mixing. (C) Schwann cells in 2% alginate scaffold different time points.

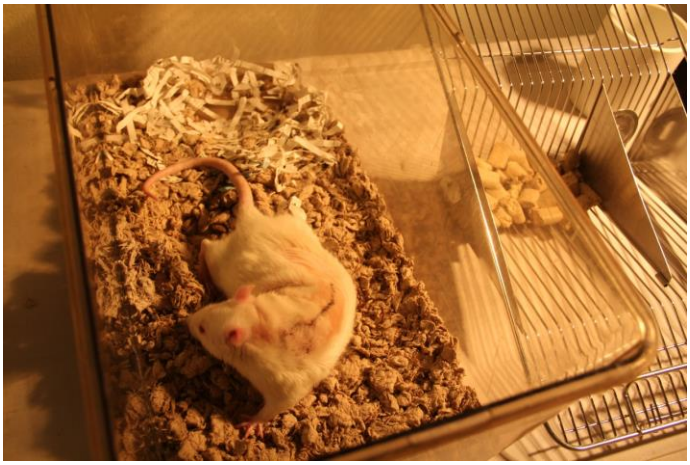

Figure 2.5. An example of poor outcome observed in post-operative care. One rat shows significant lateral curvature of the spine and had abdominal swelling on the left side.

recovery. In the second series, animals received smaller lesions. Additional improvements in the procedure to control bleeding included more care by the surgeon in avoiding blood vessels, more liberal use of GelFoam for haemostasis, and a new practice of covering the exposed spinal cord with fibrin glue.

(4) Perioperative care: Subcutaneous injections of lactated Ringer's solution immediately after surgery as a fluid replacement therapy.

(5) Weight control: Under an *ad libitum* feeding regimen the animals were gaining too much weight before and after surgery. With excessive weight gain, it was harder to control the level of anesthesia and the degree of bleeding during the surgical procedure. Weight gain may also have impaired postsurgical recovery. During the second series of surgeries we used a diet regimen of 15 g/day of rat chow, which limited weight gain to about 10 g/week. The weight control regimen appeared to contribute to better outcomes in the second series of surgeries.

(6) Wound healing: Sutures were removed at 14 days after surgery and skin repair was observed to be uniformly excellent. One rat exhibited some post surgical edema beneath the skin wound. Fluid was drained for two days, and the problem was resolved.

A general assessment of neurological function indicated that there were problems in some animals of the first surgical series indicative of excessive spinal cord damage. Postoperative observations included complete hindlimb paralysis, loss of bladder function, and severe spinal curvature, occurring in two animals of this first series.

Ideally, correct lesion placement on the left side of the spinal cord should produce partial loss of mobility in the left hindlimb, and no loss of mobility in the right hindlimb. Of the rats in

the second surgical series, eight exhibited partial loss of mobility in the left hindlimb, and no loss of mobility in the right hindlimb. One rat also has partial loss of mobility in the right hindlimb, and one rat has complete loss of mobility in the left hindlimb and partial loss of mobility in the right hindlimb. Although it appears that the lesions may have been too large in these latter two animals, they were both in good health otherwise. The healthy rats from the sham operated control group showed no loss of mobility in either hindlimb. More detailed behavioral assessment is presented in Chapter 3. All rats obtained food and water from above. No rats in the second series exhibited loss of bladder function or spinal curvature. All rats in the second series survived the full six weeks in good health, and no infection was observed.

From the outcomes of experiments, it is observed that the improvement of surgical procedures in the second series is profound as compared to the first series. As such, the surgical procedures in the second series can be used as a more improved model for the testing of other scaffolds in any future study.

Chapter 3. Behavioral Studies for SCI Repair

3.1. Introduction

Behavioral outcome from SCI can normally be considered a critical measure of both the severity of injury and the efficacy of experimental intervention. However, the connection between locomotor function and spinal cord integrity at the site of injury in an animal is not at all straightforward. Compared to human rehabilitation, rodents often display better spontaneous functional recovery of hind limb function following SCI than do humans. The validity of the behavioral measurements available for SCI animals is limited and indirect. However, there are still some tests can be done for the assessment of functional recovery in any given SCI model. These different tests can be used to evaluate either fore limb or hind limb function, or a combination of both. Some of the most commonly used scales are the Basso, Beattie and Bresnahan (BBB) open field locomotion scale (Basso, Beattie, and Bresnahan 1995), footprint analysis (Metz et al. 2000), the Tarlov open field test (Voda, Yamaji, and Gold 2005), grid walk (Merkler et al. 2001), kinematic analysis (Collazos-Castro, Lopez-Dolado, and Nieto-Sampedro 2006) and the recently developed Catwalk system (Gensel et al. 2006).

Many of the current models of SCI utilize the BBB test which is an open field locomotor test initially developed for rats to assess functional outcome. It is a simple, yet comprehensive analysis of the way rats recover from SCI. This scale evaluates the movements of the hindlimbs of the animal using a 21-point non-linear scale incorporating parameters such as joint movement, weight support, limb coordination, foot placement, and gait stability (Figure 3.1). Scores are assigned by a trained observer evaluating unrestricted locomotion on a flat surface. A score of 0 means no hindlimb movements whereas 21 means normal coordinated gait. Statistical analyses

0	No observable hindlimb (HL) movement
1	Slight movement of one or two joints, usually the hip and/or knee
2	Extensive movement of one joint or extensive movement of one joint *and* slight movement of one other joint
3	Extensive movement of two joints
4	Slight movement of all three joints of the HL
5	Slight movement of two joints *and* extensive movement of the third
6	Extensive movement of two joints *and* slight movement of the third
7	Extensive movement of all three joints of the HL
8	Sweeping with no weight support or plantar placement of the paw with no weight support
9	Plantar placement of the paw with weight support in stance only (i.e., when stationary) or occasional, frequent, or consistent weight supported dorsal stepping and no plantar stepping
10	Occasional weight supported plantar steps, no forelimb (FL)–HL coordination
11	Frequent to consistent weight supported plantar steps *and* no FL–HL coordination
12	Frequent to consistent weight supported plantar steps *and* occasional FL–HL coordination
13	Frequent to consistent weight supported plantar steps *and* frequent FL–HL coordination
14	Consistent weight supported plantar steps, consistent FL–HL coordination; *and* predominant paw position during locomotion is rotated (internally or externally) when it makes *initial contact* with the surface as well as just before it is *lifted off* at the end of stance or frequent plantar stepping, consistent FL–HL coordination, and occasional dorsal stepping
15	Consistent plantar stepping and consistent FL–HL coordination; *and* no toe clearance or occasional toe clearance during forward limb advancement; predominant paw position is parallel to the body at initial contact
16	Consistent plantar stepping and consistent FL–HL coordination during gait; *and* toe clearance occurs frequently during forward limb advancement; predominant paw position is parallel at initial contact and rotated at lift off
17	Consistent plantar stepping and consistent FL–HL coordination during gait; *and* toe clearance occurs frequently during forward limb advancement; predominant paw position is parallel at initial contact *and* lift off
18	Consistent plantar stepping and consistent FL–HL coordination during gait; *and* toe clearance occurs consistently during forward limb advancement; predominant paw position is parallel at initial contact and rotated at lift off
19	Consistent plantar stepping and consistent FL–HL coordination during gait; *and* toe clearance occurs consistently during forward limb advancement; predominant paw position is parallel at initial contact *and* lift off; and tail is down part or all of the time
20	Consistent plantar stepping and consistent coordinated gait; consistent toe clearance; predominant paw position is parallel at initial contact and lift off; tail consistently up; *and* trunk instability
21	Consistent plantar stepping and coordinated gait, consistent toe clearance, predominant paw position is parallel throughout stance, consistent trunk stability, tail consistently up

Definitions

Slight: partial joint movement through less than half the range of joint motion

Extensive: movement through more than half of the range of joint motion

Sweeping: rhythmic movement of HL in which all three joints are extended, then fully flex and extend again; animal is usually sidelying, the plantar surface of paw may or may not contact the ground; no weight support across the HL is evident

No Weight Support: no contraction of the extensor muscles of the HL during plantar placement of the paw; or no elevation of the hindquarter

Weight Support: contraction of the extensor muscles of the HL during plantar placement of the paw, or elevation of the hindquarter

Plantar Stepping: The paw is in *plantar* contact with weight support then the HL is advanced forward and *plantar* contact with weight support is reestablished

Dorsal Stepping: weight is supported through the dorsal surface of the paw at some point in the step cycle

FL–HL Coordination: for every FL step an HL step is taken and the HLs alternate

Occasional: less than or equal to half; ≤50%

Frequent: more than half but not always; 51–94%

Consistent: nearly always or always; 95–100%

Trunk Instability: lateral weight shifts that cause waddling from side to side or a partial collapse of the trunk

Figure 3.1. The 21-Point Basso, Beattie, Bresnahan Locomotor Rating Scale and Operational Definitions of Categories and Attributes (Basso, Beattie, and Bresnahan 1995).

of these scores have been attempted, but can be difficult to interpret because the scale is non-linear (Tabien 2010).

BBB scores in the range from 0 to 7 largely signify only elementary hip, knee, and ankle joint movement. Next, scores in the 8 to 13 range are based on paw placement and coordination, and scores of 14 to 21 rely heavily on paw placement, tail position, and trunk stability.

The Basso Mouse Scale (BMS) is also an analysis of hindlimb function and locomotion in an open-field and developed for mice based on the BBB scale. These two scoring methods are widely used to assess postoperative behavioral study for rat and mice models of SCI (Basso et al. 2006). The Tarlov scale is a 5-point scale only to evaluate upper and lower limb locomotion but do not reflect specific changes in motor or sensory function. Tarloy scale scores ranging from 0 (paraplegia) to 5 (normal locomotor function) are not as detailed as the BBB scale. However, they can be combined with motor evoked potential (MEP) and somatosensory evoked potential (SSEP) in muscle and nerves (Webb and Muir 2004). Footprint analysis is another good way to quantify gait coordination and placement of the feet. Kinematic analysis provides both qualitative and quantitative measurements which including the evaluation of joint and limb movements and how animals get food. It can be applied not only to thoracic level injury but also cervical spinal cord injury.

3.2. Materials and Methods

All rats in groups S, L(-), L(A) and L(A+S) in both series of surgeries were subjected to BBB behavioral tests to assess the recovery of function that is lost following a surgical lesion that disrupts the axons of gracile fasciculus and the corticospinal tract. During the BBB test rats were placed in a 150 cm x 100 cm plastic testing chamber for two minutes to make them familiar with their environment. Then the observer examined the relationship of hip, knee, and ankle joint

movement of hindlimbs and the coordination of fore and hindlimbs for five minutes. When scoring, reflections of hindlimbs caused by muscle contractions are not able to account for hindlimb movements. The animals were tested at the same time every week thereafter, until euthanasia of the rats at six weeks after surgery. The scoring sheet shown in Figure 3.1 includes categories and attributes that accompany the choice of score on the BBB Locomotor Rating Scale. Data were collected three days and six days prior to surgery, then every seventh day after surgery for the six week survival period.

3.3. Results and Discussion

All animals received a BBB score of 21 at six and three days prior to surgery (shown collectively as "pre-op" in Figure 3.2 and 3.3). The sham Group that underwent laminectomy surgery without damage to the spinal cord continued to receive consistent BBB scores of 21 during six weeks of recovery. No loss of forelimb function was observed in any animals. This suggests that the surgically placed lesions caused trauma and functional disruption at the intended spinal level. BBB scores for animals in the first surgical series that did not survive the full six weeks are excluded from the analysis.

In general, BBB scores of SCI animals initially dropped down to their lowest points when measured at one and two weeks after surgery, then slowly increased for the remaining four weeks on most rats, with incomplete recovery at the end of week six.

In the first surgical series, animals that received dorsal column lesions showed the lowest scores during the first two weeks after injury. The right hindlimb of one animal in Group L(-) was scored zero at one week, and the right hindlimb of one animal in Group L (A+S) presented zero at week two. Scores equal to 1 or 2 mean that there was no extensive movements for one of the hip, knee or ankle. Scores in this range were recorded during the first two weeks in the right

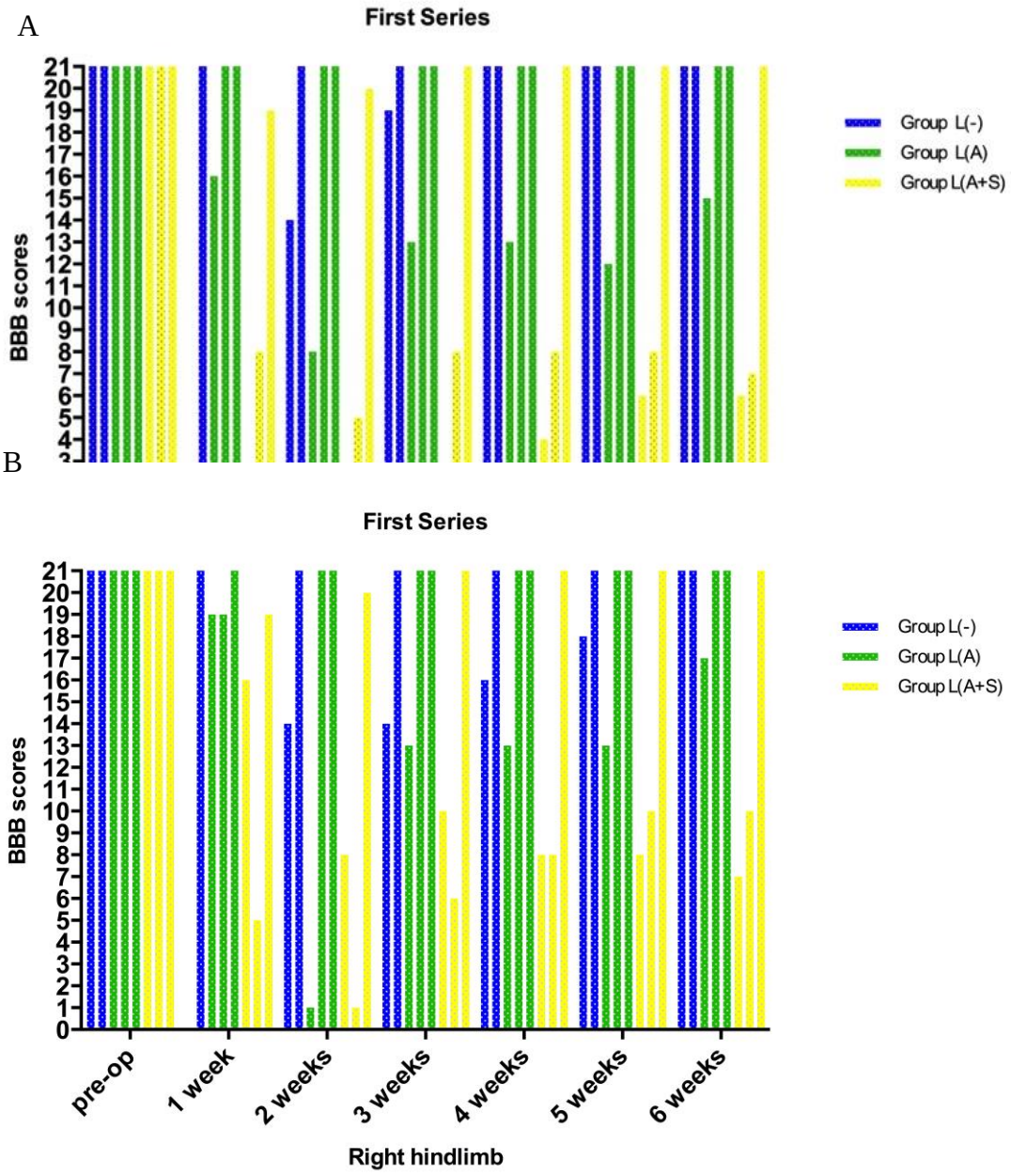

Figure 3.2. BBB scores recorded for the first series, and during six weeks post-operative survival. (A) BBB scores for first surgical series of left hindlimb. (B) BBB scores for first surgical series of right hindlimb.

A

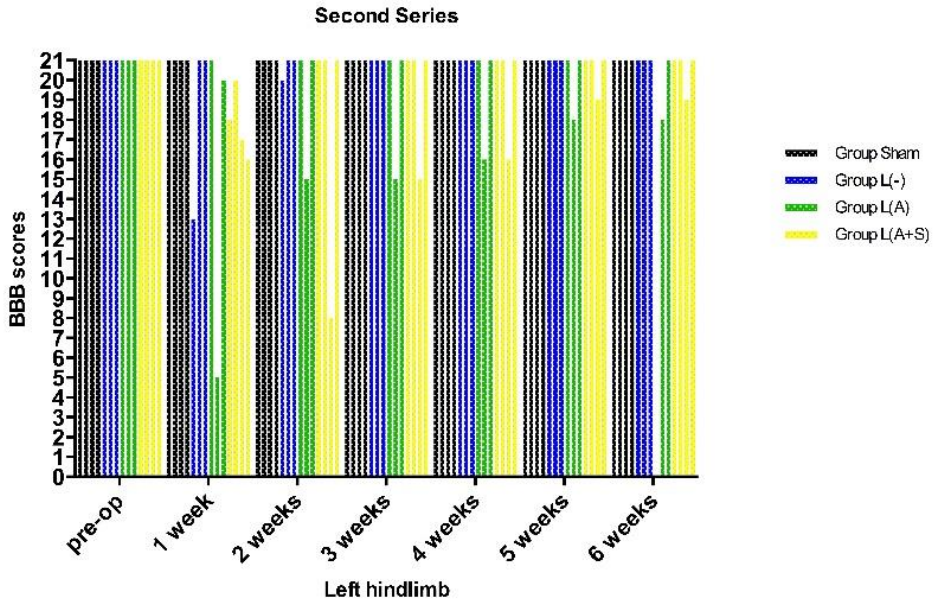

B

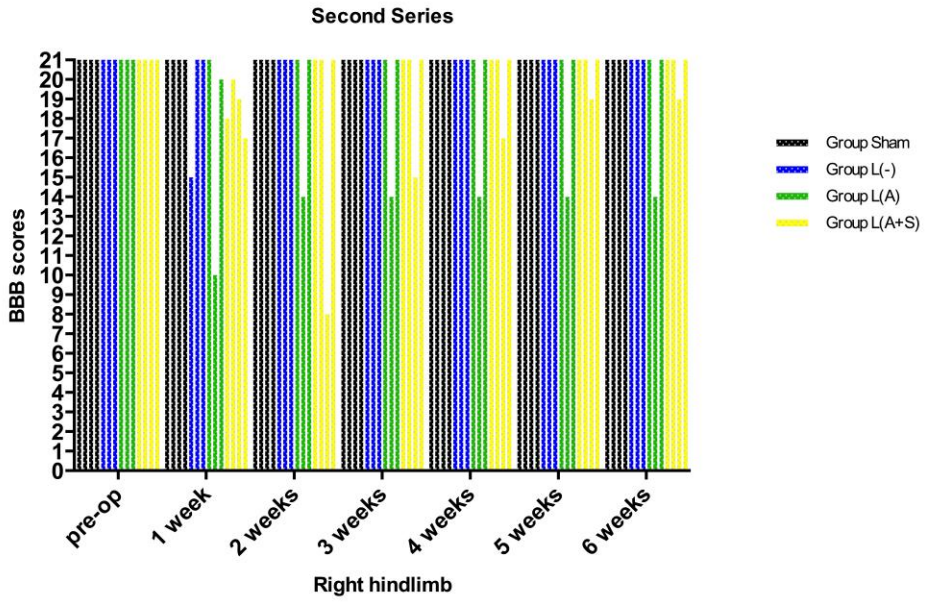

Figure 3.3. BBB scores recorded for the second series, and during six weeks post-operative survival. (A) BBB scores for second surgical series of left hindlimb. (B) BBB scores for second surgical series of right hindlimb.

hindlimb of one animal in Group L(A), both hindlimbs of one animal in Group L(-) and one animal in Group L(A+S). For all of these, BBB scores increased over the final four weeks. At the end of week six, one animal in Group L(-) reached score 21 which indicates full functional recovery. One animal in group L(A) recovered from score 0 to 18. Two animals in Group L(A+S) displayed the worst recovery progress in the first series by not exceeding a score of 10 after six weeks.

Although overall recovery trends were similar for both surgical series, generally better results were observed in the second series than in the first. In the second series, only scores from one animal of group L(A) and one animal of group L(A+S) dropped down between 5 to 10 in the first two weeks (Figure. 3.3). The other animals displayed less severe functional deficit in the first week and their BBB scores recovered to 21 during the following five weeks. One animal of group L(A) had slowly increased scores in the right hindlimb but not the left hindlimb. One animal of group L(A+S) reached a score of 19 at the end of week six from an initial score of 8 (Fig. 3.2). The somewhat better outcomes of animals in the second series is likely related to the improvement in surgical technique.

We did not expect to see significant contralateral behavioral deficits in Groups L(-), L(A) and L(A+S) that entailed unilateral placement of a lesion in the dorsal columns. If spinal cord damage had been completely confined to the intended site in the left dorsal columns, unilateral destruction of the left CST should only have disrupted motor function of the left hindlimb. (Similarly, destruction of the left gracile fasciculus should only have affected sensory function in the left hindlimb. Sensory function was not studied directly, but sensory impairment may contribute to altered motor behavior.) For animals in both surgical series, the BBB scores of left

hindlimbs showed consistency with scores of right hindlimbs in individual animals. For example, one animal in Group L(A+S) presented only slightly decreased scores in both the right and left hindlimbs during the post-surgical period.

Behavioral outcomes measured by the BBB test appeared to be influenced by scaffold implantation. In the first series, BBB scores of Group L(A+S) were lower than the other three groups. Two out of three animals of Group L(A+S) got the lowest scores during the recovery process. One animal each in Groups L(-) and L(A) received lower scores. However, in the second series, Group L(A+S) animals ultimately achieved similar BBB scores on the left side, and higher BBB scores on the right side, compared to Group L(A). No BBB scores lower than 15 were recorded after two weeks in Group L(A) animals. Due to the improvement in surgical technique, it is likely that the BBB scores observed in the second series of surgeries are more reliable. Therefore, compared to Group L(-), alginate scaffolds may not help improved locomotion recovery as measured by BBB scores. However, Group L(A+S) had better results than Group L(A) which suggests that inclusion of Schwann cells within the scaffold gel may help reverse the detrimental factors associated with the use of an alginate scaffold alone.

An important consideration in explaining the severity of the initial functional deficit, especially its bilateral pattern, is the accuracy of lesion placement during surgery. The left dorsal column was the target for removal from the spinal cord. If initial damage was restricted to the left side of the spinal cord, the BBB scores of right hindlimb should have remained high. Initial functional impairment on the right side might have occurred because the lesion unintentionally extended across the midline to involve the right CST. When the laminectomy was completed in the first surgical series, the dura and dorsal spinal cord were slit at the dorsal midline. Then, a specially designed spatula was inserted into the incision we made in the dorsal midline to protect

the right side while the left dorsal columns were aspirated. Nevertheless, the insertion of the spatula itself might have caused bilateral damage, or the spatula might have moved and compressed the right side CST when the suction was applied at the intended site. We terminated using the spatula as a bulkhead in the second surgical series, but the BBB scores of right hindlimb remained almost the same as the left, indicating that this change in surgical procedure did not solve the problem of bilateral functional deficit.

Postsurgical spinal shock (Ditunno et al. 2004) is another mechanism that could also contribute to transient impairment of spinal cord function outside the intended lesion area. Spinal shock caused by acute SCI is due to direct insult on cells, ischemia and vasospasm. It normally lasts days to weeks but is still a transient process. Decreased reflexes, loss of sensation as well as flaccid paralysis will appear at the first stage of spinal shock. Below the level of SCI, voluntary and reflex neurologic activity may absent or reduced due to supraspinal excitation deficits, missing plateau potentials, metabolic inhibition, or other factors. However, spinal shock is a reversible process such that the reflex gradually returns after areflexia/hyporeflexia. Increased positive neuron receptor function, immune cells response and synapse growth will each help to reduce the spinal shock symptoms after the acute phase.

A third biological mechanism that may contribute to an unexpectedly severe behavioral outcome is secondary injury (Mortazavi et al. 2015). There are multiple mechanisms of secondary injury that have been well explained in the past decades (Oyinbo 2011). Local invasion of inflammatory cells such as macrophages and microglia cells are considered prominent on inducing secondary injury and triggering a neuroprotection reaction. Besides that, local vasospasm can contribute to ischemia. Secondary injury can also be due to spreading mechanisms such as ischemia, glial scar, apoptosis, excitotoxicity and oxidative stress. Direct,

postmortem examination of the final extent of lesion severity in our SCI animals is reported in Chapter 4.

Some functional recovery was seen in the final four weeks in virtually all animals (Figure 3.2 and 3.3). In many cases, BBB scores returned to 21 in both hindlimbs. The purpose of this study was to establish an animal model that can be used to test how artificial tissue repair scaffolds might foster regenerative axon growth that would lead to re-establishment of synaptic connections and functional recovery. However, mechanisms other than regenerative axon growth might operate to improve functional outcome. These include resolution of spinal shock, remyelination of spared (but temporarily demyelinated) axons, sprouting of intact axons, and functional re-organization of undamaged spinal cord. Our direct, postmortem examination of axon regeneration, reported in Chapter 4, suggests that non-regenerative mechanisms were responsible for functional improvement after SCI in this study.

Chapter 4. Histology and Immunohistochemical Analysis of SCI Repair

4.1. Introduction

A thorough model for animal studies of SCI should include a histological staining technique to visualize the extent of spinal cord damage and examine any anatomical evidence of axon recovery or regeneration following injury. There are many different types of nerve tissue staining. The cresyl violet stain is a standard and widely used staining techniques for nervous tissue. To ascertain the basic structure of normal spinal cord and amount of damage caused by SCI, this method can identify neurons, or demonstrate the loss of Nissl substances in tissue sections. Cresyl violet dye is able to bind strongly to Nissl substance in the cytoplasm of neurons, which is RNA in the neuron's rough endoplasmic reticulum. The larger stained blue cells are neurons which are mainly distributed among grey matter in CNS. Nissl substances are lost after spinal cord injury and thus can be used to assess severity of spinal cord injury. Cresyl violet also identifies small glial cells, located both in the grey and white matter of the spinal cord.

Immunohistochemistry is a more specific technique that allows visualization of the distribution of individual proteins. This technique can thus provide more insightful analysis of cellular changes that occur after injury. Five different monoclonal antibodies were employed for immunohistochemical analysis in this study. ED-1 monoclonal antibody is a cellular marker which specifically recognizes a cytoplasmic antigen in activated microglia/macrophages in rats (Dijkstra et al. 1985). ED-1 positive staining indicates that the immune system is activated when there are lesions in the CNS (Jacobowitz et al. 2012) and that active phagocytosis of cellular debris is occurring. The glial fibrillary acidic protein (GFAP) monoclonal antibody recognizes a major protein found exclusively in the cytoskeleton of fibrous and protoplasmic astrocytes (Eng

1985). It is therefore useful for detecting hypertrophy and proliferation of astrocytes as part of glial scar formation. Neurofilaments (NF) are major elements of the neuronal cytoskeleton, and are widely distributed in the neuron cytoplasm, dendrites, and large diameter axons (Anderton et al. 1982). The nature of NF makes them an excellent marker to evaluate the loss of neurons and large axons after SCI. Growth-associated protein 43 (GAP-43) is found in developing and regenerating axons, particularly the axonal growth cones, (Fitzgerald, Reynolds, and Benowitz 1991) and can therefore serve to mark regenerating axons in adult spinal cord tissue. The gamma isoform of protein kinase C (PKC γ) has a very limited distribution in the rat spinal cord. PKC γ antibody can show the accurate position of CST axons in the rat spinal cord (Lu et al. 2005). The use of these several immunohistochemical markers for post-mortem analysis of spinal cord tissue following injury can thus provide more specific information about tissue organization than can be obtained using standard histological stains such as cresyl violet.

4.2. Materials and Methods

4.2.1 Transcardial perfusion

Six weeks after SCI surgery, an intraperitoneal injection of Euthanyl (65 mg/kg) was used to induce deep, terminal anesthesia in all rats. An incision was made at the ventral midline, exposing the thoracic and abdominal regions. The abdominal cavity was opened, the diaphragm was cut transversely from below, the ribs were cut and the thoracic cage was reflected rostrally. After exposure of the heart, a pair of forceps was used to hold the heart and a perfusion needle was immediately inserted through the left ventricle until it could be seen within the transparent aorta. The right atrium was quickly cut to allow blood efflux. 150 ml 10 mM PBS was pumped through the cannula within the aorta to flush the blood away through the animal. Then, 150 ml of

4% paraformaldehyde (PF) in phosphate buffer was delivered through the same route to fix all tissues in the animal. The thoracic spinal cord including the scaffold implanted was carefully removed, post-fixed in 4% PF for 24 hours, then cryoprotected in 20 % sucrose for 48 hours at 4℃. Each of the spinal cord tissue samples obtained was cut into three parts: the injury site (T7-T9), the part above injury (T4-T6), and the part below injury (T10-T13). Each part was 10 mm in length (Figure 4.1). The tissues were then put in disposable vinyl cryomolds embedded in Tissue-Tek optimal cutting temperature (O.C.T., SAKURA; Japan) compound and kept frozen at -80℃. Transverse histological sections were obtained from the bundled spinal segments of each animal, beginning at the rostral side, with a thickness of 10 µm, using a cryostat (Thermo Scientific MICROM HM550, ON). Sections were collected on Superfrost Plus™ microscope slides (Fisher, USA; 12-550-15) and air dried. Alternating sections from each animal were used for the cresyl violet staining and immunohistochemistry.

4.2.2 Cresyl violet histology staining

Sections mounted on slides were stained with 0.5% cresyl violet for two minutes. The slides were then rinsed in distilled water for one minute and dehydrated through ascending concentrations of ethanol from 50%, 70%, 90%, 95% and two 100%. Then the sections were fixed in two changes of 100% xylenes and coverslip in Permount (Fisher, SP15-500; USA). They were observed under a light microscope (Olympus Corporation BX53F; Japan).

A B

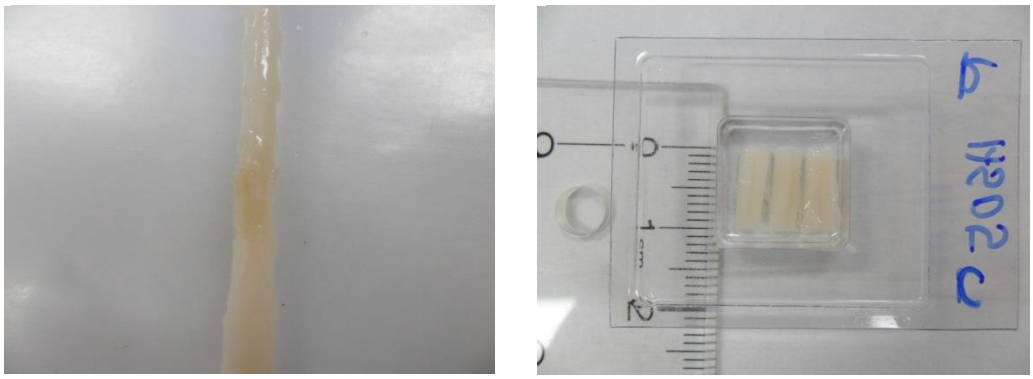

Figure 4.1 Spinal cord sample preparation for histology and immunohistochemistry. (A) Injured spinal cord with scaffold dissected from animal. (B) Tissues coated with Tissue-Tek O.C.T. compound in disposable vinyl cryomolds before freezing.

4.2.3 Measurement of lesion area

The spinal level of each animal that contained maximal damage was measured by computerized planimetry. Cresyl violet stained sections were observed at a magnification of 40x. Measurements were made using the Adobe Photoshop CS6 and the data were expressed as pixels. Traces of the circumferences of the Group S (sham operated) spinal cords were used to calculate the mean cross-sectional area of the undamaged spinal cord. Similarly, the area of remaining intact tissue was traced and measured in damaged spinal cord of Groups L(-), L(A) and L(A+S) animals. The difference between each lesioned animal and the mean of sham-operated animals was used to estimate lesion area. Differences in the lesion area (± SEM) were compared among the groups using a repeated measures one way ANOVA followed by individual Student Newman-Keuls comparisons for statistical significance ($p<0.05$).

4.2.4 Immunohistochemistry

Transverse tissue sections were prepared from spinal cord at, above and below the lesion site using a cryostat and 10 µm sections were collected on Superfrost Plus™ microscope slides. The sections were blocked against non-specific antibody binding in 2% horse serum (Vector Laboratories, Burlingame CA; S2000), 0.5% bovine serum albumin (BSA, Sigma-Aldrich, St. Louis, MO; A9647) in 0.1M PBS for one hour at room temperature. Then the slides were incubated in one of five primary antibodies, respectively (Table 3), diluted in blocking solution overnight at 4 ℃. On the next day, tissue sections were washed three times for five minutes in PBS, and then incubated with secondary antibodies, either AlexaFluor 488 anti-mouse (1:200; Mol. Probes, ON, A11017) or AlexaFluor 555 anti-rabbit (1:200; Life Technologies Inc., A21430). All secondary antibody solutions also included DAPI (1:10,000, 100 µg/ml, Life Technologies Inc., D1306) to label cell nuclei. After two hours, sections were again washed three

Table 4.1. Antibodies for immunohistochemistry studies

Primary Antibody	Supplier /Cat.No.	Host Species	Dilution Factor	Cellular Target
Anti-ED1	AbD serotec /MCA341GA	Mouse	1:200	Macrophages/microglia
Anti-GFAP	Cell Signaling /#3670	Mouse	1:300	Astrocytes
Anti-neurofilament (NF)	Sigma /N5139	Mouse	1:400	All axons
Anti-GAP-43	Millipore /MAB347	Mouse	1:500	Axons and growth cones undergoing regeneration
Anti-PKCγ	Santa Cruz /sc-211	Rabbit	1:250	Corticospinal axons (and substantia gelatinosa)

times for five minutes in PBS. Finally, the slides were coverslipped using Citifluor AF1 (VWR, USA;100496-530) and observed and photographed under a fluorescence microscope (Olympus Corporation BX53F, Japan). Images were taken from three different locations: T6, T9 (lesion site) and T13. Captured electronic images were analyzed using the CellSens Dimension software (Olympus Fluorescence, Japan).

4.3. Results and Discussion

4.3.1 Histology image analysis

In the present study, the neurons in the gray matter can be observed in the spinal cord after the cresyl violet staining (Figure 4.2). Surrounding white matter contains only small glial cells. The black lines in Figure 4.2 (A) enclose the cross-section of the left dorsal columns targeted for lesion (T9), and corresponding areas above (T6) and below (T13) the lesion target. Sham (Group S) represent a healthy spinal cord without any damage (Fig. 4.2 A1-A3).

At the surgery sites of groups which received partial spinal cord lesions (Groups L(-), L(A) and L(A+S)), all of groups featured different severities of spinal cord damage (Fig. 4.2 B2-D2). Representative samples are shown. In all cases, the left dorsal columns appeared to be entirely destroyed at the lesion site. No trace of the alginate implant was seen at the lesions sites six weeks following surgery. Unexpectedly, damage to the spinal cord typically occurred well beyond the lesion site. In almost all animals, the left dorsal horn was also destroyed. Further areas of severe damage could also extend to include the lateral columns of the white matter on the left side, more ventral regions of grey matter on the left side, and some dorsal grey and white matter structures on the right side. It thus appears that our efforts to carefully target the lesion were unsuccessful.

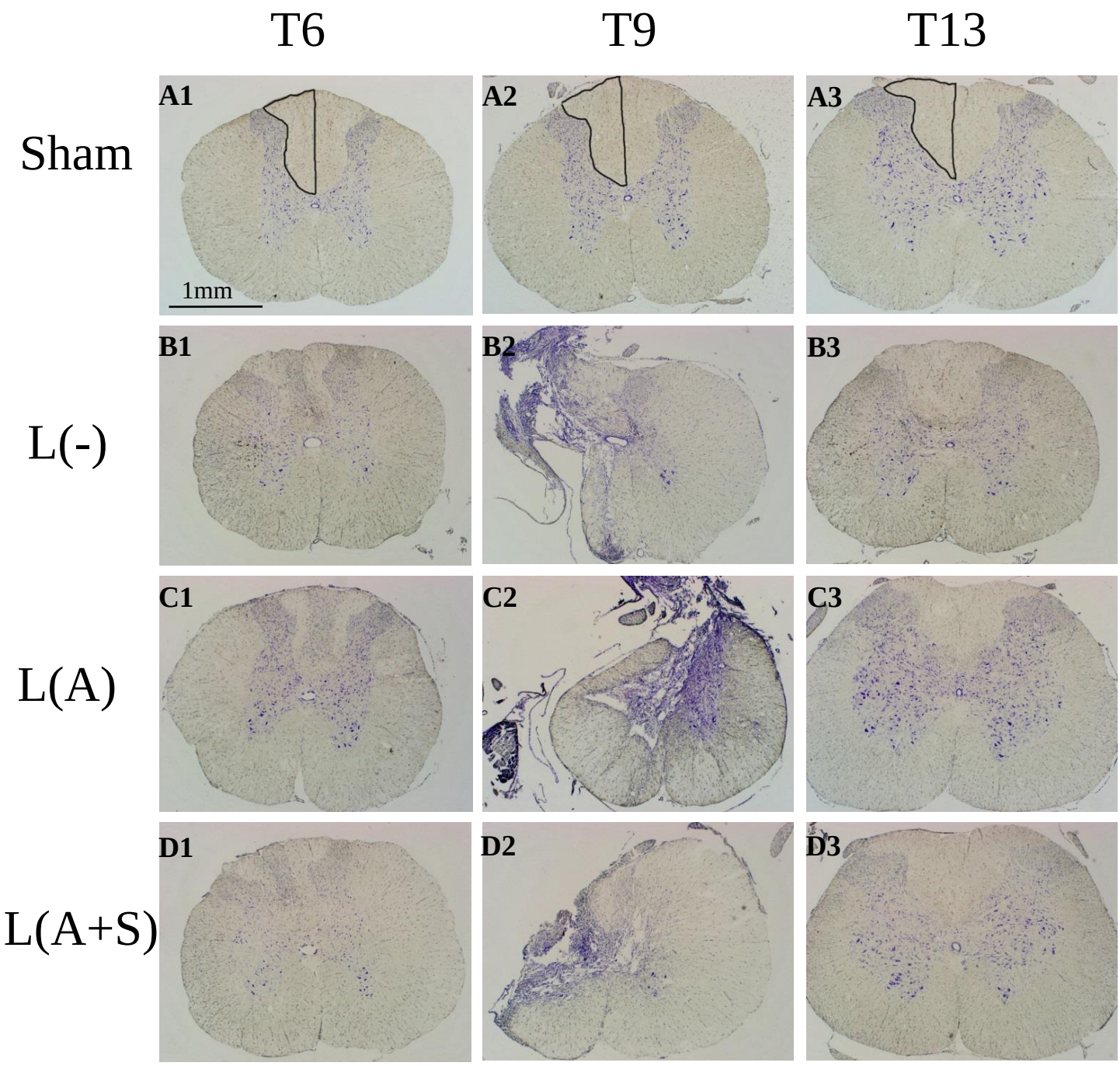

Figure 4.2. Photomicrographs of representative cresyl violet stained tissue sections. (A) Sham-operated Group S. (B) SCI without scaffold Group L(-). (C) SCI with alginate scaffold Group L(A). (D) SCI with alginate scaffold containing Schwann cells Group L(A+S). T6 (A1-D1) sections are taken above the surgery lesion site. T9 (A2-D2) sections are taken at the surgery lesion site. T13 (A3-D3) sections are taken below the surgery lesion site.

In contrast, spinal cord tissue appeared to remain remarkably intact at spinal cord levels T6 and T13, approximately 10 mm above and below the lesions, respectively. No overt sign of secondary injury elongated to these levels. All surgical groups displayed well organized white matter, normal round, well-stained neurons and compact neuropil, which are typical characteristic of healthy tissue. No disruption or morphological changes are shown at the T6 or T13 levels.

Healthy areas of spinal cords of both sham and experimental groups were measured. The average area of spinal cord cross section at T9 from sham group animals was treated as baseline (100%). The percent of uninjured spinal cord of the experimental group was evaluated in comparison to the mean of all animals from the sham group. The lesion area percent was calculated by subtracting the percent of healthy areas from 100%. The lesion area includes both the damaged and atrophic area. From Figure 4.3, it is seen that each group has similar lesion sizes. The percents of mean lesion area (% ± SEM) are 58.10% ± 9.996%, 48.55% ± 8.293%, 45.03% ± 7.883% for Groups L(A), L(A+S), and L(-), respectively. The L(A) group had the highest calculated percentage lesion area, while the L(-) has the lowest calculated percentage lesion area. One way ANOVA suggested that the apparent differences among three groups are not statistically significant.

4.3.2 Immunofluorescence image analysis

Immonohistology allows us to examine the fate of particular cellular elements within the spinal cord following targeted unilateral destruction of the dorsal columns. At the T9 level, this includes ascending sensory axons of the gracile fasciculus. The CST consists of three bilateral components. The great majority of CST axons are located in the ventral part of the dorsal columns, but minor components are also found in the dorsal aspect of the lateral columns, and

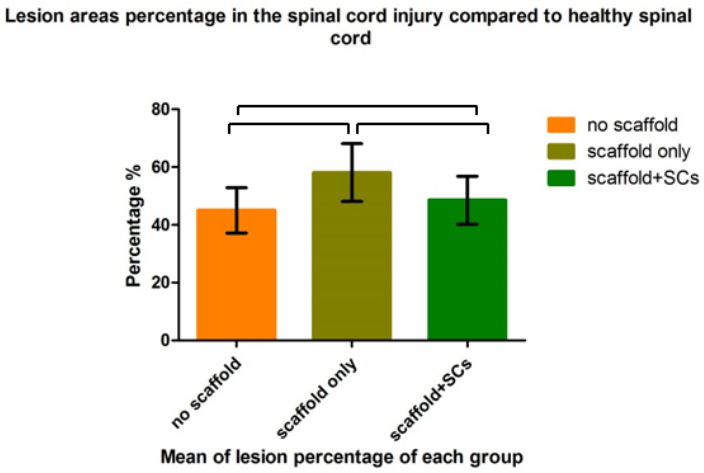

Figure 4.3. Graph of the mean lesion area (% ± SEM) for cresyl violet stained sections at T9.

the medial aspect of the ventral columns (Benowitz and Popovich 2011). In this project, by immunohistochemistry, the outgrowth and regenerative response of lesioned gracile fasciculus axons and CST axons in the dorsal and main component of the CST were examined. The physiological changes were evaluated by analyzing the responses of macrophages/microglia (ED-1) and astrocytes (GFAP), the survival of neurons and large axons (NF), any appearance of newly growing axons (GAP-43) and the particular fate of axons of the CST (PKC γ).

4.3.2.1 ED-1 image results

Inflammation plays an essential role in CNS injury and axon regeneration. Resident, activated microglia and invading macrophages are inflammatory cells that can be marked by ED-1 monoclonal antibody in rats. Figure 4.4 (A1-A3) shows an undamaged spinal cord without any ED-1 staining in Group S. In contrast, a great number of ED-1 positive microglial and macrophage cells were observed in the cavity and graft area in spinal cord lesion Groups L(-), L(A) and L(A+S). At the surgery site (T9), microglia/macrophages were also distribute more broadly. Although there was animal to animal variation, microglia/macrophages were typically found throughout white and grey matter of the left spinal cord and partially within the right grey matter all groups (Fig.4.4 B2, C2, D2). ED-1 positive microglia/macrophages were also seen at spinal cord levels above and below the surgery site in experimental Groups L(-), L(A) and L(A+S) but not Group S. Microglia/macrophages at these levels were found principally in white matter, and absent from grey matter. In T6 cross section of corresponding spinal cords, the level above the surgery site (Fig. 4.4 B1, C1, D1), most of ED-1 positive cells are distributed in the left lateral and dorsal columns. In particular, there was a striking concentration of ED-1 positive cells in the left gracile fasciculus. This corresponds to the fact that ascending left gracile fasciculus axons were targeted for surgical destruction at T9, and are expected to be degenerating

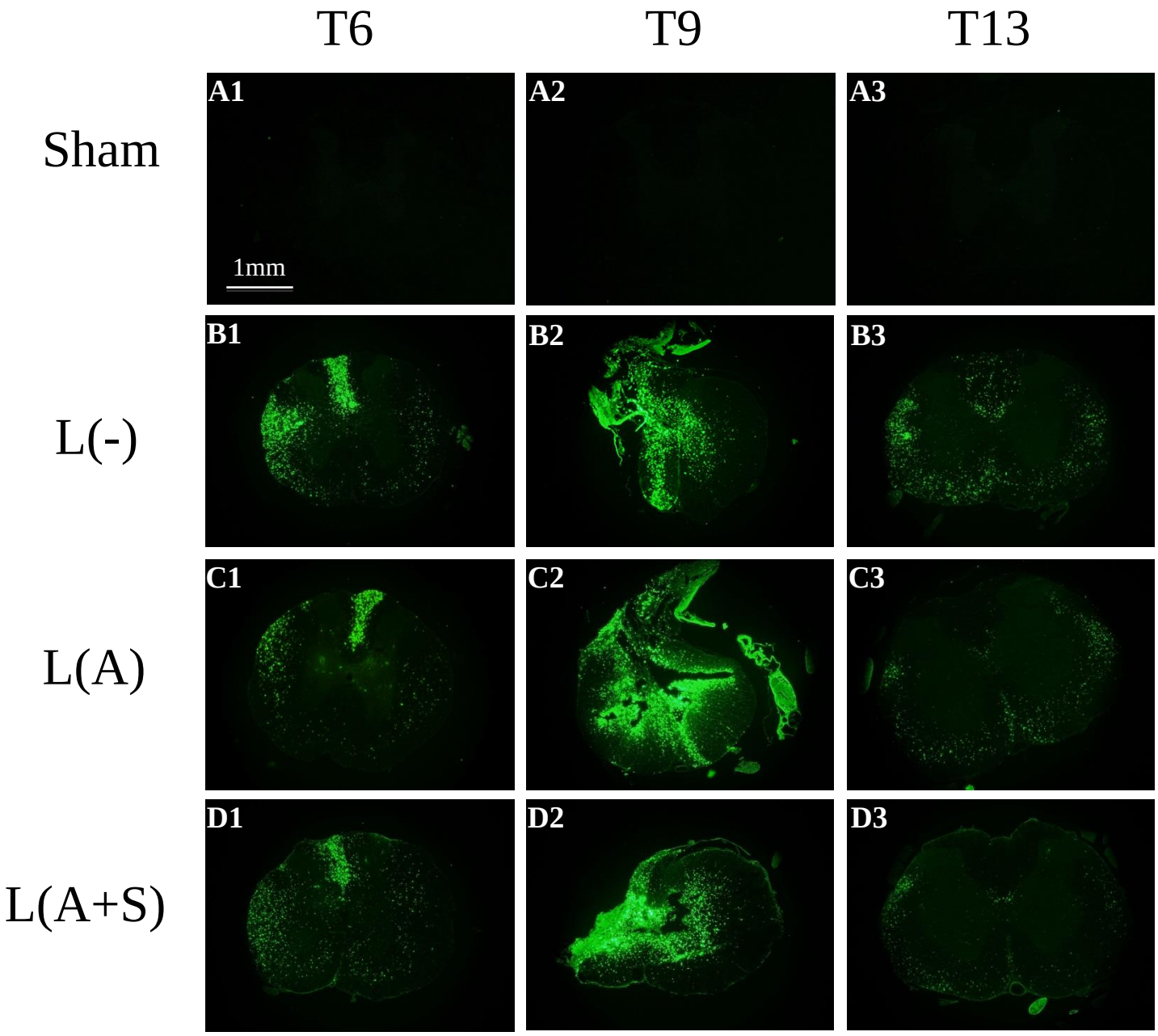

Figure 4.4. Immunofluorescent photomicrographs of macrophages staining by ED-1 antibody. (A) Sham-operated Group S. (B) SCI without scaffold Group L(-). (C) SCI with alginate scaffold Group L(A). (D) SCI with alginate scaffold containing Schwann cells Group L(A+S). T6 (A1-D1) is above the surgery lesion part. T9 (A2-D2) is the surgery lesion in the experimental groups. T13 (A3-D3) is below the surgery lesion part.

at T6. The morphological integrity of spinal cord was not disrupted at the T6 level, indicating that ED-1 positive cells in other white matter regions were present in relatively healthy tissue.

In T13 cross sections, the level below the site of surgery (Fig.4.4 B3, C3, D3), Groups L(-), L(A) and L(A+S) also showed some ED-1 positive cells distribute in white matter (but not grey matter) on both sides. The number of ED-1 positive cells was generally lower at T13 compared to T6. Again, there was no major tissue disruption at this level. Interestingly, there was no major concentration of ED-1 positive cells in the left gracile fasciculus at T13, presumable because this is an ascending tract, and gracile fasciculus axons present at this level would be uninjured, or injured only distally, and would not be expected to be degenerating. However, there did appear to be a small cluster of microglia macrophages on both sides of the dorsal columns corresponding to the bilateral position of the CST. As the CST is a descending tract, this area of ED-1 immunoreactivity may correspond to distally degenerating CST axons.

4.3.2.2 GFAP image results

Astrocytes are a type of glia cell that participate many essential activities in the normal CNS. GFAP is a hallmark protein that is often used to visualize the distribution of astrocytes. A normal distribution of astrocytes in grey and white matter was seen with anti-GFAP immunohistochemistry in Group S animals (Figure 4.5 A1, A2, A3). Immunoreactivity was seen in grey and white matter, and was particularly prominent at the glia limitans at the outer margins of the spinal cord.

Reactive astrocytes contribute to the formation of glial scar following CNS injury. Our results from SCI groups L(-), L(A) and L(A+S) (Figure 4.5 B2, C2, D2) revealed that GFAP expression density sometimes increased at the margins of the surgery sites, suggesting the formation of a glial scar. Little increase in GFAP immunoreactivity was seen in other,

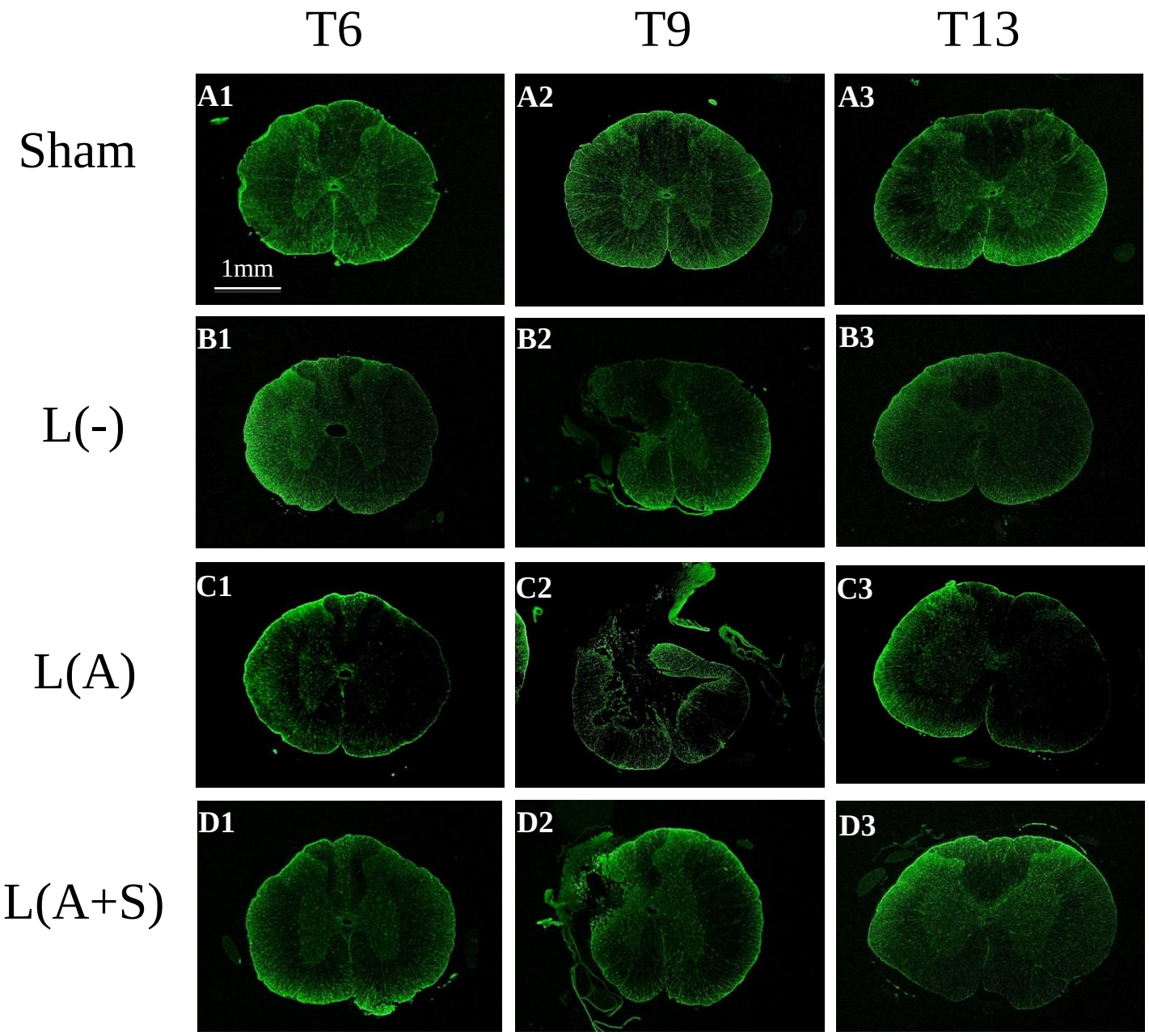

Figure.4.5. Immunofluorescent photomicrographs of macrophages staining by GFAP antibody. (A) Sham-operated Group S. (B) SCI without scaffold Group L(-). (C) SCI with alginate scaffold Group L(A). (D) SCI with alginate scaffold containing Schwann cells Group L(A+S). T6 (A1-D1) is above the surgery lesion part. T9 (A2-D2) is the surgery lesion in the experimental groups. T13 (A3-D3) is below the surgery lesion part.

undamaged areas of the spinal cord, and in some animals GFAP actually decreased in surviving white matter.

At the T6 level above the surgery sites (Figure 4.5 B1, C1, D1) a greater number of GFAP positive astrocytes was seen in the left side of the dorsal columns compared to the contralateral or sham operated spinal cord. This uneven distribution of GFAP on left and right sides demonstrates that glial scar formation may occur in the left side of dorsal columns containing degenerating gracile fasciculus axons. The assembling glial cells in this area correspond with increased ED-1 immunoreactivity in the same place. No such increase in GFAP is seen at the T13 level below the site of surgical lesions in Groups L(-), L(A) and L(A+S). Indeed, there appeared to be a generalized decrease in astrocytes in some animals (Figure 4.5).

4.3.2.3 NF200 image results

NF proteins exist in neuron cell bodies and all large diameter axons in the spinal cord, as a part of the cytoskeletal network. RT97 is one specific epitope of 200 KDa neurofilament protein expressed in rats. In Group S uninjured spinal cords NF shows higher expression in white matter than in grey matter, with the exception that the CST shows low NF immunoreactivity. NF proteins were virtually absent in the substantia gelatinosa of the dorsal horn. At the T9 level of surgical lesion, NF expression remained strong in all surviving areas of the white matter and remaining grey matter in Groups L(-), L(A) and L(A+S).

At spinal levels T6 and T13, above and below the surgery site, respectively, the expression of NF in experimental Groups L(-), L(A) and L(A+S) remained the same in most areas of the white and grey matter. However, the position normally occupied by the gracile fasciculus at T6 became devoid of NF immunoreactivity on one (Figure 4.6 B1, D1) or both (Figure 4.6 C1) sides. These results confirm that targeted gracile fasciculus axons have degenerated above the lesion.

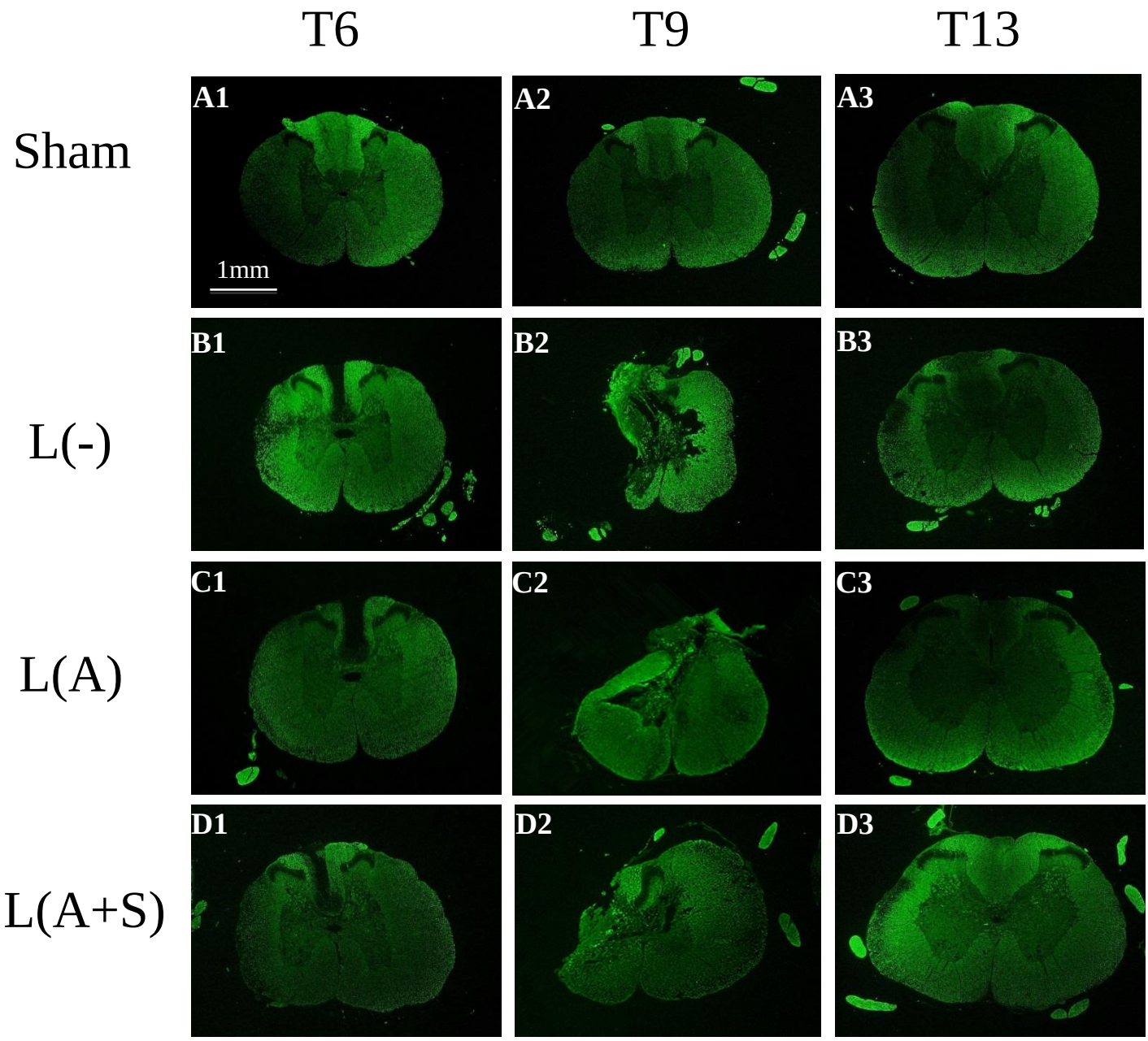

Figure.4.6. Immunofluorescent photomicrographs of macrophages staining by NF antibody. (A) Sham-operated Group S. (B) SCI without scaffold Group L(-). (C) SCI with alginate scaffold Group L(A). (D) SCI with alginate scaffold containing Schwann cells Group L(A+S). T6 (A1-D1) is above the surgery lesion part. T9 (A2-D2) is the surgery lesion in the experimental groups. T13 (A3-D3) is below the surgery lesion part.

The absence of NF in the ascending gracile fasciculus corresponds to the area with higher ED-1 and GFAP expression. No loss of NF was seen in the gracile fasciculus below the lesion at T13 (Figure 4.6). In some animals, there also appeared to be a variable loss of NF in the left lateral white matter columns at T13, below the lesion (Figure 4.6 B3, C3, D3). This corresponds with increased ED-1 seen in the same area in many animals. Thus, axon injury and degeneration may also have occurred on the left side more lateral to the intended lesion site in some animals.

4.3.2.4 GAP-43 image results

GAP-43 is one a marker for axonal regeneration, presents in high concentrations in growing axon and axonal growth cones. Healthy adult spinal cord shows GAP-43 immunoreactivity in the grey matter, particularly the substantia gelatinosa of the dorsal horns, and around the central canal (Figure 4.7 A1, A2, A3). GAP-43 immunoreactivity is generally very low in white matter, but it is seen at a high level in the normal CST at the ventral part of the dorsal columns in healthy spinal cord.

Compared to sham, GAP-43 positive staining appeared to increase throughout the cross section of spinal cord for lesion Groups L(-), L(A) and L(A+S).At the T9 surgery sites damaged areas were rimmed with increased GAP-43 in Groups L(-), L(A) and L(A+S) (Figure 4.7 A2, B2, D2). GAP-43 was also now broadly distributed in surviving white matter, usually forming a radial pattern. Increased GAP-43 was also seen at the outer margin of the spinal cord.

At the levels above and below the injury, T6 and T13, Groups L(-), L(A) and L(A+S) continue to have increased expression of GAP-43 throughout the white matter. The pattern is radial, with a bright band at the outer surface of the spinal cord (Figure 4.7). There appears to be increased GAP-43 in the gracile fasciculus at T6 above the lesions (Figure 4.7 B1, C1, D1), corresponding to increased ED-1, GFAP and decreased NF. In T13 sections below the lesion,

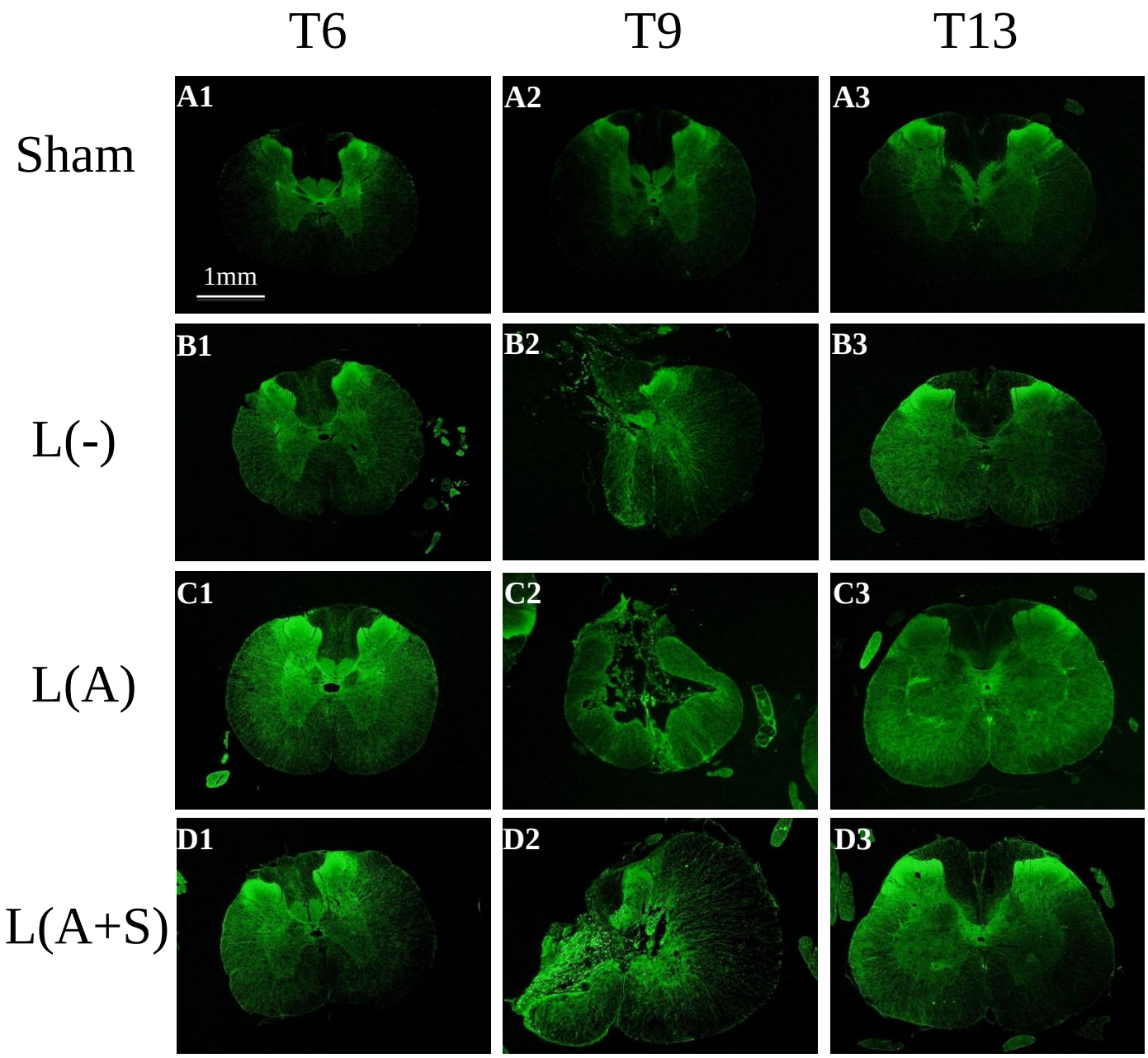

Figure 4.7. Immunofluorescent photomicrographs of macrophages staining by GAP-43 antibody. (A) Sham-operated Group S. (B) SCI without scaffold Group L(-). (C) SCI with alginate scaffold Group L(A). (D) SCI with alginate scaffold containing Schwann cells Group L(A+S). T6 (A1-D1) is above the surgery lesion part. T9 (A2-D2) is the surgery lesion in the experimental groups. T13 (A3-D3) is below the surgery lesion part.

this increase in GAP-43 is not seen in the gracile fasciculus. Below the gracile fasciculus in the dorsal columns at T13 the CST position shows reduced or absent GAP-43 immunoreactivity, compared to sham (Figure 4.7 A3, B3, C3, D3). Persistent but reduced GAP-43 in the CST below the lesion could represent either partial loss of CST axons, or initial regeneration of CST axons.

4.3.2.5 PKC γ image results

Although its cell biological significance is unclear, PKC γ expression is useful for localization of CST axons in spinal cord sections. In healthy spinal cord, PKC γ positive cells are also abundant in the substantia gelatinosa, but these are easily distinguishable from the CST (Figure 4.8). The area of expression of PKC γ is gradually reduced in the ventral part of the dorsal columns as the CST travels downward through cervical, thoracic and lumbar spinal levels Figure 4.8 A1, A2, A3).

At the surgery sites of all experimental Groups L(-), L(A) and L(A+S) no PKC γ positive sign of the CST is seen on either side of the spinal cord (Figure 4.8 B2, C2, D2) indicating that the surgical lesion consistently destroyed the CST on the target side, and on the unintended side. The PKC γ positive substantia gelatinosa was also absent at the lesion site on one or both sides (Figure 4.8 B2, C2, D2) showing again that the lesions were more extensive than we intended.

At T6 the level above the injury, there was variably reduced PKC γ expression at the position of the CST compared to sham in most lesioned animals (Figure 4.8 A1, B1, C1, D1) suggesting that there may have been some loss of the proximal regions of injured CST axons. At the T13 site below the trauma, all three experimental groups showed a complete loss of PKC γ expression distal to the injury (Figure 4.8 B3, C3, D3). The substantia gelatinosa was not damaged either at the level above or below the injury site for all groups.

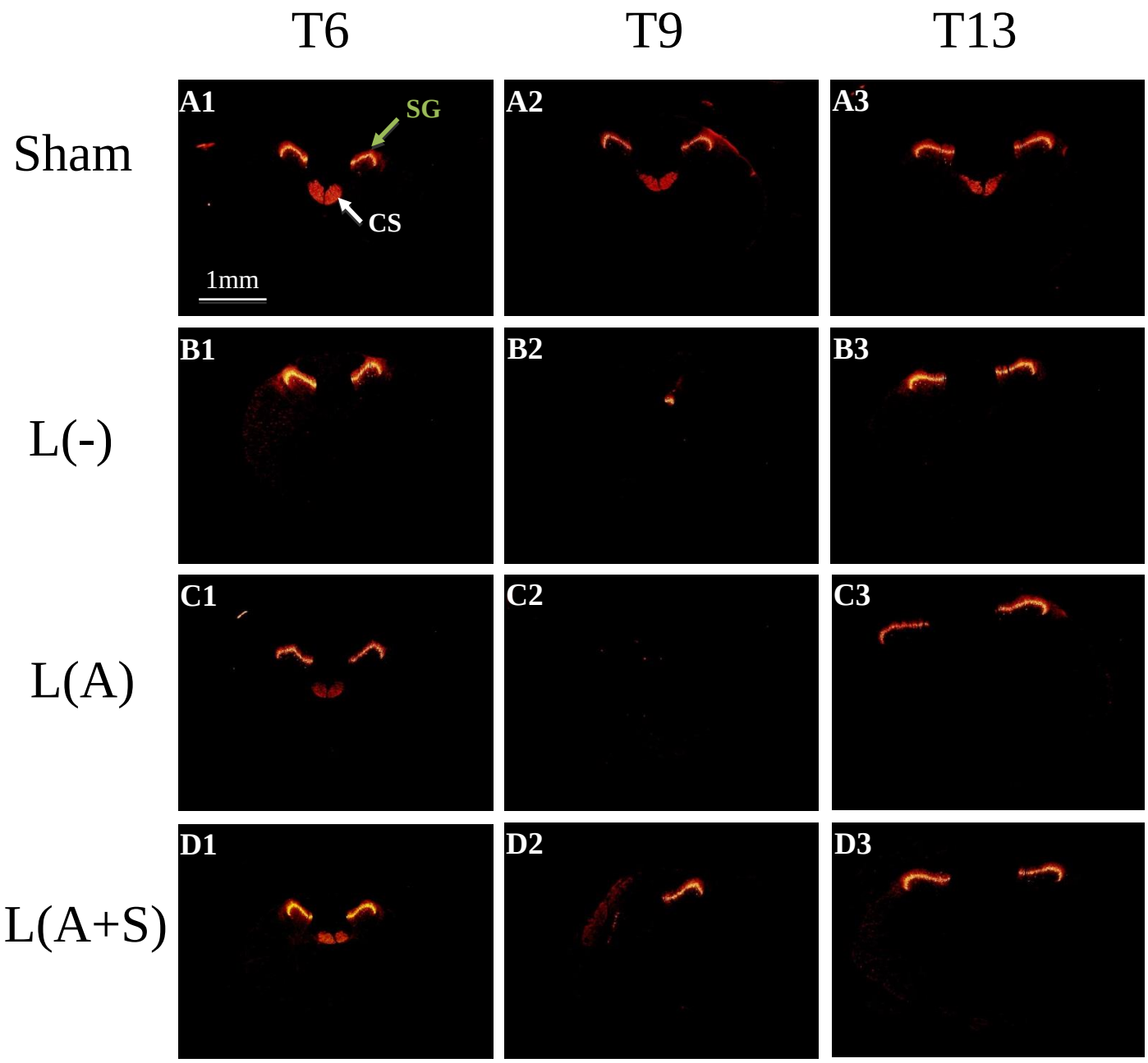

Figure 4.8. Immunofluorescent photomicrographs of macrophages staining by GAP-43 antibody. (A) Sham-operated Group S. (B) SCI without scaffold Group L(-). (C) SCI with alginate scaffold Group L(A). (D) SCI with alginate scaffold containing Schwann cells Group L(A+S). T6 (A1-D1) is above the surgery lesion part. T9 (A2-D2) is the surgery lesion in the experimental groups. T13 (A3-D3) is below the surgery lesion part.

Chapter 5. Visualization of Scaffolds Using Synchrotron Images

5.1. Introduction

The synchrotron radiation PCI-CT technique shows promise for the visualization of the low-density scaffolds that were implanted in soft tissue in this study. This chapter presents a preliminary study on the feasibility of using synchrotron PCI-CT to visualize spinal cord tissue containing alginate hydrogel scaffolds. The scaffolds are designed specifically to mechanically mimic the *in vivo* environment of the spinal cord. For future application of PCI-CT in nervous tissue engineering, a newly designed, 3D grid-pattern hydrogel scaffold is examined with the same technique as contrast.

Specifically, the spinal cord used in this study was dissected from an adult male rat under the approval by UCACS and AREB. Osmium tetroxide (OsO_4) is a heavy metal staining material that has been widely used in X-ray imaging techniques. In this project, OsO_4 was used to stain spinal cord as a comparison to the unstained spinal cord. The image data obtained from our PCI-CT study provided a novel way to examine the interaction between spinal cord tissue and scaffolds *in vivo*, which is not afforded by conventional X-ray imaging methods.

5.2. Materials and Methods

5.2.1 Sample preparation

To investigate the nerve tissue regrowth mechanism and monitor the scaffold interaction with axon tracts, the visualization and distinction of spinal cord and scaffold should be identified first. To achieve this goal, the unstained cervical region of the spinal cord was put standing up vertically in the center of the 1.5 ml tube. Then a cylinder-shaped (1.47 mm in diameter) solid alginate scaffold, spiraling two or more turns, was placed around the spinal cord. This structure

increased the contact areas between scaffold and spinal cord. This shape and arrangement of the mock scaffold ensures easy identification of the scaffold in the PCI projections. A healthy adult rat was deeply anesthetized with 3% isoflurane and euthanized by transcardial perfusion with 0.01M PBS, pH 7.4, followed by 4% PF in 0.1M PBS. After transcardial perfusion, the spinal cord was dissected without vertebral bones and cut into three parts measuring 10 mm each, for X-ray imaging. Sample I: one spinal cord part was not stained. A cylinder-shaped (1.47 mm in diameter) alginate scaffold was made as helix with unstained spinal cord in the center. The remaining two parts of spinal cord were soaked in 0.1% OsO_4 for 24 hours, and then washed with 10 mM Tris buffer with 2% $CaCl_2$ solution for another 24 hours. One of these stained samples did not undergo any further processing and is referred to as Sample II. For Sample III, an alginate scaffold was inserted into the dorsal midline of the osmium stained spinal cord.

Newer techniques in nerve tissue engineering may require more sophisticated 3D scaffolds with well-defined outer form and an open inner structure. Alginate hydrogel scaffolds with only a simple, solid structure may not be suitable for future development. With the help of a 3D-BioPlotter (EnvisionTEC, German), a 3D grid-pattern alginate-hyaluronate scaffold (Rajaram, Schreyer, and Chen 2015) was fabricated in the form of a rectagonal mesh for imaging in the present study. The scaffold was 10 mm in length and 5 mm in width and height. The inter-strand width was 0.5 - 0.7 mm and the width of one alginate-hyaluronate strand was 150 - 200 micron. This scaffold was prepared by another one of our group members, Dr. Ajay Rajaram. Samples were placed inside plastic tubes in PBS and transported to the Canadian Light Source (CLS) synchrotron facility in a cooler.

5.2.2 Imaging spinal cords with scaffolds

Synchrotron PCI was performed at the 05B1-1 Biomedical Imaging and Therapy (BMIT) bending magnet beamline. The samples were placed in a cylindrical sample holder and then mounted on the specimen stage in the beamline experimental hutch for PCI-CT scanning. PCI was performed at an energy level of 26 keV using a monochromatic beam. The sample-to-detector distance was set to approximately 1 m according to previous studies (Zhu et al. 2011). A Hamamatsu C9300-AA66-C9300-124 (Japan) detector was chosen for use with a pixel size of 8.7 microns. The sample stage was rotated at a step angle of 0.2 degrees during imaging for the total rotation angle of 180 degrees. Image processing and reconstruction were performed using the software packages of NRecon and CTVox (Bruker microCT, Germany), by another one of our group member, Dr. Ning Zhu.

5.3. Results and Discussion

Figure 5.1. shows the 3D reconstruction of Sample I that was obtained using CTVox. From the reconstructed images, the phase of the spinal cord and the scaffold can be observed without the need for any contrast agent. Additionally, the inner structure of the spinal cord, such as gray matter, can be easily distinguished. The classical butterfly structure of grey matter was visualized clearly. The results of this initial study form a basis for the future studies using our SCI model *in vivo*, including a real-time monitor of any secondary injury that develops and encroaches on healthy tissue.

The PCI technique enabled visualization and analysis of the structure of engineered scaffolds and spinal cords (including white and gray matters) without the addition of any staining agent. This structural characterization is not be possible by conventional X-ray imaging techniques.

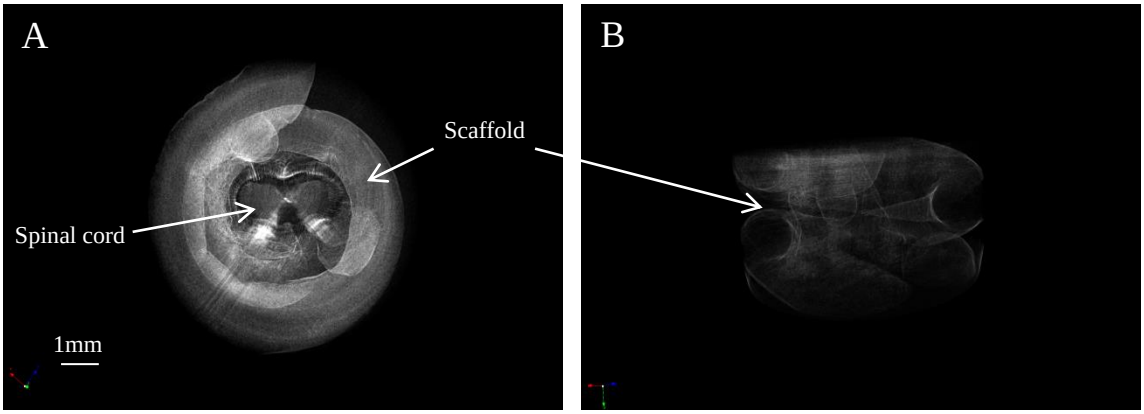

Figure 5.1. The inside region contains the spinal cord and the outside contains the cylinder alginate hydrogel scaffold as a screw shape. (A) Transverse view of model. (B) Lateral view of model.

Based on the previous studies performed by one of our group members (Yijing Guan, unpublished), we examined whether staining samples with OsO_4 could provide distinct visualization of the alginate scaffolds in spinal cord tissue using PCI. Therefore, the addition of OsO_4 as a contrast agent was also tested to visualize the alginate with the spinal cord tissue in the PCI performed in this study too.

Figure 5.2 shows reconstructions of the samples stained with OsO_4. Fig. 5.2 (A) was a 10 mm piece of healthy thoracic spinal cord (Sample II). Fig. 5.2 (B), another 10 mm thoracic spinal cord, was cut on the ventral midline (Sample III). A 0.5 mm diameter cylinder-shaped solid alginate scaffolds was inserted into the position of CST. Fig. 5.2 (A) shows the external shape of the spinal cord and the location and size of the dorsal root ganglion. Fig. 5.2 (B) shows the transverse view of spinal cord and the location of the scaffold. However, the contrast of inner structure of inner spinal cord is limited but the visualization of intensity of the external appearance is increased compared to Fig. 5.1. One explanation for this is that because OsO_4 is a heavy metal staining agent it may not be able to penetrate from the white matter into the gray matter of the spinal cord due to the limits of diffusion. Indeed, it was noticed that, due to the uneven staining, the outer layer of the spinal cord has a higher refractive index than the inner layer, which leads to the loss of information from the inner layer.

The uneven distribution of OsO_4 in the spinal cord interrupts the visualization of the spinal cord using PCI-CT. In addition, the staining procedure damages the proteins in the samples and as a result the samples cannot be used for the histological and immunohistochemical analysis.

PCI is highly sensitive to the porosity and boundaries between similar low density and low contrast materials. Figure 5.3. shows a region of interest of the 3D grid-pattern alginate-

hyaluronate scaffolds that we prepared, containing a biologically appropriate porous microstructure. The PCI-CT image clearly illustrates that the grid-pattern scaffold has higher contrast than the solid scaffold (Figure 5.1 A). The porous microstructure increased the boundary areas and increased the contact areas, which enable higher quality imaging. In addition to an improvement in image quality, the porous microstructure also encourages tissue integration and vascularization, as well as diffusion of nutrients. Furthermore, the internal and external structure of this scaffold allows any regenerating axons or tracts to reintegrate with tissue at the distal end of the severed site from the channel of the scaffold. These features of 3D grid-pattern scaffolds make them a promising avenue of research aimed at improving repair and regeneration of damaged nerve tissue.

The results obtained from this chapter represent substantial progress in the visualization and characterization of the soft tissues and alginate hydrogel scaffolds. Using PCI, the structural features of the unstained spinal cords were visible, and were comparable to PC images observed on spinal cords stained with OsO_4. The PCI technique provides an outstanding non-destructive and non-invasive method for the visualization of the low density scaffold associated with soft tissues, which will greatly facilitate *in vivo* soft tissue engineering studies in the future.

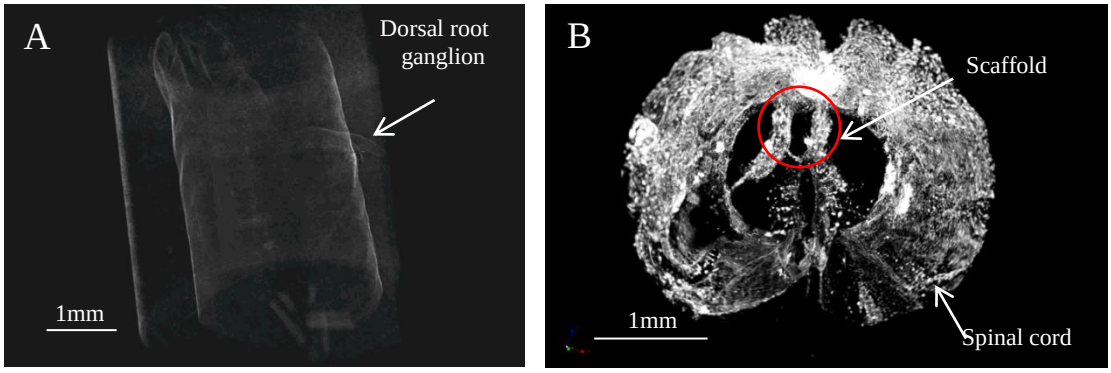

Figure 5.2. 3D reconstruction models of the spinal cord tissue using in-line PCI-CT. (A) Lateral view of the spinal cord with OsO_4 staining. (B) A transverse view of the spinal cord with a cylinder-shaped alginate scaffold by OsO_4 staining. The scaffold (red circle) inside the spinal cord can be visualized by using in-line PCI-CT with the photon energy at 26 KeV.

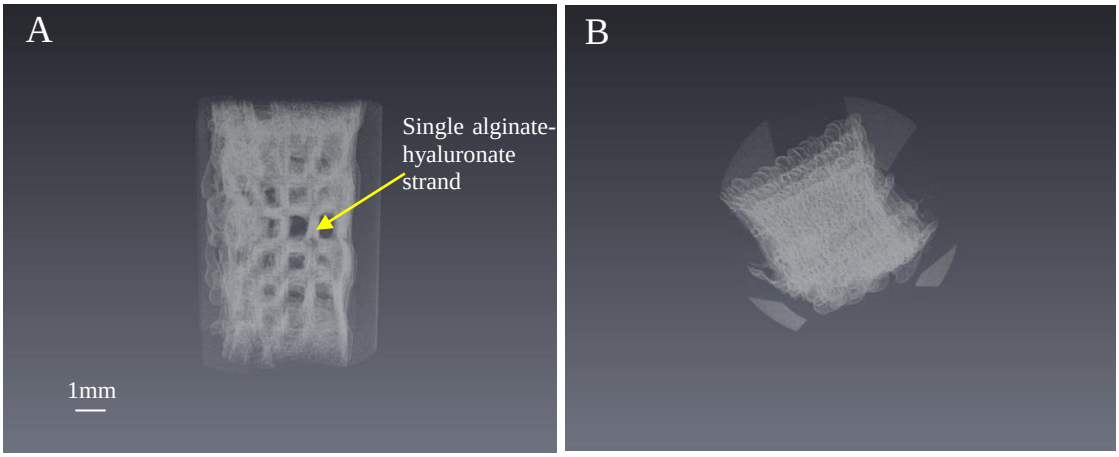

Figure 5.3. Visualization of a 3D grid-pattern scaffold using in-line PCI-CT. (A) Lateral view of the scaffold. (B) A transverse view of the scaffold.

Chapter 6. Discussion and Conclusions, Limitations of Method, and Future work

6.1. Discussion and Conclusions

This thesis presents a study on the development of an animal model to test tissue repair scaffolds made from alginate hydrogel containing living Schwann cells for the repair of SCI, as well as a preliminary study on the visualization of scaffolds in soft tissue with synchrotron based imaging. The thesis describes scaffold fabrication, the design of a SCI animal model, behavioural tests, histological and immunohistochemical analysis of lesion outcome, and the development of synchrotron imaging techniques.

The tissue repair scaffolds used in this study were composed either of a plain alginate hydrogel, or an alginate gel containing living Schwann cells. Schwann cells are widely used in nerve tissue engineering especially in PNS. Previous study also suggested that Schwann cells can be used to improve remyelination and help restore neurological functions at lower levels after SCI (Lavdas et al. 2008). Schwann cells assist recovery after SCI by expressing axonal growth-promoting molecules, such as neurotrophins, neural cell adhesion molecular and extracellular matrix proteins (Bachelin et al. 2010). Schwann cells play an important role in maintaining homeostasis and therefore reduce secondary damage (Zhang et al. 2013). In addition, Schwann cells improved signal conduction by forming myelin sheaths around CNS axons (Kanno et al. 2015). Schwann cells are easy to access, can be maintain in culture and show good survival compared to other cells. These features make Schwann cells an attractive candidate in this project. However, some studies reported that introducing Schwann cells into the lesion may lead to Schwannoma formation and neuropathic pain (Norenberg, Smith, and Marcillo 2004,

Campana 2007). Also, tracking survival of implanted Schwann cells in CNS *in vivo* is difficult due to the possible presence of invading host Schwann cells.

Experiments were conducted to confirm the survival and proliferation of Schwann cells inside of alginate hydrogel in the short term (up to 72 hours). We found that Schwann cells survived very well in the alginate hydrogel environment for several days *in vitro*. However, we were not able to track the fate of Schwann cells after six weeks implantation *in vivo*.

Measurements of cresyl violet stained spinal cord sections indicated that surgery sites in Group L(A) animals ultimately had more damage than Group L(-) and L(A+S) animals. The results from BBB scores also indicated that behavioural outcomes were improved in Group L(A+S) animals compared to Group L(A). Neither of these results could be shown to reach statistical significance, however. Nevertheless, if true, these findings would indicate that the inclusion of living Schwann cells at the alginate gel implantation site is beneficial. The nature of any beneficial effect of Schwann cells in our study, whether through secretion of growth factors, construction of extracellular matrix, or amelioration of spinal shock or secondary injury, remains unknown.

In order to provide a proper scientific evaluation of tissue repaired scaffolds, the lesion placement in the present study is fundamentally different from other spinal cord lesion studies in an important way. In other studies that utilize a partial transection model, the tissue damage is confined to a single transverse plane. In our study, a rostrocaudal length of white matter tract which included the gracile fasciculus and the CST is extirpated, so that a cavity is created to receive the 3D scaffold and axon growth within the alginate hydrogel environment of the scaffold can be evaluated. Our method therefore entails more difficult surgery, and an increased likelihood of severe spinal shock, spreading secondary damage and a strong inflammatory

response. Moreover, the placement of the scaffold requires more extensive axon regeneration before severed axons can reconnect with healthy tissue.

There are two reasons that we chose the lower thoracic region of the spinal cord for lesion and scaffold placement in this study. One reason is that lesions at this level ideally only produce functional impairment of one hindlimb and therefor moderate the degree of postsurgical care which must be provided. The second reason is that functional recovery following this type of lesion can be evaluated with the BBB tests of hindlimb locomotion. A possible alternative procedure is to create the lesion and place the scaffold at a cervical level of the spinal cord. Despite the presence of considerably more muscle mass that must be traversed, the exposure of cervical vertebral column is very easy. Meanwhile, the vertebrae of the cervical segments are much less substantial than those of the lower thoracic segments, so that the laminectomy can be done much more quickly. However, a few features of the cervical spinal region still work against the thoracic level. First, the cervical segments are too short to expose enough spinal cord to implant a reasonable length scaffold. Instead of two thoracic vertebrae removed, the laminectomy of cervical vertebrae would require four to six vertebrae to be removed to expose enough spinal cord. Second, the vertebral column and enclosed spinal cord are curved in the cervical region, whereas they are straight and parallel to the long axis of the animal in the lower thoracic region. The stereotaxic manipulators were used to guide the knife blade that makes the lesion in the thoracic spinal cord, and then to carefully deliver the scaffold implant. These manipulators can guide precise parallel movements in the horizontally positioned thoracic cord, but would not be able to do the work in the curved and angled cervical cord.

There were two series of surgical procedures carried out in these studies. The first series was aimed at exploring the possible procedures for this new type of highly invasive surgery. Lessons

learned during the first series were used to develop improved procedures for the second series. The two runs of surgery were compared from the aspects of anesthesia, bleeding control, weight control and neurological function. The survival rate of animals during the surgical procedure and post-surgery period was significantly increased from 57.89% in the first series to 100% in the second series. The first reason for this is that we shortened the length of the lesion and the length of scaffolds, from 10 mm to 5 mm, for implantation. The shorter the scaffold is, the less overall tissue damage is required, and a shorter time under anesthesia can be achieved. But, if the length of the scaffold is too short, it is not scientifically meaningful. Secondly, the animal physiology and depth of anesthesia were continually monitored, which prevented the animals from dying under anesthesia in the second run. Thirdly, improvements were made to speed up the surgical procedure and control bleeding, including more care by the surgeon to avoid damage to blood vessels, more liberal use of GelFoam for haemostasis, and a new practice of covering the exposed spinal cord with fibrin glue. Finally, it was noticed that when animals gain too much weight, it was hard to control the depth of anesthesia, thus likely leading to bleeding during the surgical procedure and the postsurgical recovery as well. Therefore, in the second run, a weight control regime was carried out. These improvements lead to the better behavioural and morphological outcomes in the second series of surgeries.

The evaluation of neurological function recovery is based on the BBB behavior tests. Excessive spinal cord damage included complete hindlimb paralysis, loss of bladder function, and severe spinal curvature, which were commonly observed in the first surgical series. Of all the rats that received surgery, there likely was a spinal shock period at the first week after the surgery (Furlan et al. 2011). This shock damages the homeostasis of rats, corresponding with very low BBB scores drop to the bottom. However, spinal shock is transient, and marked

recovery of BBB scores was seen after the first two weeks in virtually all animals. It is very unlikely that regenerative repair or functional compensation could have happened this quickly, so these are unlikely explanations for improved BBB scores at three weeks.

During six weeks post-surgery period, central cavitation spread and eventually expanded to become much larger than the initial surgery lesion size. It is well-established that inflammatory cell infiltration, hemorrhage, ischemia, and excitotoxicity can contribute to cavitation enlargement (Oyinbo 2011). Although surgery created a physical lesion with a small lesion initially, we observed that central hemorrhage started immediately after the damage in spinal cord. At the early edge of secondary injury, vasospasm and vascular damage likely led to spreading ischemia. Subsequent deprivation of oxygen and glucose likely then caused failure of ion pumps that regulate intracellular Ca^{+}, Na^{+}, K^{+} and Cl^{-}. Meanwhile, injury causes depolarization of the cells that induces increased glutamate release. High glutamate is the major factor causing excitotoxicity thus more damage happened. Cell necrosis, apoptosis and membrane damage trigger an inflammatory cascade reaction. When macrophages started to "clean up" debris of neurons and membranes, one drawback of the inflammation cascade reaction is that the macrophage mannose receptor and type 3 β2 integrin receptor may induce astrocytes to accumulate around the lesion and create scars and cavities (Fitch et al. 1999). Histological examination at six weeks showed that spinal cord damage was always more extensive than intended, whether due to surgical error or secondary injury processes. In this project, histologic and immunohistochemical analysis were done only at six weeks post-operative survival, so we have no information about tissue changes at intermediate time points. The damage in the spinal cord in the surgery groups caused the Wallerian degeneration of gracile fasciculus and CST axons, which results in evident shrinkage of the ventral part of the dorsal

column and substantia gelatinosa (SG) on the left side at regions well above the site of trauma. The midline glial boundary between the left and right CST underwent a leftward shift and sometimes the intact CST on the right bulged to the left due to this shrinkage, which was also reported in previous studies (Sharp et al. 2013). Collateral damage to gray matter structures and even other white matter was often seen on the left side, and sometimes even on the right. This unintended damage may have contributed to functional deficits.

We expect that significant inflammation would accompany spinal cord damage of the magnitude created during our surgical procedures (Benowitz and Popovich 2011). At the cellular level of physiology, the macrophages/microglia are critical in nervous tissue damage control. When the injury occurred, axons began to degenerate distal to the site of injury and myelin debris was produced. By six weeks after injury, the macrophages/microglia appeared and accumulated at the injury site to engulf degenerating myelinated axons. This process of Wallerian degeneration is much slower in the CNS than in the PNS (Patrick R. Hof 2010) and is likely a factor leading to poor recovery after CNS injury.

In our study, the presence of ED-1 positive macrophages/microglia also indicated the severity of the injury. The more macrophages/microglia that were present, the more severe the injury is. From the surgery site imaging, all three experimental groups shows massive macrophages accumulated surround the cavity even extended to the grey matter in the other hemisphere. The presence of macrophages/microglia was also a convenient way to monitor axon degeneration above the injury in the gracile fasciculus. Less noticeable accumulation of macrophages/microglia below the injury may have marked degenerating CST distal axons, and perhaps some axons of the lateral column white matter. More macrophages/microglia were present in Group L(A) than in Groups L(-) and L(A+S) which, taken together, may signify that

the inclusion of Schwann cells helped reduce inflammatory activity caused by the presence of alginate.

Astrocytes are thought to respond to CNS injury by undergoing "reactive astrocytosis", including proliferation, hypertrophy and migration (Sofroniew and Vinters 2010). They also contribute to the formation of a glial scar (Wanner et al. 2013). Although we saw evidence of GFAP positive glial scarring at the edges of the damaged areas, there did not appear to be a general astrocytosis in regions distant from the lesion at the T9 level, or above and below the lesion at T6 and T13. If anything, GFAP immunoreactivity was decreased in Groups L(-), L(A) and L(A+S) outside the immediate lesion area. However, we did see an increase in GFAP in the gracile fasciculus above the lesion, corresponding with increased ED-1 and distal axon degeneration. Thus, the responsiveness of astrocytes appeared to be closely tied to the degenerative process.

In this study, the intended lesion area includes both the gracile fasciculus and the CST. At the injury level, the left dorsal horn was destroyed in almost all animals and the damage also extended to include the lateral columns of the white matter on the left side. In contrast, spinal cord tissue appeared to remain remarkably intact at spinal cord levels T6 and T13. At level T6, cresyl violet staining showed dark staining of the gracile fasciculus on left side for Group L(-) and L(A+S) as well as the gracile fasciculus on both sides for Group L(A). ED-1 and GFAP results showed that macrophages and astrocytes accumulated at the same gracile fasciculus area as shown in cresyl violet staining. It is indicated that secondary injury may expand to degenerating proximal gracile fasciculus that triggered the inflammatory reaction. However, GAP-43 and NF results suggested that new neurites sprouted at the same position as shown by ED-1 and GFAP. Taken together, these results suggest that the inflammation process and neurite

sprouting were present at the T6 gracile fasciculus limited to the left side of Group L(-) and L(A+S) and were present on both sides of Group L(-) animals.

PKC γ expression is a convenient marker to determine the completeness of a spinal lesion of the CST. Transection of CST fibers in our animals resulted in a complete loss of PKC γ expression distal to the injury. There is no evidence that CST fibers regenerate at the injury level or at distal levels. However, at the T6 level, Group L(A) and L(A+S) showed normal or increased expression of CST, especially Group L(A+S), whereas Group L(-) showed no expression of PKC γ in the CST. There are three hypotheses. One hypothesis is that Schwann cells may still survive and proliferate proximal to the lesion and form myelin sheaths around CST and gracile fasciculus axons, and help to prevent secondary injury. The other hypothesis is that expression of PKC γ in Group L(-) was inhibited by secondary injury but not in the other two groups because of the scaffold. The CST may still exist in Group L(-) but cannot been detected because of decreased PKC γ. Another hypothesis is that surgery caused different severity of injury among the three groups. Thus the regeneration rates were different. However, histology and other staining clearly illustrated that Group L(A) had larger damage then the other two groups. Combined with results from NF and GAP-43, the first hypothesis may contribute more to our results in this research.

Perhaps the most remarkable finding of this study is that most animals eventually displayed functional recovery to near normal at six weeks following SCI based on behavior results, even though spinal cord damage was greater than intended. Good recovery from SCI is often seen in rodents (MacKay-Lyons 2002, Guertin 2012, Dietz 2003). There are two reasons why high spontaneous recovery might occur. At the end of the spinal shock period, a local pattern generator in undamaged lumbar spinal cord might begin to cause coordinated hindlimb

movement even without descending motor signals. A larger thoracic lesion may disrupt coordination of hindlimb and forelimb movements, but we did not study overall coordination of limb movements. Secondly, different mechanisms of neural plasticity can lead to improved function even without axons regeneration. For example, local axons sprouting and synapse re-arrangement within the spinal cord could allow undamaged axons to participate in new functions. Also, similar plasticity in the CNS above the spinal cord could redirect functional signalling through remaining undamaged tissue at the level of the lesion.

Taken together, histology and immunohistochemistry results suggest that alginate scaffold may cause a larger cavity at the injury site, and does not support axon regeneration into the bridge area. However, inclusion of Schwann cells may reduce secondary injury. The animal model designed in this research offers several advantages for studying the repair of SCI by means of artificial tissue scaffolds. First, this partial transection model was only targeted to remove one side of the dorsal columns including the CST and the fasciculus graculis by cutting instruments or needle aspiration. The lesion was initially designed to be small. Second, the lesions in the spinal cord were not supposed to cause the animals to be totally paralyzed or to lose bladder control, and they still held the ability to walk. Besides, SD rats are easy to access and raise, relatively inexpensive and easy to care for post-operatively, with few surgical infections. In the course of developing this model, we made several amendments to the procedure, and the surgery became more precise and standardized such as to shorten time under anaesthesia, improve control of bleeding to obtain a good survival rate and no complication.

However, there are still some aspects of the model that could be improved. For instance, the size of cavity initially created in the spinal cord may not consistent for all animals due to the lack of suitable stereotaxic lesion and cavity creation procedure. Also, the method to identify the

Schwann cells (or other living cells) encapsulated in the implanted scaffold needs to be developed. In addition, the BBB behavior test alone was not enough to evaluate all aspects of functional recovery related to the axons regeneration. A combination of two or three different behavior tests would be a better choice. Besides that, monitoring scaffold degradation *in vivo* is still a challenge. However, with the help of development of synchrotron radiation PCI technique, live animal imaging should show remarkable progress for both tissue engineering and imaging technique. These issues remain to be addressed in the future work.

This project involved the use of synchrotron based imaging techniques for the visualization of spinal cords and scaffolds. Effective tissue visualization and scaffold tracking are crucial for observing scaffold fate and the axon regeneration process after implantation. Using conventional X-ray imaging, it is hard to distinguish soft tissues from hydrogels because of their similarity in X-ray attenuation coefficients. To visualize weakly absorbing materials such as nerve tissues, image contrast can be enhanced by the X-ray in-line PCI technique. Coupled with CT, PCI-CT can reveal the 3D structure of the sample. It has previously been shown that it is possible to visualize low-density hydrogel scaffolds within brain tissues without OsO_4 staining by using DEI-CT and PCI-CT (Guan, 2010). Given that spinal cord tissue is similar to brain tissue, PCI-CT was applied in this project to illustrate and develop the visualization technique for studies of nerve tissue engineering.

The 05B1-1 BMIT-BM beamline at the CLS provides a range of photon energy from 10 to 40 keV. For PCI-CT, photon energy is positively correlated with image definition which means that the higher the photon energy, the higher image definition. However, higher photon energy comes with lower photon flux, which results in longer scan times. Consequently, the longer times required at high photon energies leads to overheating samples and subsequent denaturation.

Therefore, in this project, an optimal photon energy of 26 keV was chosen to ensure both clear image projections, whilst also maintaining a modest scan time.

In this project, three different samples were created and the feasibility of PCI-CT to visualize and characterize the microstructure of low-density hydrogel scaffolds and soft tissue were evaluated, with the aim of providing a means to monitor new tissue regeneration and scaffold degradation *in vivo*. The first sample was selected to demonstrate that the scaffold with spinal cord can be visualized by PCI-CT. The second sample was designed to compare the effectiveness of visualization between unstained tissues and OsO_4 stained tissues. The third sample was created with a 3D grid-pattern structure to more closely model future tissue repair scaffolds designed to incorporate internal porosity. Both the sample to detector distance and photon energy are factors that influence the quality of the images produced. The values of these parameters were determined based on previous studies in our group as well as the limits of the beamline at the CLS.

The results illustrate that PCI-CT is able to sufficiently image the structures and features of spinal cords and hydrogel scaffolds without the use of any staining agents. Indeed, staining with OsO_4 may hamper visualization of this type of material. It is hoped that our findings may help allow PCI to be employed to monitor scaffold degradation and new tissues regeneration in live animals. In conclusion, PCI is a feasible method to analyze the structure of engineered scaffolds and could differentiate white and gray matter in the spinal cord. Currently, such structural characterization is not possible with conventional X-ray imaging techniques. PCI was able to reveal the structural features of the spinal cord in unstained tissue and was comparable to that observed in the OsO_4 stained sample. As such, PCI is able to provide a non-destructive and non-invasive method for the visualization of the low-density scaffold associated with soft tissues,

illustrating the promise of this technique to evaluate soft tissue engineering studies during the process of tissue repair *in vivo*.

6.2. Limitations of Method

The results obtained from this study provide useful information about the potential use of an alginate hydrogel tissue repair scaffold with Schwann cells to support repair of SCI. Meanwhile, there are still some limitations of the present work, and the model system could be improved.

We were unable to fully study the contribution of including living cells in a tissue repair scaffold because detection of implanted Schwann cells and their survival and proliferate *in vivo* was not completed. Our techniques did not allow us to identify Schwann cells potentially surviving in the spinal cord cavity for six weeks. This was due, in part to the fact that there is no specific immunohistochemical marker to detect implanted Schwann cells in CNS and differentiate them from Schwann cells that may have invaded from the rat's own PNS. Anti-S-100 is a classic antibody to stain Schwann cells in PNS; however, it is also an astrocyte marker in some regions of CNS such as rat cerebellum (Slemmer, Weber, and De Zeeuw 2004).

In this study, only the BBB behavior test was used and that the nature of this test (classification of behaviour into categories) does not allow us to determine if there was a statistically significant difference between the control group and scaffold-treated groups. The use of more sophisticated behavioural test might allow a more quantitative analysis of behavioural recovery, focussing on the contribution of the CST (Girgis et al. 2007). A larger, more intractable problem with the use of rats as a model species is that they can exhibit high levels of spontaneous recovery following different kinds of SCI (Onifer, Smith, and Fouad 2011). Moreover, partial transection models exhibit more spontaneous recovery than complete transection models (Sakai et al. 2012). This will always create a difficulty in trying to isolate

how anatomical recovery may underlie behavioural recovery.

Our results indicate that unintentional secondary injury of spinal cord tissue may have expanded the size of the lesions beyond what was intended. Some strategies can be used to limit the extent of secondary injury, particularly the use of immunosupressants, or agents that can reduce oxidative stress or excititoxicity. Indeed, methylpredisone is already in use to limit secondary injury in human SCI (Cristante et al. 2012). However, the addition of pharmacological treatments to supress secondary injury adds another layer of complication to the model, even as it helps focus on the contribution of regenerative axon growth to behavioural recovery.

6.3. Future Work

With the successes presented previously, this project forms a basis for future studies in the development of 3D alginate scaffolds as applied to the repair of SCI as well as the visualization of swollen and degradation properties of scaffolds.

First, according to the limited detection of the Schwann cells in this study, the visualization in Schwann cells should be developed. Recently, green fluorescent protein (GFP) from jellyfish is popularly used as a marker to identify Schwann cells and assess the size and number of the transplants in the repair of spinal cord injury (Fehlings and Nguyen 2010). GFP is different from other cell markers. The GFP gene integrated into the genome of the donor Schwann cells can provide a marker that is not attenuated by time. There are two ways to acquire GFP positive Schwann cells. One is choosing suitable commercial GFP transgenic rats, which are especially Schwann cell-GFP positive. These exist, but are difficult to access in North America. The other is to isolate Schwann cells from the peripheral nerve of a rat, then transfect the GFP gene into the isolated Schwann cells. GFP expression in Schwann cells is stable and visualized clearly. Thus, employing GFP to mark donor cells in the animal model may be an essential and significant

improvement that can be made in the future.

Second, the surgery process of creating cavities in the spinal cord for scaffolds implanted should be further improved. Currently, the device available for creating accurate triangular prism cavities in the spinal cord is cumbersome and difficult, and errors may have occurred during the surgery. It is possible that a laser knife would have better performance in creating cavities in the spinal cord. The cutter head of laser knife is as small as 0.1 mm. The laser knife can cut the spinal cord more cleanly without creating mechanical stress on intact tissues. In addition, the thermal effects of laser knife could help reduce bleeding during the surgery.

Last, visualization techniques of hydrogel scaffolds by means of synchrotron-based techniques are still in their early stage. In this study, the alginate hydrogel scaffolds can be characterized and distinguished from the surrounding soft tissues without OsO_4 staining. It would be very informative to monitor the degradation properties of the scaffold throughout the post-injury survival period. According to our preliminary results, PCI-CT is the only X-ray imaging technique that can be used to monitor the microstructure of low-density hydrogel scaffolds and soft tissue *in vivo.* We would also like to be able to monitor the formation of new or regenerated tissue, which should be visualized at different time points during the recovery time of spinal cord injury on live animals. The resolution available from current synchrotron radiation PCI-CT is too low to detect individual axons, but bundles of axons such as regenerating tracts might be visualized. Moreover, future developments in synchrotron imaging technology might offer increased resolution.

REFERENCES

Agudo, M., A. Woodhoo, D. Webber, R. Mirsky, K. R. Jessen, and S. B. McMahon. 2008. "Schwann cell precursors transplanted into the injured spinal cord multiply, integrate and are permissive for axon growth." *Glia* 56 (12):1263-70. doi: 10.1002/glia.20695.

Anderton, B. H., D. Breinburg, M. J. Downes, P. J. Green, B. E. Tomlinson, J. Ulrich, J. N. Wood, and J. Kahn. 1982. "Monoclonal-Antibodies Show That Neurofibrillary Tangles and Neurofilaments Share Antigenic Determinants." *Nature* 298 (5869):84-86. doi: Doi 10.1038/298084a0.

Andrews, Melissa R., and Dennis J. Stelzner. 2007. "Evaluation of olfactory ensheathing and Schwann cells after implantation into a dorsal injury of adult rat spinal cord." *Journal of Neurotrauma* 24 (11):1773+.

Assun, #xe7, #xe3, Rita C. o-Silva, Eduardo D. Gomes, Nuno Sousa, Nuno A. Silva, Ant Salgado, #xf3, and nio J. "Hydrogels and Cell Based Therapies in Spinal Cord Injury Regeneration." *Stem Cells International*.

Bachelin, C., V. Zujovic, D. Buchet, J. Mallet, and A. Baron-Van Evercooren. 2010. "Ectopic expression of polysialylated neural cell adhesion molecule in adult macaque Schwann cells promotes their migration and remyelination potential in the central nervous system." *Brain* 133 (Pt 2):406-20. doi: 10.1093/brain/awp256.

Banerjee, A., M. Arha, S. Choudhary, R. S. Ashton, S. R. Bhatia, D. V. Schaffer, and R. S. Kane. 2009. "The influence of hydrogel modulus on the proliferation and differentiation of encapsulated neural stem cells." *Biomaterials* 30 (27):4695-9. doi: S0142-9612(09)00547-X [pii]

10.1016/j.biomaterials.2009.05.050.

Basso, D. M., M. S. Beattie, and J. C. Bresnahan. 1995. "A sensitive and reliable locomotor rating scale for open field testing in rats." *J Neurotrauma* 12 (1):1-21.

Basso, D. M., L. C. Fisher, A. J. Anderson, L. B. Jakeman, D. M. McTigue, and P. G. Popovich. 2006. "Basso Mouse Scale for locomotion detects differences in recovery after spinal cord injury in five common mouse strains." *J Neurotrauma* 23 (5):635-59. doi: 10.1089/neu.2006.23.635.

Benowitz, L. I., and P. G. Popovich. 2011. "Inflammation and axon regeneration." *Curr Opin Neurol* 24 (6):577-83. doi: 10.1097/WCO.0b013e32834c208d.

Brittis, P. A., and J. G. Flanagan. 2001. "Nogo domains and a Nogo receptor: implications for axon regeneration." *Neuron* 30 (1):11-4. doi: S0896-6273(01)00258-6 [pii].

Brosamle, C., A. B. Huber, M. Fiedler, A. Skerra, and M. E. Schwab. 2000. "Regeneration of lesioned corticospinal tract fibers in the adult rat induced by a recombinant, humanized IN-1 antibody fragment." *J Neurosci* 20 (21):8061-8.

Campana, W. M. 2007. "Schwann cells: activated peripheral glia and their role in neuropathic pain." *Brain Behav Immun* 21 (5):522-7. doi: 10.1016/j.bbi.2006.12.008.

Canada, Spinal Cord Injury. 2014. "Spinal Cord Injury Canada Facts."

Catharyn T. Liverman, Bruce M. Altevogt, Janet E. Joy, and Richard T. Johnson,. 2005. "Spinal cord injury; progress, promise, and priorities." *SciTech Book News*, 2005/12//.

Chen, G., Y. R. Hu, H. Wan, L. Xia, J. H. Li, F. Yang, X. Qu, S. G. Wang, and Z. C. Wang. 2010. "Functional recovery following traumatic spinal cord injury mediated by a unique

polymer scaffold seeded with neural stem cells and Schwann cells." *Chin Med J (Engl)* 123 (17):2424-31.
Chodobski, A., B. J. Zink, and J. Szmydynger-Chodobska. 2011. "Blood-brain barrier pathophysiology in traumatic brain injury." *Transl Stroke Res* 2 (4):492-516. doi: 10.1007/s12975-011-0125-x.
Collazos-Castro, J. E., E. Lopez-Dolado, and M. Nieto-Sampedro. 2006. "Locomotor deficits and adaptive mechanisms after thoracic spinal cord contusion in the adult rat." *J Neurotrauma* 23 (1):1-17. doi: 10.1089/neu.2006.23.1.
Consortium for Spinal Cord, Medicine. 2008. "Early acute management in adults with spinal cord injury: a clinical practice guideline for health-care professionals." *J Spinal Cord Med* 31 (4):403-79.
Cote, M. P., A. A. Amin, V. J. Tom, and J. D. Houle. 2011. "Peripheral nerve grafts support regeneration after spinal cord injury." *Neurotherapeutics* 8 (2):294-303. doi: 10.1007/s13311-011-0024-6.
Courtine, G., M. B. Bunge, J. W. Fawcett, R. G. Grossman, J. H. Kaas, R. Lemon, I. Maier, J. Martin, R. J. Nudo, A. Ramon-Cueto, E. M. Rouiller, L. Schnell, T. Wannier, M. E. Schwab, and V. R. Edgerton. 2007. "Can experiments in nonhuman primates expedite the translation of treatments for spinal cord injury in humans?" *Nature Medicine* 13 (5):561-566. doi: 10.1038/nm1595.
Cristante, A. F., T. E. Barros Filho, R. M. Marcon, O. B. Letaif, and I. D. Rocha. 2012. "Therapeutic approaches for spinal cord injury." *Clinics (Sao Paulo)* 67 (10):1219-24.
Cui, F. Z., W. M. Tian, S. P. Hou, Q. Y. Xu, and I. S. Lee. 2006. "Hyaluronic acid hydrogel immobilized with RGD peptides for brain tissue engineering." *Journal of Materials Science-Materials in Medicine* 17 (12):1393-1401. doi: 10.1007/s10856-006-0615-7.
de Guzman, R. C., E. S. Ereifej, K. M. Broadrick, R. A. Rogers, and P. J. VandeVord. 2008. "Alginate-matrigel microencapsulated schwann cells for inducible secretion of glial cell line derived neurotrophic factor." *J Microencapsul* 25 (7):487-98.
Deng, L. X., J. Hu, N. Liu, X. Wang, G. M. Smith, X. Wen, and X. M. Xu. 2011. "GDNF modifies reactive astrogliosis allowing robust axonal regeneration through Schwann cell-seeded guidance channels after spinal cord injury." *Exp Neurol* 229 (2):238-50. doi: 10.1016/j.expneurol.2011.02.001.
Deumens, R., G. C. Koopmans, W. M. Honig, F. P. Hamers, V. Maquet, R. Jerome, H. W. Steinbusch, and E. A. Joosten. 2006. "Olfactory ensheathing cells, olfactory nerve fibroblasts and biomatrices to promote long-distance axon regrowth and functional recovery in the dorsally hemisected adult rat spinal cord." *Exp Neurol* 200 (1):89-103. doi: 10.1016/j.expneurol.2006.01.030.
Dietz, V. 2003. "Spinal cord pattern generators for locomotion." *Clin Neurophysiol* 114 (8):1379-89.
Dijkstra, C. D., E. A. Dopp, P. Joling, and G. Kraal. 1985. "The heterogeneity of mononuclear phagocytes in lymphoid organs: distinct macrophage subpopulations in the rat recognized by monoclonal antibodies ED1, ED2 and ED3." *Immunology* 54 (3):589-99.
Ditunno, J. F., J. W. Little, A. Tessler, and A. S. Burns. 2004. "Spinal shock revisited: a four-phase model." *Spinal Cord* 42 (7):383-95. doi: 10.1038/sj.sc.3101603.
Eng, L. F. 1985. "Glial fibrillary acidic protein (GFAP): the major protein of glial intermediate filaments in differentiated astrocytes." *J Neuroimmunol* 8 (4-6):203-14.

Fehlings, M. G. 2001. "Editorial: recommendations regarding the use of methylprednisolone in acute spinal cord injury: making sense out of the controversy." *Spine (Phila Pa 1976)* 26 (24 Suppl):S56-7.

Fehlings, M. G., and D. H. Nguyen. 2010. "Immunoglobulin G: a potential treatment to attenuate neuroinflammation following spinal cord injury." *J Clin Immunol* 30 Suppl 1:S109-12. doi: 10.1007/s10875-010-9404-7.

Fernandez, E., R. Pallini, E. Marchese, and G. Talamonti. 1991. "Experimental studies on spinal cord injuries in the last fifteen years." *Neurol Res* 13 (3):138-59.

Field-Fote, E. C. 2001. "Combined use of body weight support, functional electric stimulation, and treadmill training to improve walking ability in individuals with chronic incomplete spinal cord injury." *Arch Phys Med Rehabil* 82 (6):818-24. doi: 10.1053/apmr.2001.23752.

Fitch, M. T., C. Doller, C. K. Combs, G. E. Landreth, and J. Silver. 1999. "Cellular and molecular mechanisms of glial scarring and progressive cavitation: in vivo and in vitro analysis of inflammation-induced secondary injury after CNS trauma." *J Neurosci* 19 (19):8182-98.

Fitzgerald, M., M. L. Reynolds, and L. I. Benowitz. 1991. "GAP-43 EXPRESSION IN THE DEVELOPING RAT LUMBAR SPINAL-CORD." *Neuroscience* 41 (1):187-199. doi: 10.1016/0306-4522(91)90209-7.

Friedman, J. A., A. J. Windebank, M. J. Moore, R. J. Spinner, B. L. Currier, and M. J. Yaszemski. 2002. "Biodegradable polymer grafts for surgical repair of the injured spinal cord." *Neurosurgery* 51 (3):742-51; discussion 751-2.

Furlan, J. C., V. Noonan, D. W. Cadotte, and M. G. Fehlings. 2011. "Timing of decompressive surgery of spinal cord after traumatic spinal cord injury: an evidence-based examination of pre-clinical and clinical studies." *J Neurotrauma* 28 (8):1371-99. doi: 10.1089/neu.2009.1147.

Gensel, J. C., C. A. Tovar, F. P. Hamers, R. J. Deibert, M. S. Beattie, and J. C. Bresnahan. 2006. "Behavioral and histological characterization of unilateral cervical spinal cord contusion injury in rats." *J Neurotrauma* 23 (1):36-54. doi: 10.1089/neu.2006.23.36.

Girgis, J., D. Merrett, S. Kirkland, G. A. Metz, V. Verge, and K. Fouad. 2007. "Reaching training in rats with spinal cord injury promotes plasticity and task specific recovery." *Brain* 130 (Pt 11):2993-3003. doi: 10.1093/brain/awm245.

Gorio, A., L. Madaschi, B. Di Stefano, S. Carelli, A. M. Di Giulio, S. De Biasi, T. Coleman, A. Cerami, and M. Brines. 2005. "Methylprednisolone neutralizes the beneficial effects of erythropoietin in experimental spinal cord injury." *Proc Natl Acad Sci U S A* 102 (45):16379-84. doi: 0508479102 [pii]

10.1073/pnas.0508479102.

Goto, E., M. Mukozawa, H. Mori, and M. Hara. 2010. "A rolled sheet of collagen gel with cultured Schwann cells: model of nerve conduit to enhance neurite growth." *J Biosci Bioeng* 109 (5):512-8. doi: 10.1016/j.jbiosc.2009.11.002.

GrandPre, T., S. Li, and S. M. Strittmatter. 2002. "Nogo-66 receptor antagonist peptide promotes axonal regeneration." *Nature* 417 (6888):547-51. doi: 10.1038/417547a

417547a [pii].

Guan, Yijing. 2010. "Characterization of Alginate Scaffolds Using X-RAY Imaging Techniques." Master of Science, Biomedical Engineering, University of Saskatchewan.

Guertin, P. A. 2012. "Central pattern generator for locomotion: anatomical, physiological, and pathophysiological considerations." *Front Neurol* 3:183. doi: 10.3389/fneur.2012.00183.
Hill, C. E., L. D. Moon, P. M. Wood, and M. B. Bunge. 2006. "Labeled Schwann cell transplantation: cell loss, host Schwann cell replacement, and strategies to enhance survival." *Glia* 53 (3):338-43. doi: 10.1002/glia.20287.
Hu, F., and S. M. Strittmatter. 2004. "Regulating axon growth within the postnatal central nervous system." *Semin Perinatol* 28 (6):371-8.
Huang, S., and X. Fu. 2010. "Naturally derived materials-based cell and drug delivery systems in skin regeneration." *J Control Release* 142 (2):149-59. doi: S0168-3659(09)00713-5 [pii]

10.1016/j.jconrel.2009.10.018.
Jacobowitz, D. M., J. T. Cole, D. P. McDaniel, H. B. Pollard, and W. D. Watson. 2012. "Microglia activation along the corticospinal tract following traumatic brain injury in the rat: a neuroanatomical study." *Brain Res* 1465:80-9. doi: 10.1016/j.brainres.2012.05.008

S0006-8993(12)00845-1 [pii].
Joosten, E. A., R. L. Schuitman, M. E. Vermelis, and P. J. Dederen. 1992. "Postnatal development of the ipsilateral corticospinal component in rat spinal cord: a light and electron microscopic anterograde HRP study." *J Comp Neurol* 326 (1):133-46. doi: 10.1002/cne.903260112.
Jun Chen, Xiao-Ming Xu, Zao C. Xu. 2009. "Animal Models of Acute Neurological Injuries." In.
Kanno, H., D. D. Pearse, H. Ozawa, E. Itoi, and M. B. Bunge. 2015. "Schwann cell transplantation for spinal cord injury repair: its significant therapeutic potential and prospectus." *Rev Neurosci*. doi: 10.1515/revneuro-2014-0068.
Kataoka, K., Y. Suzuki, M. Kitada, T. Hashimoto, H. Chou, H. Bai, M. Ohta, S. Wu, K. Suzuki, and C. Ide. 2004. "Alginate enhances elongation of early regenerating axons in spinal cord of young rats." *Tissue Eng* 10 (3-4):493-504. doi: 10.1089/107632704323061852.
Khan, T., R. M. Havey, S. T. Sayers, A. Patwardhan, and W. W. King. 1999. "Animal models of spinal cord contusion injuries." *Lab Anim Sci* 49 (2):161-72.
Kim, B. I., K. H. Kim, H. S. Youn, S. Jheon, J. K. Kim, and H. Kim. 2008. "High resolution X-ray phase contrast synchrotron imaging of normal and ligation damaged rat sciatic nerves." *Microsc Res Tech* 71 (6):443-7. doi: 10.1002/jemt.20571.
Kwon, B. K., T. R. Oxland, and W. Tetzlaff. 2002. "Animal models used in spinal cord regeneration research." *Spine* 27 (14):1504-1510. doi: Doi 10.1097/01.Brs.0000018791.75972.A5.
Lam, T., J. J. Eng, D. L. Wolfe, J. T. Hsieh, M. Whittaker, and Scire Research Team the. 2007. "A systematic review of the efficacy of gait rehabilitation strategies for spinal cord injury." *Top Spinal Cord Inj Rehabil* 13 (1):32-57. doi: 10.1310/sci1301-32.
Lavdas, A. A., F. Papastefanaki, D. Thomaidou, and R. Matsas. 2008. "Schwann cell transplantation for CNS repair." *Curr Med Chem* 15 (2):151-60.
Lawrence S Chin, Robert B and Molly G King. 2013. "Spinal Cord Injuries ".
Lee, D. H., and J. K. Lee. 2013. "Animal models of axon regeneration after spinal cord injury." *Neurosci Bull* 29 (4):436-44. doi: 10.1007/s12264-013-1365-4.
Lee, K. Y., and D. J. Mooney. 2012. "Alginate: properties and biomedical applications." *Prog Polym Sci* 37 (1):106-126. doi: 10.1016/j.progpolymsci.2011.06.003.

Lemon, R. N., and J. Griffiths. 2005. "Comparing the function of the corticospinal system in different species: organizational differences for motor specialization?" *Muscle Nerve* 32 (3):261-79. doi: 10.1002/mus.20333.

Lu, G. M., D. M. Liu, Z. L. Jiang, F. Ding, X. S. Gu, and Z. G. Wang. 2005. *Immunohistochemical localization of the corticospinal tract in normal rat spinal cord as a stereotactic guidance for implantation of microelectronic chip*. Edited by J. P. He, S. K. Gao and J. R. Lin, *2005 First International Conference on Neural Interface and Control Proceedings*. New York: Ieee.

MacKay-Lyons, M. 2002. "Central pattern generation of locomotion: a review of the evidence." *Phys Ther* 82 (1):69-83.

Mahdi Sharif-Alhoseini, Vafa Rahimi-Movaghar. 2014. *Animal Models in Traumatic Spinal Cord Injury, Topics in Paraplegia*: Yannis Dionyssiotis (Ed.).

Mano, J. F., G. A. Silva, H. S. Azevedo, P. B. Malafaya, R. A. Sousa, S. S. Silva, L. F. Boesel, J. M. Oliveira, T. C. Santos, A. P. Marques, N. M. Neves, and R. L. Reis. 2007. "Natural origin biodegradable systems in tissue engineering and regenerative medicine: present status and some moving trends." *J R Soc Interface* 4 (17):999-1030. doi: R44P66156484711X [pii]

10.1098/rsif.2007.0220.

McKinley, W. O., A. B. Jackson, D. D. Cardenas, and M. J. DeVivo. 1999. "Long-term medical complications after traumatic spinal cord injury: a regional model systems analysis." *Arch Phys Med Rehabil* 80 (11):1402-10. doi: S0003999399000520 [pii].

Merkler, D., G. A. Metz, O. Raineteau, V. Dietz, M. E. Schwab, and K. Fouad. 2001. "Locomotor recovery in spinal cord-injured rats treated with an antibody neutralizing the myelin-associated neurite growth inhibitor Nogo-A." *J Neurosci* 21 (10):3665-73.

Metz, G. A., D. Merkler, V. Dietz, M. E. Schwab, and K. Fouad. 2000. "Efficient testing of motor function in spinal cord injured rats." *Brain Res* 883 (2):165-77. doi: S0006-8993(00)02778-5 [pii].

Mietto, B.S., A.M.B. Martinez, R.M. Costa, S.T. Ferreira, and S.V. de Lima. 2011. *Wallerian Degeneration in Injury and Diseases: Concepts and Prevention*: INTECH Open Access Publisher.

Miselis, Richard. 2011. Laboratory 12 : Tract Systems I. University of Pennsylvania School of Veterinary Medicine.

Moon, L., and M. B. Bunge. 2005. "From animal models to humans: strategies for promoting CNS axon regeneration and recovery of limb function after spinal cord injury." *J Neurol Phys Ther* 29 (2):55-69.

Mortazavi, M. M., K. Verma, O. A. Harmon, C. J. Griessenauer, N. Adeeb, N. Theodore, and R. S. Tubbs. 2015. "The microanatomy of spinal cord injury: a review." *Clin Anat* 28 (1):27-36. doi: 10.1002/ca.22432.

Naseri, K., E. Saghaei, F. Abbaszadeh, M. Afhami, A. Haeri, F. Rahimi, and M. Jorjani. 2013. "Role of microglia and astrocyte in central pain syndrome following electrolytic lesion at the spinothalamic tract in rats." *J Mol Neurosci* 49 (3):470-9. doi: 10.1007/s12031-012-9840-3.

Nomura, H., C. H. Tator, and M. S. Shoichet. 2006. "Bioengineered strategies for spinal cord repair." *J Neurotrauma* 23 (3-4):496-507. doi: 10.1089/neu.2006.23.496.

Nor, J. E. 2006. "Tooth regeneration in operative dentistry." *Oper Dent* 31 (6):633-42. doi: 10.2341/06-000.

Norbert Pallua, Christoph V. Suscheck. 2011. *Tissue Engineering*: Springer Berlin Heidelberg.
Norenberg, M. D., J. Smith, and A. Marcillo. 2004. "The pathology of human spinal cord injury: defining the problems." *J Neurotrauma* 21 (4):429-40. doi: 10.1089/089771504323004575.
Nyberg-Hansen, R., and A. Brodal. 1963. "Sites of termination of corticospinal fibers in the cat. An experimental study with silver impregnation methods." *J Comp Neurol* 120:369-91.
Onifer, S. M., G. M. Smith, and K. Fouad. 2011. "Plasticity after spinal cord injury: relevance to recovery and approaches to facilitate it." *Neurotherapeutics* 8 (2):283-93. doi: 10.1007/s13311-011-0034-4.
Oudega, M., and M. A. Perez. 2012. "Corticospinal reorganization after spinal cord injury." *J Physiol* 590 (Pt 16):3647-63. doi: 10.1113/jphysiol.2012.233189

jphysiol.2012.233189 [pii].
Oudega, M., and X. M. Xu. 2006. "Schwann cell transplantation for repair of the adult spinal cord." *J Neurotrauma* 23 (3-4):453-67. doi: 10.1089/neu.2006.23.453.
Oyinbo, C. A. 2011. "Secondary injury mechanisms in traumatic spinal cord injury: a nugget of this multiply cascade." *Acta Neurobiol Exp (Wars)* 71 (2):281-299. doi: 7128 [pii].
Patrick R. Hof, Charles V. Mobb. 2010. *Handbook of the Neuroscience of Aging* Academic Press.
Popovich, P. G., and T. B. Jones. 2003. "Manipulating neuroinflammatory reactions in the injured spinal cord: back to basics." *Trends Pharmacol Sci* 24 (1):13-7. doi: S0165-6147(02)00006-8 [pii].
Pritchard, C. D., J. R. Slotkin, D. Yu, H. N. Dai, M. S. Lawrence, R. T. Bronson, F. M. Reynolds, Y. D. Teng, E. J. Woodward, and R. S. Langer. 2010. "Establishing a model spinal cord injury in the African green monkey for the preclinical evaluation of biodegradable polymer scaffolds seeded with human neural stem cells." *Journal of Neuroscience Methods* 188 (2):258-269. doi: DOI 10.1016/j.jneumeth.2010.02.019.
Rajaram, A., D. J. Schreyer, and D. X. Chen. 2015. "Use of the polycation polyethyleneimine to improve the physical properties of alginate-hyaluronic acid hydrogel during fabrication of tissue repair scaffolds." *J Biomater Sci Polym Ed*:1-13. doi: 10.1080/09205063.2015.1016383.
Ramon-Cueto, A., and J. Avila. 1998. "Olfactory ensheathing glia: properties and function." *Brain Res Bull* 46 (3):175-87.
Rotshenker, S. 2011. "Wallerian degeneration: the innate-immune response to traumatic nerve injury." *J Neuroinflammation* 8:109. doi: 10.1186/1742-2094-8-109.
Rupenthal, I. D., C. R. Green, and R. G. Alany. 2011. "Comparison of ion-activated in situ gelling systems for ocular drug delivery. Part 1: physicochemical characterisation and in vitro release." *Int J Pharm* 411 (1-2):69-77. doi: S0378-5173(11)00259-6 [pii]

10.1016/j.ijpharm.2011.03.042.
Sakai, K., A. Yamamoto, K. Matsubara, S. Nakamura, M. Naruse, M. Yamagata, K. Sakamoto, R. Tauchi, N. Wakao, S. Imagama, H. Hibi, K. Kadomatsu, N. Ishiguro, and M. Ueda. 2012. "Human dental pulp-derived stem cells promote locomotor recovery after complete transection of the rat spinal cord by multiple neuro-regenerative mechanisms." *J Clin Invest* 122 (1):80-90. doi: 10.1172/JCI59251.
Schmidt, C. E., and J. B. Leach. 2003. "Neural tissue engineering: strategies for repair and regeneration." *Annu Rev Biomed Eng* 5:293-347. doi: 10.1146/annurev.bioeng.5.011303.120731.

Sharp, K. G., K. M. Yee, T. L. Stiles, R. M. Aguilar, and O. Steward. 2013. "A re-assessment of the effects of treatment with a non-steroidal anti-inflammatory (ibuprofen) on promoting axon regeneration via RhoA inhibition after spinal cord injury." *Exp Neurol* 248:321-37. doi: 10.1016/j.expneurol.2013.06.023.

Siemionow, M., W. Duggan, G. Brzezicki, A. Klimczak, C. Grykien, J. Gatherwright, and D. Nair. 2011. "Peripheral nerve defect repair with epineural tubes supported with bone marrow stromal cells: a preliminary report." *Ann Plast Surg* 67 (1):73-84. doi: 10.1097/SAP.0b013e318223c2db.

Slemmer, J. E., J. T. Weber, and C. I. De Zeeuw. 2004. "Cell death, glial protein alterations and elevated S-100 beta release in cerebellar cell cultures following mechanically induced trauma." *Neurobiol Dis* 15 (3):563-72. doi: 10.1016/j.nbd.2003.11.027.

Sofroniew, M. V., and H. V. Vinters. 2010. "Astrocytes: biology and pathology." *Acta Neuropathol* 119 (1):7-35. doi: 10.1007/s00401-009-0619-8.

Sriamornsak, P., and S. Sungthongjeen. 2007. "Modification of theophylline release with alginate gel formed in hard capsules." *AAPS PharmSciTech* 8 (3):E51. doi: 10.1208/pt0803051.

Starkweather, AR. 2013. "Spinal Cord Injury Facts and Figures at a Glance." *The Journal of Spinal Cord Medicine* 36 (2):170-171. doi: DOI: http://dx.doi.org/10.1179/1079026813Z.000000000148.

Straley, K. S., C. W. Foo, and S. C. Heilshorn. 2010. "Biomaterial design strategies for the treatment of spinal cord injuries." *J Neurotrauma* 27 (1):1-19. doi: 10.1089/neu.2009.0948.

Tabien, Hortense Elizabeth Nsoh. 2010. "THE NEUROPROTECTIVE ACTIONS OF QUERCETIN." Doctor of Philosophy, Anatomy and Cell Biology, University of Saskatchewan.

Teng, Y. D., E. B. Lavik, X. Qu, K. I. Park, J. Ourednik, D. Zurakowski, R. Langer, and E. Y. Snyder. 2002. "Functional recovery following traumatic spinal cord injury mediated by a unique polymer scaffold seeded with neural stem cells." *Proc Natl Acad Sci U S A* 99 (5):3024-9. doi: 10.1073/pnas.052678899

052678899 [pii].

Tortora, Gerard J., and Bryan Derrickson. 2011. *Principles of anatomy and physiology*. Hoboken, N.J.: Wiley.

Usov, A. I. 1999. "Alginic acids and alginates: Methods for analysis, determination of the composition and structure elucidation." *Uspekhi Khimii* 68 (11):1051-1061.

Vacanti, C. A., and J. P. Vacanti. 2000. "The science of tissue engineering." *Orthopedic Clinics of North America* 31 (3):351-6.

Vawda, R., J. Wilcox, and M. Fehlings. 2012. "Current stem cell treatments for spinal cord injury." *Indian J Orthop* 46 (1):10-8. doi: 10.4103/0019-5413.91629.

Verdu, E., X. Navarro, G. Gudino-Cabrera, F. J. Rodriguez, D. Ceballos, A. Valero, and M. Nieto-Sampedro. 1999. "Olfactory bulb ensheathing cells enhance peripheral nerve regeneration." *Neuroreport* 10 (5):1097-101.

Voda, J., T. Yamaji, and B. G. Gold. 2005. "Neuroimmunophilin ligands improve functional recovery and increase axonal growth after spinal cord hemisection in rats." *J Neurotrauma* 22 (10):1150-61. doi: 10.1089/neu.2005.22.1150.

Voron, Stephen. 2011. The Vestibular System. University of Utah School of Medicine.

Wanner, I. B., M. A. Anderson, B. Song, J. Levine, A. Fernandez, Z. Gray-Thompson, Y. Ao, and M. V. Sofroniew. 2013. "Glial scar borders are formed by newly proliferated, elongated astrocytes that interact to corral inflammatory and fibrotic cells via STAT3-dependent mechanisms after spinal cord injury." *J Neurosci* 33 (31):12870-86. doi: 10.1523/JNEUROSCI.2121-13.2013.

Webb, A. A., and G. D. Muir. 2004. "Course of motor recovery following ventrolateral spinal cord injury in the rat." *Behav Brain Res* 155 (1):55-65. doi: 10.1016/j.bbr.2004.04.002.

Whitwell, Helen L, ed. 2005. *Forensic Neuropathology* illustrated ed: CRC Press.

Wilcox, J. T., K. Satkunendrarajah, J. A. Zuccato, F. Nassiri, and M. G. Fehlings. 2014. "Neural precursor cell transplantation enhances functional recovery and reduces astrogliosis in bilateral compressive/contusive cervical spinal cord injury." *Stem Cells Transl Med* 3 (10):1148-59. doi: 10.5966/sctm.2014-0029.

Wilhelm, J. C., M. Xu, D. Cucoranu, S. Chmielewski, T. Holmes, K. S. Lau, G. J. Bassell, and A. W. English. 2012. "Cooperative roles of BDNF expression in neurons and Schwann cells are modulated by exercise to facilitate nerve regeneration." *J Neurosci* 32 (14):5002-9. doi: 10.1523/JNEUROSCI.1411-11.2012.

Wong, F. S., B. P. Chan, and A. C. Lo. 2014. "Carriers in cell-based therapies for neurological disorders." *Int J Mol Sci* 15 (6):10669-723. doi: 10.3390/ijms150610669.

Xu, W., L. Chi, R. Xu, Y. Ke, C. Luo, J. Cai, M. Qiu, D. Gozal, and R. Liu. 2005. "Increased production of reactive oxygen species contributes to motor neuron death in a compression mouse model of spinal cord injury." *Spinal Cord* 43 (4):204-13. doi: 3101674 [pii]

10.1038/sj.sc.3101674.

Zhang, N., Y. Yin, S. J. Xu, Y. P. Wu, and W. S. Chen. 2012. "Inflammation & apoptosis in spinal cord injury." *Indian J Med Res* 135:287-96.

Zhang, S. X., F. Huang, M. Gates, and E. G. Holmberg. 2013. "Role of endogenous Schwann cells in tissue repair after spinal cord injury." *Neural Regen Res* 8 (2):177-85. doi: 10.3969/j.issn.1673-5374.2013.02.011.

Zhang, X., H. N. Wenk, C. N. Honda, and G. J. Giesler, Jr. 2000. "Locations of spinothalamic tract axons in cervical and thoracic spinal cord white matter in monkeys." *J Neurophysiol* 83 (5):2869-80.

Zhu, N., D. Chapman, D. Cooper, D. J. Schreyer, and X. Chen. 2011. "X-ray diffraction enhanced imaging as a novel method to visualize low-density scaffolds in soft tissue engineering." *Tissue Eng Part C Methods* 17 (11):1071-80. doi: 10.1089/ten.tec.2011.0102.